



**HAL**  
open science

## Dealing with interfering users in LoRa Networks

Angesom Ataklity Tesfay

► **To cite this version:**

Angesom Ataklity Tesfay. Dealing with interfering users in LoRa Networks. Micro and nanotechnologies/Microelectronics. Université de Lille, 2021. English. NNT : 2021LILUN005 . tel-03526526

**HAL Id: tel-03526526**

**<https://theses.hal.science/tel-03526526v1>**

Submitted on 14 Jan 2022

**HAL** is a multi-disciplinary open access archive for the deposit and dissemination of scientific research documents, whether they are published or not. The documents may come from teaching and research institutions in France or abroad, or from public or private research centers.

L'archive ouverte pluridisciplinaire **HAL**, est destinée au dépôt et à la diffusion de documents scientifiques de niveau recherche, publiés ou non, émanant des établissements d'enseignement et de recherche français ou étrangers, des laboratoires publics ou privés.

**Thèse de doctorat**  
présentée à  
l'UNIVERSITÉ DE LILLE

Pour l'obtention du grade de  
**Docteur en Sciences**  
Spécialité: **Systèmes de Télécommunication**

par  
**Angesom Ataklity TESFAY**

**Laboratoire d'accueil:** Institut d'Électronique de Microélectronique et de Nanotechnologie  
IEMN– UMR CNRS 8520

**École doctorale:** 072 Sciences pour l'Ingénieur (SPI), Lille Nord-de-France

---

Dealing with interfering users in LoRa Networks  
Gérer les interférences des utilisateurs dans les réseaux LoRa

---

Soutenance prévue le 01/10/2021, devant le jury composé de:

Rapporteur **Matthieu CRUSSIÈRE**, Maître de Conférences, HDR, INSA Rennes, France.

Rapporteur **Lina MROUEH**, Professeur, Institut Supérieur d'Electronique de Paris, Paris, France.

Président du jury **Laurent ROS**, Professeur, Université de Grenoble, Grenoble, France.

Examinateur **Mohammad-Ali KHALIGHI**, Professeur, Ecole Centrale Marseille, Marseille, France.

Examinateur **Nathalie MITTON**, Directeur de recherche, Inria, Lille, France.

Examinateur **Joumana FARAH**, Professeur, Faculty of Engineering, Lebanese University, Lebanese.

Directeur de thèse **Laurent CLAVIER**, Professeur, IMT Lille Douai, France.

Co-encadrante **Eric Pierre SIMON**, Maître de Conférences, HDR, IEMN, University de Lille, France.



---

In memory of the victims of the war in Tigray.

Dedicated to my mother Trhas, wife Hana, son Nathan, and my family for their unconditional love and support during my journey.

---



# Acknowledgments

The first time I came to France was in July 2017 for my internship and M.Sc. thesis at IRCICA with the supervision of Professor Laurent CLAVIER. That was the moment that shaped my future research career. After I finished my M.Sc. degree, I got an offer on this great Ph.D. project from Professor Laurent CLAVIER; then, I decided to return to France to pursue my Ph.D. at the University of Lille.

First and foremost, I thank God for all the blessings. I want to express my special gratitude to my supervisors, who helped me most, Professor Laurent CLAVIER, and Dr. Eric Pierre Simon, for their guidance, support, and patient throughout my Ph.D. candidature. It would be difficult to complete this thesis without their guidance.

I would like to thank Dr. Sofiane Kharbech, who was my mentor in research and social life. He was beside me in every step of my journey. His excellent work habit and discipline are infectious. I learned a lot from working with him.

I thank all my former and colleges in the IRCICA lab, Ce Zheng, Meysem Mayahi, Yasser Mestrah, Nicolas de Araujo Moreira, and Umber Noreen.

Last but not least, I have a special thanks to my family, my grandmother Adey (Abrehet Brhane), my mother Trhas Zerezgi, my father Ataklity Tesfay, my brother Merhawi, my sister Freweyni, and my wife, Hana Teshome. They supported me unconditionally throughout my life as well as during my study. I am very grateful for the love and support from my wife, Hana Teshome, during this difficult time. I thank God for giving me the gift of life, my son Nathan. You gave me the strength to finish my Ph.D. as planned. You and your mother become the light in the darkness. I want to thank my uncle Dr. Berhe G. Tokola, and his family for always being there during my Ph.D. This work is dedicated to you all. Trhasey (mother), I can't thank you enough for supporting me and opening opportunities to reach where I am today.



# Résumé | Abstract

**Résumé** La technologie de l'Internet des objets (IoT) est devenue omniprésente dans de nombreuses applications et son utilisation se développe très rapidement. Cependant, l'expansion de l'IoT se heurte à une difficulté importante d'évolutivité, c'est-à-dire que le déploiement très dense d'appareils communicants est actuellement limité. Cette thèse se concentre sur la fourniture de solutions aux problèmes liés à l'évolutivité des réseaux de type LoRa dans les deux sens de communication, la liaison montante et la liaison descendante. Dans les réseaux longue portée, comme LoRa, la liaison descendante est critique car elle limite le nombre d'accusés de réception pouvant être envoyés, et par conséquent, la fiabilité. Cela limite également la possibilité de mettre à jour les appareils, ce qui pourrait être critique lorsqu'ils sont déployés pendant des décennies. Pour surmonter ces problèmes, nous proposons une solution, inspirée des techniques d'accès multiple non orthogonal (NOMA), pour augmenter d'au moins un ordre de grandeur le nombre de dispositifs pouvant être adressés. Si l'approche différencie les appareils par la puissance qui leur est allouée, elle diffère de la grande majorité des travaux antérieurs sur le domaine de puissance NOMA car elle ne nécessite pas d'annulation des interférences. Au lieu de cela, il bénéficie de l'étalement spectral du schéma de modulation (chirp spread spectrum), où, à la fin de la phase de décodage, l'information portée par un symbole se retrouve à la position d'un pic dans le domaine de Fourier. Dans la plupart des cas, les informations provenant de différents utilisateurs entraînent des positions de pic différentes, ne créant aucune interférence. En ce sens, on se rapproche des schémas d'évitement comme le saut de temps ou de fréquence, mais sans utiliser de code. Cette thèse propose une nouvelle solution s'appuyant sur du NOMA dans le domaine de la puissance qui ne souffre pas des limitations induites par les résidus d'annulation d'interférence. Le système proposé, y compris la détection de préambule et l'estimation de canal, est présenté et évalué par des simulations. Nous montrons que notre schéma permet d'augmenter le nombre d'appareils connectés d'un ordre de grandeur par rapport au

système actuel, tout en maintenant une compatibilité totale avec la norme de couche physique LoRa.

Concernant la liaison montante, nous présentons un nouveau récepteur capable de démoduler plusieurs utilisateurs transmis simultanément sur le même canal de fréquence avec le même facteur d'étalement. Du point de vue de l'accès multiple non orthogonal, il est basé sur le domaine des puissances et utilise l'annulation des interférences en série. Les résultats de simulation montrent que le récepteur permet une augmentation significative du nombre d'appareils connectés dans le réseau. Enfin, cette thèse traite de la détection de signaux, en liaison montante, d'un réseau LoRa à travers une approche basée sur l'apprentissage profond. Deux stratégies sont proposées : la régression pour la détection de bits basée sur un réseau de neurones *deep feedforward* et la classification pour la détection de symboles basée sur un réseau de neurones convolutif. Ces récepteurs peuvent décoder les signaux d'un utilisateur sélectionné lorsque plusieurs utilisateurs émettent simultanément sur la même bande de fréquences avec le même facteur d'étalement. Les résultats de simulation montrent que les deux récepteurs surpassent le LoRa classique en présence d'interférences. De plus, les résultats montrent que l'approche introduite est pertinente pour traiter la question de l'évolutivité.

**Mots-clefs** LoRa, LoRaWAN, IoT, Annulation des interférences série, Détecteur multi-utilisateurs, Allocation de puissance, évolutivité, Deep-Learning, Chirp Spread Spectrum.

---

**Abstract** Internet of Things (IoT) technology has become ubiquitous in many applications, and its use is growing very fast. However, the expansion of IoT faces a significant difficulty of scalability, which is, the very dense deployment of communicating devices is currently limited. This thesis focuses on providing solutions to issues related to the scalability of LoRa-like networks in both communication directions, the uplink, and downlink. In long-range networks, such as LoRa, the downlink is critical because it limits the number of acknowledgments that can be sent, and consequently, reliability. It also limits the possibility of updating the devices, which could be critical when deployed for decades. To overcome those problems, we propose a solution, inspired by Non-Orthogonal Multiple Access (NOMA) techniques, to increase by at least one order of magnitude the number of devices that can be addressed. While the approach differentiates the devices by the power allocated to them, it differs from the vast majority of previous works on power domain NOMA because it does not require interference cancellation. Instead, it benefits from the spectrum spreading of the modulation scheme (chirp spread spectrum), where, at the end of the decoding phase, the information carried by a symbol is found in the position of a peak in the Fourier domain. In most cases, the information from different users results in different peak positions, not creating any interference. In that sense, we get closer to avoidance schemes such as time or frequency hopping, but without using a code. This thesis proposes a new solution for NOMA in the power domain that does not suffer from the limitations induced by interference cancellation residues. The proposed system, including preamble detection and channel estimation, is presented and evaluated by simulations. We demonstrate that our proposed scheme increases the number of devices by one order of magnitude compared to the current system, which allows addressing only one user at a time and maintains full compatibility with the LoRa physical layer standard.

In addition to that, we present a new receiver design, which significantly improves performance in the uplink communication of LoRa networks, i.e., having asynchronous transmissions. The proposed receiver is able to demodulate multiple users simultaneously transmitted over the same frequency channel with the same spreading factor. From a non-orthogonal multiple access point of view, it is based on the power domain and uses serial interference cancellation. Simulation results show that the receiver allows a significant increase in the number of connected devices in the network. Finally, this thesis deals with signal detection in the uplink of a LoRa network through a deep learning-based approach. Two strategies are proposed: regression for bit detection based on a deep feedforward neural network and classification for sym-

bol detection based on a convolutional neural network. These receivers can decode a selected user's signals when multiple users simultaneously transmit over the same frequency band with the same spreading factor. Simulation results show that both receivers outperform the classical LoRa one in the presence of interference. Furthermore, the results show that the introduced approach is relevant to deal with the scalability issue.

**Keywords** LoRa, LoRaWAN, IoT, Serial Interference Cancellation, Multiuser Detector, Power Allocation, scalability, Deep-Learning, Chirp Spread Spectrum.

# Contents

<b>Acknowledgments</b>	<b>i</b>
<b>Résumé   Abstract</b>	<b>iii</b>
<b>Contents</b>	<b>vii</b>
<b>Table of Figures</b>	<b>xi</b>
<b>List of Table</b>	<b>xv</b>
<b>List of Algorithms</b>	<b>xvii</b>
<b>List of Abbreviations</b>	<b>xix</b>
<b>Mathematical Notations</b>	<b>xxi</b>
<b>General Introduction</b>	<b>1</b>
<b>1 Introduction</b>	<b>5</b>
1.1 Introduction . . . . .	6
1.2 LoRaWAN . . . . .	6
1.3 LoRa PHY . . . . .	9
1.4 State of the Art: Scalability . . . . .	12
1.4.1 Physical Layer . . . . .	12
1.4.2 MAC Layer . . . . .	15
<b>2 Downlink Communication in LoRa-like Networks</b>	<b>19</b>
2.1 Introduction . . . . .	21
2.2 System Model . . . . .	22

2.3	Proposed Signal Detection Scheme . . . . .	23
2.3.1	Transmitted signal . . . . .	24
2.3.1.1	Power considerations . . . . .	24
2.3.1.2	Channel Model . . . . .	25
2.3.2	Receiver Design . . . . .	25
2.3.2.1	Cross-Entropy Multiuser Detector . . . . .	27
2.3.2.2	Proposed Low-Complexity Detector . . . . .	30
2.3.2.3	Direct Peak Detection . . . . .	35
2.3.3	Power allocation scheme . . . . .	36
2.3.3.1	Power Allocation 1: Suppressing ambiguities . . . . .	36
2.3.3.2	Power Allocation 2: Fair Spacing . . . . .	36
2.4	Results . . . . .	37
2.4.1	Simulation setup . . . . .	37
2.4.2	Performance of the three receivers . . . . .	38
2.4.3	Power allocation performance . . . . .	40
2.4.4	Fairness . . . . .	40
2.4.5	Computational Complexity Analysis . . . . .	44
2.4.5.1	Direct peak detection . . . . .	44
2.4.5.2	Cross Entropy Method . . . . .	45
2.4.5.3	Proposed Method . . . . .	45
2.4.5.4	Comparison . . . . .	46
2.4.6	SF Orthogonality . . . . .	46
	Conclusion . . . . .	49
<b>3</b>	<b>Uplink Communication in LoRa-like Networks</b>	<b>51</b>
3.1	Multi-user Detection: Serial Interference Cancellation . . . . .	52
3.1.1	System Model . . . . .	53
3.1.2	Proposed SIC Receiver . . . . .	57
3.1.3	Results . . . . .	58
3.1.3.1	Performance for a given selected link . . . . .	59
3.1.3.2	Mean Performance . . . . .	59
3.1.3.3	SF Orthogonality . . . . .	60
3.2	Single User Detection: Deep learning-based . . . . .	65
3.2.1	System Model . . . . .	66
3.2.2	Deep Learning-based Receiver . . . . .	67
3.2.2.1	Deep Feedforward Neural Network-based receiver . . . . .	68

---

3.2.2.2	Convolutional Neural Networks-based receiver . . .	68
3.2.3	Results . . . . .	69
3.2.3.1	Results for $N_i \sim \mathcal{P}(\lambda)$ . . . . .	70
3.2.3.2	Capture Effect – $N_i = 1$ . . . . .	71
3.2.3.3	Computational complexity . . . . .	71
Conclusion	. . . . .	75
<b>Conclusion and Perspectives</b>		<b>77</b>
<b>A Appendix related to Down-link Communication in LoRa</b>		<b>81</b>
A.1	Power allocation 2 . . . . .	81
<b>B Appendix related to Up-link Communication in LoRa-like Networks</b>		<b>83</b>
B.1	Chirp Formulation . . . . .	83
B.2	Received Signal and De-chirping . . . . .	87
B.3	Amplitudes of the Peaks . . . . .	92
<b>Bibliographie</b>		<b>103</b>



# List of Figures

1.1	LoRaWAN Network Architecture. . . . .	7
1.2	LoRaWAN devices classes. . . . .	8
1.3	LoRa PHY frame format. . . . .	9
1.4	Spectrum plot of a LoRa packet. . . . .	9
1.5	Raw up-chirp and Coded chirp associated with $m_q^{(i)}$ . . . . .	11
2.1	CEM-MUD as per Algorithm 2.1, with $N = 8$ users and SF = 7. This figure represent $f_{\mathbf{m}} = \mathbb{P}(m = k)$ at the beginning of the first iteration. Only one user is represented because the Probability Mass Function (PMF) $f_{\mathbf{m}}$ is the same for all users. . . . .	30
2.2	CEM-MUD as per Algorithm 2.1, with $N = 8$ users and SF = 7. In this example two collisions occur ( $\mathbf{m}_q = \{6, 79, 115, 79, 100, 100, 51, 87\}$ ). The figures represent $f_{\mathbf{m}}$ at the beginning of the 16th iteration. We can see that if values tend to gain in probability, the decision cannot be made yet. . . . .	31
2.3	CEM-MUD as per Algorithm 2.1, with $N = 8$ users and SF = 7. In this example two collisions occur ( $\mathbf{m}_q = \{6, 79, 115, 79, 100, 100, 51, 87\}$ ). The figures represent $f_{\mathbf{m}}$ at the beginning of the 31st iteration. We can see that the probability is clearly converging towards a single value equal to one for each user, all the others being zero. We also see that the decision is good despite the two collisions between users 2 and 4 and users 5 and 6. . . . .	32
2.4	SER for different SNR values of a single user, when SF = 7, and $B = 250$ kHz. . . . .	39
2.5	Performance of the proposed MUD when SNR = -10 dB, SF = 8, and $B = 250$ kHz. . . . .	41

2.6	Performance of the proposed MUD when SNR = -12 dB, SF = 8, and $B = 250$ kHz. . . . .	42
2.7	SER of the proposed MUD for different $N$ , Noise level of -114 dBm, SF=7, 8, and $B = 250$ kHz. . . . .	43
2.8	SER of the proposed MUD for different $N$ , Noise level of -114 dBm, SF=9, 10, and $B = 250$ kHz. . . . .	43
2.9	SER of individual users when $N = 7$ and 13, SF = 8, Noise level of -114 dBm, and $B = 250$ kHz. . . . .	44
2.10	SER for fixed 5 users using SF = 8, for different SF and interfering users, when $B = 250kHz$ . . . . .	48
2.11	SER for fixed 10 users using SF = 8, for different SF and interfering users, when $B = 250kHz$ . . . . .	48
3.1	LoRa-like Interfering symbols. . . . .	55
3.2	FFT of coded chirp of the user of interest at the values of 4 and 99 in the presence of one interfering user using SF = 8, $B = 250$ KHz. . . . .	56
3.3	SER for $N_u = 1, 4, 7,$ and 10, with SF = 8, $B = 250$ kHz. . . . .	60
3.4	SER for different values of $N_u$ , SF = 8, $B = 250$ kHz. . . . .	61
3.5	SER of each users for SF = 8, $B = 250$ kHz, Noise level of -114 dBm. . . . .	62
3.5	SER of each users for SF = 8, $B = 250$ kHz, Noise level of -114 dBm. . . . .	63
3.6	SER of Fixed 10 users using SF = 8 and additional interfering users using different SF (9, 10, 12), $B = 250$ kHz, Noise level of -114 dBm. . . . .	64
3.7	Uniform distribution of interfering user around the gateway. There exist no interfering devices within the radius of the guard-zone. . . . .	66
3.8	Collision between a symbol of selected user and two consecutive symbols of the interfering user. . . . .	67
3.9	Deep Feedforward Neural Network architecture. . . . .	68
3.10	Plot of $ Y_q[k] $ ( $k = 0, \dots, M - 1$ ) for a symbol of $m_q = 20$ with SNR = -10 dB and SF = 7. . . . .	69
3.11	Convolutional Neural Network architecture. . . . .	70
3.12	Symbol error rate as a function of the SNR for different detection approaches: classical decoder [∇], DFNN-based [*], and CNN-based [○]. For all figures, two scenarios are considered: no possible interference (plots in dash-dot line [-.-]) and when interference can happens (plots in solid line [—]). The plot inside show the probability mass function (pmf) related to the number of interfering users. . . . .	72

---

<p>3.12 Symbol error rate as a function of the SNR for different detection approaches: classical decoder [∇], DFNN-based [*], and CNN-based [○]. For all figures, two scenarios are considered: no possible interference (plots in dash-dot line [-.-]) and when interference can happens (plots in solid line [—]). The plot inside show the probability mass function (pmf) related to the number of interfering users. . . . .</p> <p>3.13 SER as a function of the SIR for the classical detector [∇], the DFNN-based [*], and the CNN-based [○]. The SNR for the selected user is set to <math>-6</math> dB. Two different cases are considered: networks trained for <math>\lambda = 0.25</math>[—], networks trained for each SIR value [-.-] . . . . .</p> <p>B.1 Interfering symbols at the receiver. . . . .</p>	<p>73</p> <p>74</p> <p>84</p>
--	-------------------------------



# List of Tables

2.1	Number of different combinations $M_c$ when $N_c$ collisions occur leading to $N_{pk}$ observed peaks when $N_{exp}$ were expected. . . . .	47
2.2	Average computational time $R_t$ (in second) to decode a single user (jth) when SF = 7, and $N$ users. . . . .	49



# List of Algorithms

2.1	CEM-MUD for downlink LoRa. . . . .	29
2.2	Proposed Multiuser Detection Algorithm (single symbol) . . . . .	35
3.1	SIC Receiver for LoRa-like Networks . . . . .	58



# List of Abbreviations

**B** Bandwidth

**BER** Bit-error Rate

**CDMA** Code Division Multiple Access

**CEM** Cross Entropy Method

**CSS** Chirp Spread Spectrum

**CR** Code Rate

**CRC** Cyclic Redundancy Check

**ETSI** European Telecommunications Standards Institute

**FFT** Fast Fourier transform

**FEC** Forward Error Correction

**ICS** Interleaved Chirp Spreading

**IoT** Internet of Things

**ISM** Industrial, Scientific and Medical

**LPWAN** Low Power Wide Area Networks

**ML** Maximum Likelihood

**MLD** Maximum Likelihood Detector

**MUD** Multi User Detector

**NOMA** Non Orthogonal Multiple Access

**PMF** Probability Mass Function

**PA** Power Allocation

**PHY** Physical

**SF** Spreading Factor

**SIC** Serial Interference Cancellation

**SNR** signal-to-Noise Ratio

**SINR** Signal-to-Interference-plus-Noise Ratio

**SIR** Signal-to-Interference Ratio

**TDMA** Time Division Multiple Access

# Mathematical Notations

$\text{sign}(\cdot)$

Fonction signe

$\|\cdot\|_\ell$

Norme d'ordre  $\ell$



# General Introduction

## Context

The Internet of Things (IoT) technology has been well integrated into our daily lives. However, we are still far from solving all significant challenges in a single network [1–3]. Nevertheless, IoT is growing fast and has become ubiquitous in many applications, such as smart cities, smart animal farming, smart agriculture, smart buildings, smart environment, smart metering, smart water recycling, and disaster alerting. These IoT applications require low power operations, long-range communication, and scalable network technologies. Low Power Wide Area Networks (LPWAN) provides a good solution for such requirements, and LoRa is one of those protocols which can enable such methods. However, the expansion of IoT faces a major difficulty: scalability, that is, very dense deployment of communicating devices, which is currently limited. This thesis brings solutions to enhance the scalability in LoRa-like networks.

## Motivation

This thesis aims to study the scalability challenges of IoT networks from the physical layer perspective and design receivers to increase the number of connected IoT devices. This work is mainly motivated by one of the prominent LPWAN, LoRaWAN. In this thesis, the following challenges are addressed:

1. **Signal detection in LoRa Downlink Communication:** In long-range networks, such as LoRa, the downlink is critical because it limits the number of acknowledgments that the gateway can send, and consequently, reliability. In fact, the access point is constrained by the duty cycle; therefore, it cannot address many devices. It also limits the possibility of updating the devices, which could be critical when deployed for decades. Therefore, these problems

need to be addressed to increase the number of devices that the network can support.

2. **Signal detection in LoRa Uplink Communication:** As we mentioned, the number of connected IoT devices is significantly increasing. Over recent years, LPWAN technologies, like LoRa in unlicensed bands, are proposed to face this growth. Several transmission settings enable quasi-orthogonal transmissions for the IoT devices. However, when two or more devices transmit simultaneously using the same transmission settings, a collision occurs at the receiver. This collision generally results in the loss of all colliding packets from the devices. As a result, the network capacity is limited in terms of scalability as well as reliability. Therefore, there is a need for a receiver design that enables multiple users to transmit simultaneously using the same transmission settings.

## Plan of document

The thesis is organized as follows:

- In Chapter 1, we describe some key features of LoRa technology and review the state-of-the-art LoRa scalability.
- In Chapter 2, we focus on designing a receiver for **downlink communication** in LoRa-like networks inspired by Non Orthogonal Multiple Access (NOMA) techniques:
  - We applied a superposition transmission scheme for LoRa-like Networks, which does not require Serial Interference Cancellation (SIC);
  - We proposed two different Power Allocation (PA) schemes to minimize error probabilities and increase fairness between users who have good or bad channels.
- Chapter 3 focuses on designing receivers for **uplink communication** in LoRa-like networks, which can cope with interference coming from other LoRa users.
  - We implemented a SIC technique to decode multiple signals in the uplink LoRa-like Networks;
  - We consider Co-Spreading Factor interference users;
  - Two deep learning-based receivers are modeled for single-user detection:

based on deep feedforward neural network and a convolutional neural network.

- Finally, the conclusion and future perspectives are drawn.

## Publications

This section summarizes the publications, conferences, and collaborations based on work that I have done during my Ph.D. candidature.

### Journal Papers

- **Angesom Ataklity Tesfay**, Eric Pierre Simon, Ido Nevat and Laurent Clavier, "Power Domain NOMA Without SIC in downlink CSS-Based LoRa Networks," In *Distributed Computer and Communication Networks. DCCN 2020. Lecture Notes in Computer Science*, vol 12563. Springer, Cham.
- **Angesom Ataklity Tesfay**, Eric Pierre Simon, Ido Nevat and Laurent Clavier, "Multiuser Detection for Downlink Communication in LoRa- Like Networks," In *IEEE Access*, vol. 8, pp. 199001-199015, 2020.

### International conference papers

- **Angesom Ataklity Tesfay**, Eric Pierre Simon, Sofiane Kharbech and Laurent Clavier, "Deep Learning-Based Signal Detection for Uplink in LoRa-Like Networks," In *2021 IEEE 32nd Annual International Symposium on Personal, Indoor and Mobile Radio Communications*, pp. 1-6, 2021.
- **Angesom Ataklity Tesfay**, Eric Pierre Simon, Guillaume Ferré and Laurent Clavier, "Serial Interference Cancellation for Improving Uplink in LoRa-like Networks," In *2020 IEEE 31st Annual International Symposium on Personal, Indoor and Mobile Radio Communications*, pp. 1-6, 2020.
- **Angesom Ataklity Tesfay**, Eric Pierre Simon, and Laurent Clavier, "Multi-user Detection to Improve Downlink Communication of CSS-based LoRa-like Networks," In *23rd International Conference on Distributed Computer and Communication Networks (DCCN): Control, Computation, Communications*, 2020.



# Chapter 1

## Introduction

### Contents

---

<b>1.1</b>	<b>Introduction</b>	<b>6</b>
<b>1.2</b>	<b>LoRaWAN</b>	<b>6</b>
<b>1.3</b>	<b>LoRa PHY</b>	<b>9</b>
<b>1.4</b>	<b>State of the Art: Scalability</b>	<b>12</b>
1.4.1	Physical Layer	12
1.4.2	MAC Layer	15

---

## 1.1 Introduction

The IoT is growing rapidly and is expected to connect more than 20 billion devices in the next 5 years [4–6], including more than 2 billion devices connected via LPWAN [7]. IoT provides connections between different devices used for different applications, such as smart metering [8,9], parking space monitoring [10,11], building monitoring [12], and smart agriculture [13,14]. These applications require low-power operation (devices are battery-powered), and a wide range of communications (devices are scattered in a large area) [15]. For these applications, wireless networks are necessary to cover a large area of farms, cities, or buildings [16]. Ordinary wireless technologies (such as ZigBee, Bluetooth, and Wi-Fi) used for this purpose can range up to several meters, and a multi-hop communication in a mesh network topology can be implemented to increase the coverage [17]. In recent years, LPWAN provides a good solution for the requirements of IoT applications [18,19] and LoRa is one of the protocols that can enable such methods. LoRa employs a Chirp Spread Spectrum (CSS) Modulation technique to encode information [20,21]. Several Spreading Factor (SF) and bandwidth settings enable quasi-orthogonal transmissions for LoRa end-devices [22,23]. However, when two or more end devices transmit simultaneously on the same band and with the same SF, a collision occurs at the receiver. This collision generally results in the loss of all colliding packets but sometimes the first arrived signal might be fully decoded due to a capture effect. Capture effect is a phenomenon associated with FM reception in which only the stronger of two signals at, or near, the same frequency or channel will be demodulated [24]. Therefore, there are still challenges to provide robust and reliable communication links, while there is a huge increase in communication devices. The organization of the rest of this chapter is as follows: sections 1.2 and 1.3 present the description of LoRaWAN and LoRa, which define the MAC layer and the PHY layer, respectively. Section 1.4 reviews the state-of-the-art on LoRa network scalability.

## 1.2 LoRaWAN

LoRaWAN is an open standard defining a MAC protocol [20] proposed for LoRa and provides the ability to control SF and Bandwidth (B). This also allows nodes to transmit with the possible highest rate in bi-directional transmission. A LoRa network is typically based on end devices (sensors, actuators, or both), gateways, and a network server. The architecture of the LoRaWAN network follows a star-

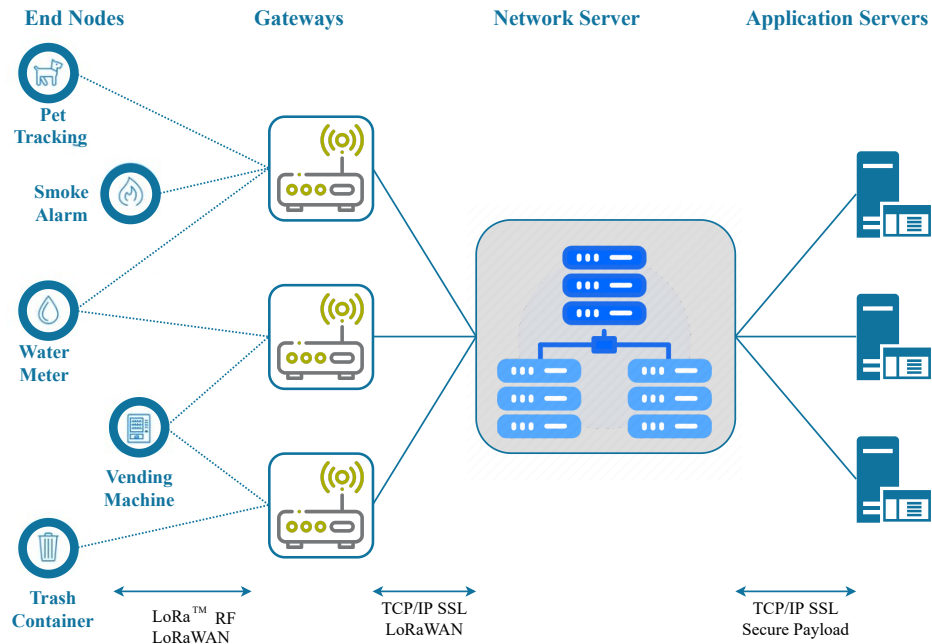


Figure 1.1: LoRaWAN Network Architecture.

of-stars topology in which gateways are used to relay messages between end-devices and a central network server, as represented in Fig. 1.1. By exploiting the long-range characteristics of the LoRa physical layer, the end devices are connected to one or several gateways through a single-hop LoRa wireless link. The gateways are connected to the network server through a standard IP-based network and provide the bridging from end devices to the IP world [25–28].

The capabilities of LoRa nodes differ depending on the node class (A, B, or C) with different specifications [25, 29]:

- Class A devices are of the lowest cost and energy-consuming nodes. They initiate the communication with a pure ALOHA [30, 31] medium access. uplink transmission is followed by two short downlink windows to receive a response from the gateway. downlink transmission is only allowed after a successful uplink transmission is decoded by the gateway. This is because the first downlink window’s data rate is considered a function of the uplink data rate and the receive window offset. Thus, if the downlink traffic is received in the first window, the second is disabled, see Fig. 1.2a.

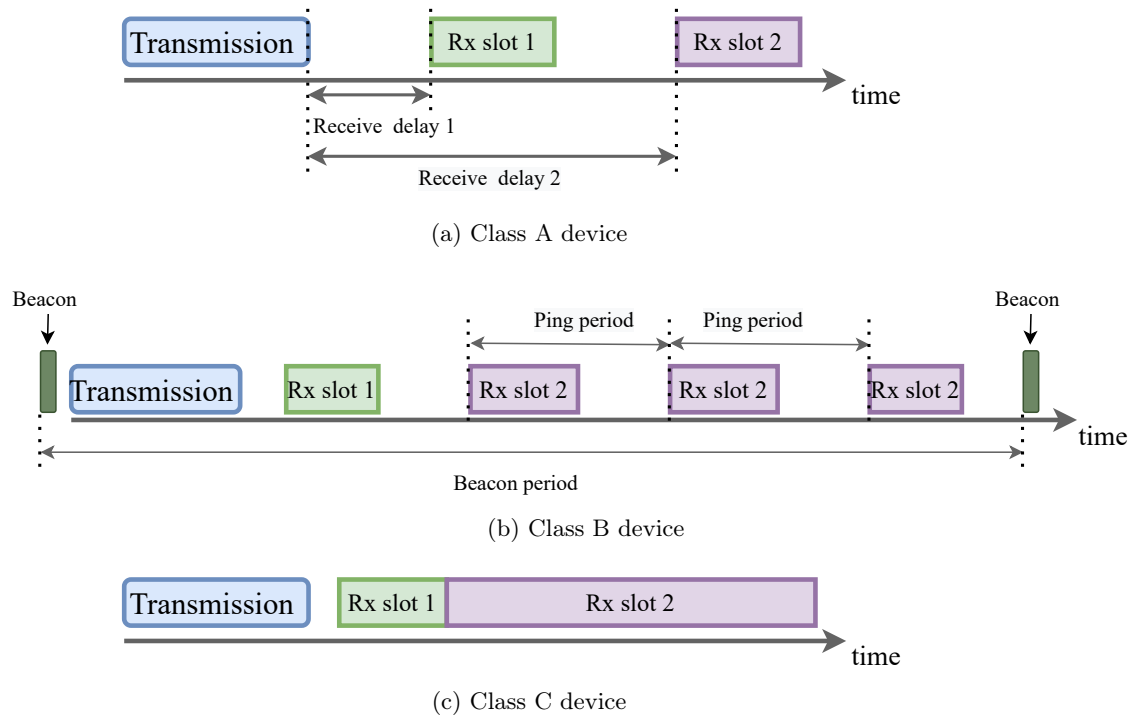


Figure 1.2: LoRaWAN devices classes.

- Class B devices allow additional downlink windows. They are synchronized using periodic beacons sent by the gateway to open an additional receive window regardless of prior successful uplink transmissions. Thus, these devices are preferred for applications that have more downlink traffic. However, this is achieved at the expense of some additional power consumption in the end nodes, see Fig. 1.2b.
- Class C devices are always listening and, consequently, can receive packets at any time. In this class, there is more power consumption as compared with other classes. Therefore, they usually require a permanent power source, see Fig. 1.2c.

LoRaWAN provides a maximum frame size of 256 bytes, and it has a preamble, header, and payload fields, as illustrated in Fig. 1.3. The preamble field contains a sequence of constant up chirps which enables the detection of the beginning of a packet, two down chirps, and a quarter of up chirp, which represents a gap used to allow the receiver to adjust the time [20] (see Fig. 1.4).

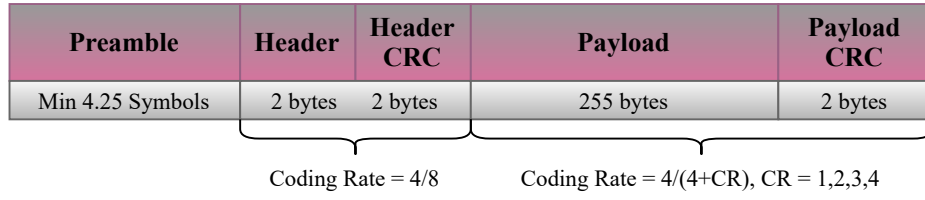


Figure 1.3: LoRa PHY frame format.

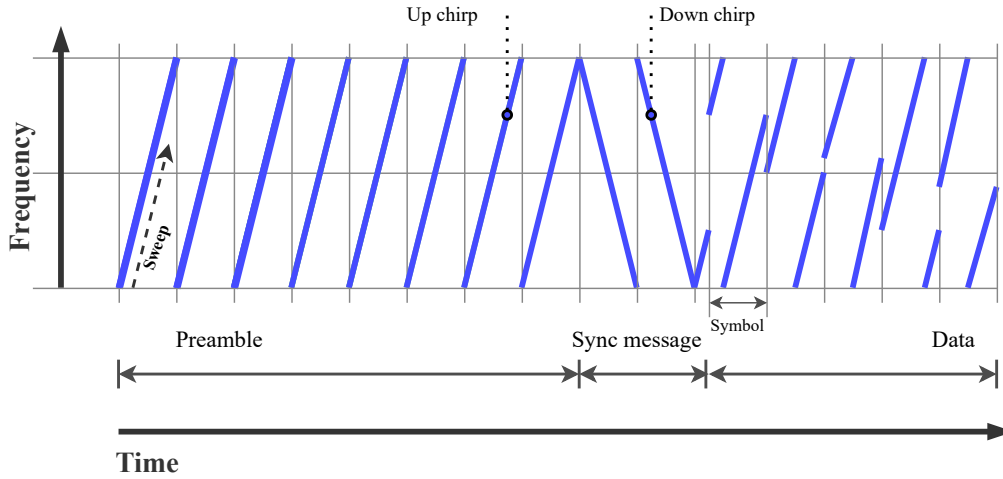


Figure 1.4: Spectrum plot of a LoRa packet.

The header field (existing only in explicit header mode) specifies the payload length, Forward Error Correction (FEC), Code Rate (CR), and Cyclic Redundancy Check (CRC). The integrity of the header is protected by the header CRC field, which is also included in the header. The actual data is contained in the payload field, and for error correction in the payload, an optional CRC field can be used [25]. The LoRa packet time on-air can be computed as:

$$T_A = (n_{Preamble} + n_{Payload} + 4.25) \times T_s \quad (1.1)$$

where  $n_{Preamble}$  and  $n_{Payload}$  are the numbers of programmed preamble symbols and the number of payload symbols, respectively. The constant value 4.25 represents the minimum length of the fixed part of the preamble.

### 1.3 LoRa PHY

LoRa physical layer has been patented by Semtech [20]. LoRa is implemented based on the CSS modulation [21] scheme and each LoRa chirp consists of a linear fre-

quency change over the symbol duration ( $T_s$ ). CSS is one of the spread-spectrum approaches which employs broadband frequency modulated chirp pulses (sinusoidal pulses with varying frequency) to carry information hence improving the robustness against Doppler effect, interference, and multipath. Transmissions are identified by the duration  $T_s$  of the coded chirp, which depends on the SF used, i.e., longer chirps correspond to higher SF value and shorter chirps to lower SF value. Higher SF can increase robustness to natural interference and noise but also decreases available bandwidth for data. LoRa signal model is an  $M$ -ary digital modulation based on frequency shift chirp spread spectrum. The  $M$  possible waveforms are chirps modulated over the bandwidth  $B$  with  $M$  different initial frequencies. A modulating symbol carries  $\text{SF} = \log_2(M)$  bits, with SF ranging from 7 to 12, (SF = 6 also exists but corresponds in fact to a very different modulation scheme and smaller SF also exists in the 2.4 GHz band). The orthogonal nature of these SFs enables simultaneous and collision-free communication in the network. The symbol duration is  $T_s = MT$ , where  $T = 1/B$  is the sampling period. Each modulated chirp is based on a raw chirp, whose instantaneous frequency is given by  $f(t) = \frac{B}{T_s}t$ . Recall that the instantaneous phase ( $\vartheta(t)$ :  $f(t) = \frac{1}{2\pi} \frac{d\vartheta(t)}{dt}$ ) is the integral of  $f(t)$ , which yields the following baseband expression for the raw chirp:

$$c(t) = \exp\left(2j\pi \frac{B}{2T_s}t^2\right), \quad t \in \left[-\frac{T_s}{2}, \frac{T_s}{2}\right]. \quad (1.2)$$

The transmitted modulating symbol of the  $i$ th user at time  $qT_s$ ,  $q = 0, \dots, Q - 1$ , with  $Q$  the number of symbols transmitted in a packet, is denoted by  $m_q^{(i)} \in \{0, \dots, M - 1\}$ . The corresponding modulated chirp is obtained by left-shifting the raw chirp of  $\tau_q^{(i)} = m_q^{(i)}T$  in the time domain, yielding a shift of  $\frac{m_q^{(i)}}{T_s}$  in the frequency domain (see Fig. 1.5). The coded chirp  $x_q^{(i)}(t)$  is expressed as:

$$x_p^{(i)}(t) = \begin{cases} \exp\left(2j\pi \left[\frac{B}{2T_s}t^2 + \frac{m_q^{(i)}}{T_s}t\right]\right), & t \in \left[-\frac{T_s}{2}, \frac{T_s}{2} - \tau_q^{(i)}\right), \\ \exp\left(2j\pi \left[\frac{B}{2T_s}t^2 + \left(\frac{m_q^{(i)}}{T_s} - B\right)t\right]\right), & t \in \left[\frac{T_s}{2} - \tau_q^{(i)}, \frac{T_s}{2}\right]. \end{cases} \quad (1.3)$$

Finally, the complex envelope of the transmitted signal of user  $i$ ,  $s^{(i)}(t)$  is given by:

$$x^{(i)}(t) = \sum_{q=0}^{Q-1} x_q^{(i)}(t - qT_s). \quad (1.4)$$

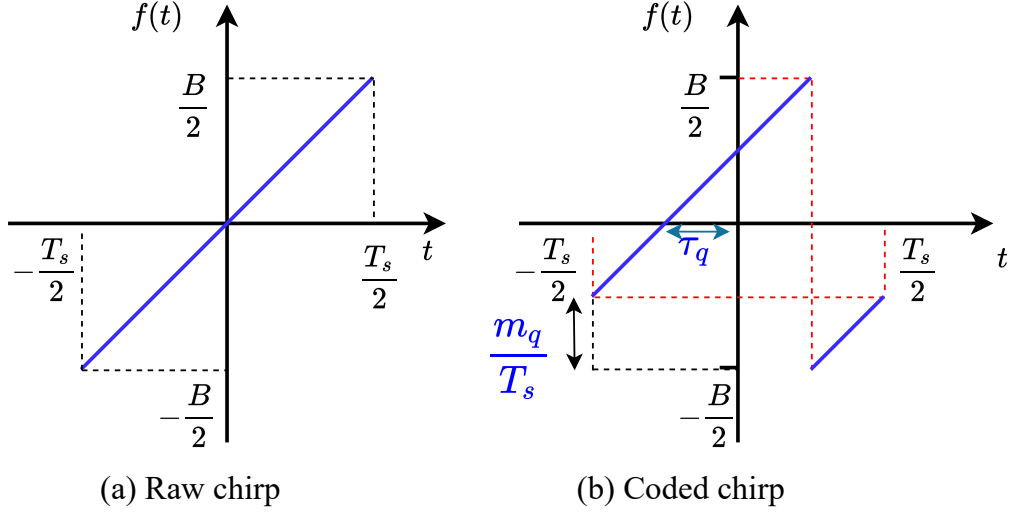


Figure 1.5: Raw up-chirp and Coded chirp associated with  $m_q^{(i)}$ .

The transmitted LoRa packet is then obtained by adding the preamble consisting of a sequence of raw chirps. The sampled received signal is multiplied by the conjugate form of the raw chirp used on the transmitter side to detect the transmitted symbols. Taking the Fast Fourier transform (FFT) of the de-chirped signal, each stream after the demodulation, the symbols can be determined by obtaining the maximum or strongest component of each FFT.

To improve the robustness against noise and interference, LoRa applies an interleaving and FEC code with a coding rate of  $4/(CR + 4)$ , where the CR value is between 1 and 4. The symbol rate  $R_s$  and data rate  $R_b$  can be computed by:

$$R_s = \frac{B}{M} \quad (1.5)$$

$$R_b = SF \frac{4}{\frac{CR+4}{M} \frac{M}{B}} \quad (1.6)$$

It can be seen from equation (1.5) that increasing the SF increases the symbol time and decreases the symbol rate. From equation (1.6), it can be noted that the data rate decreases as the SF increasing.

## 1.4 State of the Art: Scalability

### 1.4.1 Physical Layer

Few works have been done at the PHY layer in the literature, but open issues remain, and scalability is among the main issues. This section reviews the scalability of LoRa networks and some proposed PHY layer techniques to address this problem.

LoRa is claimed to be robust to inter-SF interference due to different orthogonal SFs. However, authors in [32] have shown that a LoRa network cell cannot be considered as a simple composition of independent networks operating on different channels because of the imperfect orthogonality between different SFs. Specifically, they showed that if the received power of the interference is strong, the collision between packets with different SFs can be destructive and hence limits the scalability. The work in [33] presented the theoretical analysis of the achievable LoRa throughput in the uplink, where capture conditions such as signal-to-Noise Ratio (SNR) reception level, Signal-to-Interference-plus-Noise Ratio (SINR) level for co-SF and inter-SF captures are included. Their results showed a significant impact of SF imperfect orthogonality and the effects of different SF allocation based on the end-devices distance from the gateway on the system performance. In [34] LoRaWAN scalability study is introduced. The authors developed a numerical model of the transmission process to evaluate the scalability of LoRaWAN. They inferred that the network limit is just 0.151 byte payload for every second. This limit relates to 5000 devices, each communicating two messages every day.

The effect of interference on a LoRa network brought by concurrent transmissions utilizing a similar SF and various SFs is analyzed in [35]. The interference field is modeled as Poisson point process with duty-cycled ALOHA, and the distributions of signal to interference ratio are derived by considering different interference scenarios. The authors showed in their results that in the LoRa network, the number of end devices that can transmit successfully is limited due to the combined impact of the co-SF and inter-SF interference.

In LoRa, the single-hop star topology has a great advantage in terms of low power consumption; however, it is a bottleneck to realize a LoRa network that is efficient, scalable, and with high coverage ability. Evaluation of multi-hop LoRa receiver performance under concurrent transmission with all SFs is discussed in [36]. The authors demonstrated that with adequate power offset, the concurrent transmission-based multi-hop LoRa showed good performance in the presence of packet collision

under the same SFs. The work in [37] introduced the performance of the LoRaWAN network in an urban environment where the unconfirmed mode was implemented. The authors present the SF allocation to every device depending on the sensitivity of the gateway by analyzing the power signal at the gateway. Accordingly, both the probability of collisions and time on-air (ToA) were reduced. The gateway configuration is based on 8 receiving paths with 3 channels, and these paths are reserved for the uplink traffic. However, the downlink traffic is not considered. The effect of the same SF interfering signal on the decoding performance of the useful signal has studied in [38,39]. The authors introduced the hypothetical models of the interference. However, the study is performed to the detriment of the interfering signal whose data is lost, and no solution has proposed any technique to deal with the interference problem.

Authors in [40] implemented simulators to assess the effect of intra and inter SF interference on LoRaWAN performance. The authors demonstrated that the SFs are not completely orthogonal; as a result, a collision can occur, and it can be very destructive if the Signal-to-Interference Ratio (SIR) is lower than a given threshold value for each SF. In addition, for co-SF collisions, the useful signal can be successfully decoded by applying a capture effect only if the received power of the useful signal is 6 dB higher than the total power of interfering signals. In [41], the authors presented a technique to detect a signal of the desired transmission in the presence of an interfering signal with received power 6 dB larger than the desired. They considered several cases where a receiver has a candidate list of expected signals.

Mainly in the uplink, the capture effect is analyzed in [42,43] and gives a general idea of differentiating users based on their received power. The authors in [44] proposed to decode two desynchronized LoRa-like signals, received concurrently in the same channel, with the same SF. The approach is based on estimating the time shift between the two received signals, but the decoding works only if the signal that has the highest power is received first. In [45] a different approach is also proposed that decodes superposed LoRa signals using the chirps timing information. However, the approach requires receivers to be perfectly synchronized or slightly desynchronized and only dealt with the uplink case, which is not practical in ALOHA-based LoRa networks.

Those ideas have been further developed and extended using a SIC scheme to decode signals from multiple users in the uplink [42,46]. However, the first one considers that all transmitting nodes are perfectly synchronized, which is not the case in the

uplink communication, whereas the second only considers not more than 4 users. To increase the scalability, in [47], we proposed a SIC receiver that allows recovering multiple signals transmitted in the same time slot (but not necessarily synchronized) and with the same SF. A complete receiver structure, with detection of packets, channel estimation, detection of symbols, and interference cancellation, is proposed and shown to support 20 times more nodes than the classic LoRa receiver. This leads to a significant increase in the possible number of devices connected to the network. Practical implementation issues remain, however, to be addressed.

To increase end-nodes density, the authors in [48] have proposed the use of multiple gateways and directional antennas, which reduces the number of end-nodes connected to a single antenna. In this work, the effect of interference between multiple LoRa networks is limited using directional antennas and multiple gateways.

The performance of uplink communication of a LoRa link in a multi-cell LoRa system is modeled and analyzed in [49]. Stochastic geometry and geometric probability are used to model the spatial distribution of LoRa devices. The effects of the massive number of LoRa cells and the quasi-orthogonal spreading factors assignment on the success probability of the LoRa transmissions were represented by the model. LoRaWAN vulnerability to the inter-network interferences is studied in [50]. The authors determined the impact of LoRaWAN data rates of the transmitter and the interference source on the probability of successfully transmitting data packets when operating in the EU 868 MHz frequency band. The results show that, in fact, transmissions with different data rates in the same channel will have an impact on the transmitted signals, and high data rates are more severely affected by interference than low data rates.

The deployment of Interleaved Chirp Spreading (ICS) LoRa to create a new overlapping logical network that co-exists with the classical LoRa network is studied in [51]. The author particularly focuses on the study of the inter-network interference between the classical LoRa and the Interleaved Chirp Spreading LoRa logic network under different SIR as well as different SNR. The simulation results show that ICS-LoRa interference has a slight impact on the Bit-error Rate (BER) performance of the classical LoRa decoding, and vice versa. In addition, it has been proven that better cross-correlation characteristics provide a better opportunity to eliminate inter-network interference signals successfully. The authors in [52] discussed the co-existence of LoRaWAN networks in the same frequency band, as well as existing applications of the short-range devices, which cover everything from door openers to

traditional home automation technologies of different types of equipment.

### 1.4.2 MAC Layer

Most of the LoRaWAN scalability researches have mainly focused on the MAC layer considering the uplink communication, and some are discussed in this section. Challenges of radio channel access and LoRa network scalability are discussed in [43]. Real-world deployments of IoT networks and LoRaWAN experimental analyses have been conducted. The impact of an adaptive data rate is illustrated, and the impact of duty cycle restrictions on the LoRa network. Scalability limits of LoRaWAN have been studied in [53–55]. It is limited because of the regulatory constraints on the channel and the use of random channel access rather than because of LoRa technical limitations.

In [55], it is shown that the network can support only up to 120 nodes with a data extraction rate over 0.9 and using a single gateway, an SF of 12, a bandwidth of 125 kHz, and forward error correction with Code Rate 4/5. The authors proposed a dynamic channel parameter setting (transmission power, SF, bandwidth, and code rate) with multiple gateways. They showed a possible increase by one order of magnitude of the number of users.

The solutions proposed in the previously mentioned papers concentrate solely on the uplink direction. However, it has been shown [56] that the duty cycle restricts both the scalability and the network's reliability. However, only a few works tackle this important aspect of scalability issues of LoRa downlink traffic to date. The authors in [57] present and evaluate gateway selection solutions to improve the performance of LoRaWAN downlink communications in terms of throughput. They consider gateway selection algorithms based on load balancing and received signal strength indicators with different deployment scenarios. The authors conclude that balancing the load per gateway improves the performance. However, the downlink benefits from a crucial advantage: the transmission to all users originates in the access point allowing accurate synchronization of signals. The authors in [58–60], evaluated the effect of downlink traffic on the performance of LoRaWAN. They have shown that the uplink traffic is extremely impacted when the number of downlink feedback frames rises. They identified the duty cycle as the main limiting factor in the scalability problem. In these papers, no solution is proposed to improve the situation. Van et al. [61] analyze the downlink frame issue using the ns-3 network simulator. The authors illustrate the main reasons behind the gateways congestion by emphasizing

the duty cycle limitation and the half-duplex problem. They also propose a multi-gateway system and assess the improvements based on lower duty cycle saturation and load balancing among the gateways. However, there is no explanation of how the load balancing is performed.

The authors in [62] presented a spreading factor allocation algorithm for a large-scale LoRa network based on K-means clustering. They illustrate the impact of the number of nodes in each spreading factor and their distance from the gateway on the network performance. The algorithm works by defining a number of nodes and range boundaries for each spreading factor. Farhad et al. in [63] investigated LoRa network scalability under a dense urban environment for confirmed and unconfirmed transmission modes. Their result indicated that the distribution of the spreading factor is highly affected by the dense urban environment. The scalability of the network is limited by the use of acknowledgment in the downlink. Moreover, they show that the network's performance can be improved by increasing the antenna height in a dense urban area. A comprehensive analysis of the effects of downlink traffic on LoRaWAN capacity was provided in a recent paper [64]. The authors describe how the gateway's half-duplex mode and the sequential transmission lead to the duty cycle saturation for downlink traffic. They also propose a multi-gateway deployment, parallel transmission of downlink frames on the same channel but with different orthogonal SF, and load balancing among the deployed multiple gateways. However, deploying multiple gateways can cost, and implementing the gateway selection algorithm to balance the load can bring another level of complexity to the system.

To improve the reliability and scalability of LoRaWAN, a new method, RS-LoRa MAC protocol, is proposed in [65]. RS-LoRa operates in two significant steps; in the initial step, the gateway schedules the devices inside its reach by estimating the Received Signal Strength Indicator (RSSI) and SF for each channel. In the second step, every device chooses its transmission setting, such as; transmission power, SF, and channel depending on the scheduling data of the gateway. The authors showed that the proposed scheduling approach decreases the impact of a collision by cautiously choosing an SF to improve the network quality, scalability, and capture effect.

In [66] an SF allocation technique for massive LoRaWAN networks is proposed. This technique targets to improve the success rate by analyzing the interference between similar SFs and channels. The interference brought by the collision of two

packets is recognized by fixing the collision time between the packets of similar SFs over a similar channel. The SIR and received power are determined at that point. After comparing it with a threshold, the interference will not affect the packets if it surpasses the threshold. If that is not the case, the packets are lost because of interference.

Most of the proposed schemes in the previously mentioned papers mainly focus on uplink communication, and few works are proposed to tackle the scalability issue from the MAC layer perspective. However, we are interested in alleviating the issues related to scalability from the PHY layer point of view. Therefore in [67], we proposed a Non-Orthogonal Multiple Access (NOMA) based new joint multiuser detection technique for downlink traffic in LoRa networks. We proposed transmitting multiple frames simultaneously, with the same SF, and on the same frequency band. On the receiver side, the devices are differentiated by the allocated power on their dedicated frame. It was demonstrated that the proposed joint multiuser detector increases the number of connected devices at least by 10 and maintains the symbol error rate below  $10^{-3}$  without implementing error-correcting codes.

The next chapter studies the downlink transmission in the LoRa-like networks. It addresses issues related to the duty cycle by proposing a solution to enhance the scalability of the networks.



## Chapter 2

# Downlink Communication in LoRa-like Networks

### Contents

---

<b>2.1</b>	<b>Introduction</b>	<b>21</b>
<b>2.2</b>	<b>System Model</b>	<b>22</b>
<b>2.3</b>	<b>Proposed Signal Detection Scheme</b>	<b>23</b>
2.3.1	Transmitted signal	24
2.3.1.1	Power considerations	24
2.3.1.2	Channel Model	25
2.3.2	Receiver Design	25
2.3.2.1	Cross-Entropy Multiuser Detector	27
2.3.2.2	Proposed Low-Complexity Detector	30
2.3.2.3	Direct Peak Detection	35
2.3.3	Power allocation scheme	36
2.3.3.1	Power Allocation 1: Suppressing ambiguities	36
2.3.3.2	Power Allocation 2: Fair Spacing	36
<b>2.4</b>	<b>Results</b>	<b>37</b>
2.4.1	Simulation setup	37
2.4.2	Performance of the three receivers	38
2.4.3	Power allocation performance	40
2.4.4	Fairness	40
2.4.5	Computational Complexity Analysis	44

2.4.5.1	Direct peak detection . . . . .	44
2.4.5.2	Cross Entropy Method . . . . .	45
2.4.5.3	Proposed Method . . . . .	45
2.4.5.4	Comparison . . . . .	46
2.4.6	SF Orthogonality . . . . .	46
<b>Conclusion</b>	. . . . .	<b>49</b>

---

*In this chapter, we present the proposed receiver for downlink communication in LoRa-like networks inspired by Non-Orthogonal Multiple Access (NOMA) techniques. The proposed receiver improves the scalability of the network by increasing the number of devices that can be addressed at least by one order of magnitude. While the approach differentiates the devices by the power allocated to them, it differs from the vast majority of previous works on power-domain NOMA because it does not require interference cancellation. Instead, it benefits from the spectrum spreading of the modulation scheme (chirp spread spectrum) where, at the end of the decoding phase, the information carried by a symbol is found in the position of a peak in the Fourier domain.*

## 2.1 Introduction

Compared to the uplink, the downlink benefits from a crucial advantage: the transmission to all users originates from the same access point, allowing accurate synchronization of signals and power allocation. Leveraging on this, we propose a power-domain NOMA scheme [68] that limits the impact of the duty cycle, half-duplex mode, and sequential transmission of a LoRa network. Besides, the complexity at the receiver level must remain low, prohibiting the implementation of many advanced methods. Therefore, applying Serial Interference Cancellation (SIC) significantly limits the possible number of simultaneous transmissions in practical systems in the downlink. Taking benefit from the CSS modulation, the main novelty in our work is to propose a power domain NOMA scheme without the need of a SIC receiver. In addition to reducing the complexity, it also avoids the residual error resulting from signal cancellation, which means a significantly easier and less limited scheme to be implemented in real systems.

The main contributions of this chapter can be summarized as follows:

1. We propose a superposition transmission scheme for synchronized (downlink) CSS modulation, which does not require SIC.
2. We derive the Maximum Likelihood (ML) optimal Multi User Detector (MUD). Due to its high complexity, it cannot be implemented in practice, and we, therefore, develop an approximation via the Cross Entropy Method (CEM). Still too complex for end devices, this receiver serves us as a reference.
3. We develop a suboptimal detection scheme that significantly reduces the com-

putation time compared with the CEM, specifically designed for low-cost devices. This scheme does not require interference cancellation. It benefits from the collision avoidance inherent in CSS. This is a significant advantage of the method since it avoids the limitations due to the propagation of residual errors after each cancellation. Preamble detection and channel estimation scheme are included in our simulation results.

4. We propose Power Allocation (PA) schemes to minimize error probabilities and increase fairness between users having good or bad channels.

Our scheme is very different from traditional NOMA, both for the decoding approach and the PA scheme. Indeed, the information in the decoded signal is carried by a frequency, i.e., a peak in the Fourier domain. Most of the time, users carry different information so that their peaks fall at different positions, avoiding each other, and the interference does not accumulate. The scheme is more similar to time or frequency hopping than to superposition coding or Direct Sequence Code Division Multiple Access (CDMA) and does not require a specific code. As far as we know, this is the first time such a NOMA scheme is proposed. A few papers have studied downlink NOMA without SIC. In [69], a Pulse-Amplitude modulation is studied and the Gray labeling without SIC very close to a system using SIC. In [70], a downlink NOMA technique without SIC is proposed using an algebraic lattice to design modulations that guarantee all users achieve full diversity gain. These approaches, although not relying on SIC, use a superposition coding scheme and try to maximize capacity or diversity gain. Besides, they are limited in the number of users and only consider two. On the contrary, the CSS that is used in LoRa is not maximizing the transmission rate, but our proposal can handle many more users. The avoidance rather than superposition approach avoids the cancellation residue that significantly limits the possible simultaneous transmissions. We keep our analysis at the PHY layer level, although characterizing in terms of good-put and latency could also certainly highlight the benefits of our method. However, it would be necessary to include channel coding schemes, protocol solutions, and re-transmission strategies beyond this thesis's scope.

## 2.2 System Model

As mentioned in section 1.2, the downlink capabilities of LoRa devices differ depending on the node class (A, B, or C) [25]. For battery-operated class A or B devices

and with an expected lifetime of several years, the downlink is very limited in terms of the quantity of information transmitted because a very limited number of slots are available. However, this is not the only limitation. LoRa operates in the license-free Industrial, Scientific and Medical (ISM) radio band, and consequently, suffers severe limitations concerning channel access. Because the devices do not listen to the channel before transmitting, the devices must adhere to the duty cycle regulation imposed by the regulatory bodies, such as the European Telecommunications Standards Institute (ETSI) [71]. This restriction limits a transmitting device when it can occupy the channel, for instance, 1% in Europe (868 – 868.6 MHz band). This duty cycle is significant for the downlink transmission. The gateway is extremely affected since it cannot send downlink frames to all of the devices after receiving multiple uplink frames. This constraint limits the capacity of downlink transmission in terms of the maximum traffic supported and, consequently, impacts the scalability of LoRaWAN networks.

Recall from section 1.3, the transmitted chirp of user  $i$  at time  $qT_s$ ,  $q \in \{0, \dots, Q-1\}$ , where  $Q$  is the number of symbols transmitted in a packet, is generated by applying left-shifting of the raw up-chirp by  $\tau_q^{(i)} = m_q^{(i)}T$ . The transmitted data symbol is represented by  $m_q^{(i)} \in \{0, \dots, 2^{SF} - 1\}$ . The coded chirp of user  $i$  associated with the  $q$ th symbol is:

$$x_q^{(i)}(t) = \begin{cases} \exp\left(2i\pi\left[\frac{B}{2T_s}t^2 + \frac{m_q^{(i)}}{T_s}t\right]\right), & t \in \left[-\frac{T_s}{2}, \frac{T_s}{2} - \tau_q^{(i)}\right), \\ \exp\left(2i\pi\left[\frac{B}{2T_s}t^2 + \left(\frac{m_q^{(i)}}{T_s} - B\right)t\right]\right), & t \in \left[\frac{T_s}{2} - \tau_q^{(i)}, \frac{T_s}{2}\right]. \end{cases} \quad (2.1)$$

Finally, the complex envelope of the transmitted signal of the  $i$ th user is:

$$x^{(i)}(t) = \sum_{q=0}^{Q-1} x_q^{(i)}(t - qT_s). \quad (2.2)$$

## 2.3 Proposed Signal Detection Scheme

In this section, we present the proposed scheme. We first present the transmitter design and the wireless channel model. We then present our method for the receiver, starting from the optimal detector formulation via the Maximum Likelihood Detector (MLD), which we show has a combinatorial complexity. To overcome this limitation, we propose an algorithm that approximates the MLD with a much lower complexity based on the CEM [72]. To further reduce the computational complexity, we propose a low-complexity multiuser detector that only searches for the closest peak to the

expected one. It is to be noted that the CEM-based and the low-complexity detectors will be used as references for comparison. We did not find any competitive method in the literature or theoretical bounds for a method equivalent to our NOMA proposal. The only one which would be relevant would be a pure ALOHA scheme or a perfect Time Division Multiple Access (TDMA) approach. Even if it is impractical in real networks, this latter approach will also be used as a comparison, but our scheme significantly outperforms both. In addition to that, we propose two PA schemes. The first one avoids ambiguities when two users transmit the same information at the same time. The second one distributes the powers to ensure a constant distance between the power of the selected peak and that of the nearest lower peak to improve equity.

### 2.3.1 Transmitted signal

To avoid the limitation due to the duty cycle, we propose to transmit  $N$  frames simultaneously, with the same SF and on the same frequency band. It is possible with Class B devices that can be synchronized and in receive mode during the same time frame. The objective is then to design a communication strategy that allows us to superimpose  $N$  users in the duration of a single packet. The idea is to generate information streams for  $N$  end-devices, modulate them using the CSS scheme, then add all signals with different allocated powers to form a single packet. A preamble and a common header are added at the packet start. The information about the number of users and the PA scheme is added in the header. At the receiver side, the receivers select and decode the signal which corresponds to their allocated power. The combined transmitted signal is:

$$x(t) = \sum_{i=1}^N \sqrt{p^{(i)}} x^{(i)}(t), \quad (2.3)$$

where  $p^{(i)}$  is the power allocated to user  $i$ .

#### 2.3.1.1 Power considerations

The maximum transmission power in an ISM band is restricted. For LoRa (at 868 MHz), in Europe, this maximum is set to 14 dBm for uplink and 27 dBm for downlink. The noise level of a receiver at room temperature is:

$$N_0(\text{dBm}) = -174 + 10 \log_{10}(B) + \text{NF}, \quad (2.4)$$

where the first term is the thermal noise in 1 Hz of bandwidth and can only be affected by changing the receiver's temperature. NF is the receiver noise figure, which depends on the hardware implementation, and a typical 6 dB noise figure is considered [21]. If we consider  $B = 250$  kHz, the noise power density at the receiver is  $-114$  dBm.

### 2.3.1.2 Channel Model

We consider one cell of radius  $R$  with the gateway placed at the center. Many devices are uniformly distributed within the cell, and the gateway has to send information to  $N$  of them. The distance from end-device  $i$  to the gateway is denoted by  $d^{(i)}$ . The propagation channel is considered block and flat fading, so a single constant coefficient throughout the packet's duration. We consider path loss and Rayleigh multipath fading  $\chi_i$ . The signal amplitude decays with increasing distance according to  $d^{(i)-\eta/2}$ , where  $\eta$  is the path loss exponent. The channel attenuation (in amplitude) is expressed as  $h^{(i)} = d^{(i)-\eta/2} \cdot \chi^{(i)}$ .

In the following, the user we are trying to decode is denoted by  $j$ , and the signal it receives is:

$$r^{(j)}(t) = h^{(j)} \sum_{i=1}^N \sqrt{p^{(i)}} x^{(i)}(t) + w^{(j)}(t), \quad (2.5)$$

where  $w^{(j)}(t)$  is a complex Gaussian noise and  $h^{(j)}$  the channel between the access point and device  $j$ .

### 2.3.2 Receiver Design

The receiver acts in two steps: preamble detection and demodulation process.

First, the correlation between the received signal and the known preamble sequence is calculated to detect the packet and its start. This detection is easy because the preamble is common to all the users; hence the power dedicated to it is large. This step also allows us to estimate the user's channel from the maximum value of the correlation.

Second, we are interested in the decoding of symbol  $q$ . We sample the received signal and it is expressed as:

$$r_q^{(j)}[n] = r^{(j)}(nT + qMT), \quad (2.6)$$

where  $n$  is limited to the set  $\Omega = \{0, \dots, 2^{SF} - 1\}$ . Then we have:

$$r_q^{(j)}[n] = h^{(j)} \sum_{i=1}^N \sqrt{p^{(i)}} x_q^{(i)}[n] + w_q^{(j)}[n], \quad (2.7)$$

where  $w_q^{(j)}[n] \sim \mathcal{N}_{\mathbb{C}}(0, \sigma_n^2)$  is a complex Gaussian thermal noise (discussed in section 2.3.1.1) and  $x_q^{(i)}[n] = x_q^{(i)}(nT)$ .

The received samples  $r_q^{(j)}[n]$  are then multiplied by the complex conjugate form of the sampled up-chirp. The sampled up-chirp is defined for  $n \in \Omega$  and denoted by  $x[n] = x(nT)$ . The signal corresponding to the  $q$ th symbol after de-chirping is written as:

$$\begin{aligned} y_q^{(j)}[n] &= r_q^{(j)}[n] x^*[n], \\ &= h^{(j)} \sum_{i=1}^N \sqrt{p^{(i)}} e^{2i\pi \frac{m_q^{(i)}}{2^{SF}} n} + \tilde{w}_q^{(j)}[n]. \end{aligned} \quad (2.8)$$

To make a decision, we use the ML estimator. It is equivalent to work with  $r_q^{(j)}[n]$ ,  $y_q^{(j)}[n]$  or even in the Fourier domain. We did not get any tractable solution in the time domain so, after compensating for the channel gain multiplying  $y_q^{(j)}[n]$  by  $h^{(j)*}$  (the  $*$  denotes the complex conjugate -in the following formulations, we assume a perfect channel estimation but in the simulation part the estimated channel will be used), we perform a FFT, as the traditional LoRa receiver:

$$\begin{aligned} Z_q^{(j)}[k] &= \text{Re} \left\{ \sum_{n=0}^{2^{SF}-1} \left( h^{(j)*} y_q^{(j)}[n] \right) e^{-2i\pi \frac{nk}{2^{SF}}} \right\}, \\ &= |h^{(j)}|^2 \sum_{i=1}^N \sqrt{p^{(i)}} \delta[k - m_q^{(i)}] + W_q^{(j)}[k]. \end{aligned} \quad (2.9)$$

where  $W_q^{(j)}[k] \sim \mathcal{N}_{\mathbb{C}}(0, |h^{(j)*}|^2 \sigma_n^2 / 2)$  is the FFT of the noise,  $\delta[\cdot]$  is Kronecker delta function,  $\delta[n] = 1$  for  $n = 0$  and  $\delta[n] = 0$  for  $n \neq 0$ . We observe that the obtained vector presents peaks at the positions corresponding to the source symbols ( $\delta[k - m_q^{(i)}]$ ).

The basic LoRa detector searches for the strongest peak to decode a single user. This observation will be used in the receiver architectures we propose.

Based on (2.9), we note:

$$\mathbf{Z}_q^{(j)} = |h^{(j)}|^2 \mathbf{X}_q^{(j)} + \mathbf{W}_q^{(j)}, \quad (2.10)$$

which is the  $2^{SF}$ -dimensional received vector after FFT. We want to implement a multiuser detection scheme. To do so, we express the log likelihood function.  $\mathbf{m}_q = \{m_q^{(1)}, \dots, m_q^{(N)}\}$  is the information vector and we assume an independent and identically distributed noise vector  $\mathbf{W}_q^{(j)}$ :

$$\begin{aligned} \Lambda &= \log \mathbb{P} \left( \mathbf{Z}_q^{(j)} \mid h^{(j)}, \mathbf{m}_q \right), \\ &= \log \prod_{k=0}^{2^{SF}-1} \mathbb{P} \left( Z_q^{(j)}[k] \mid h^{(j)}, \mathbf{m}_q \right), \\ &= \sum_{k=0}^{2^{SF}-1} \log \mathbb{P} \left( |h^{(j)}|^2 X_q^{(j)}[k] + W^{(j)}[k] \mid h^{(j)}, \mathbf{m}_q \right). \end{aligned} \quad (2.11)$$

Because all operations are linear and given  $\mathbf{m}_q$ ,  $|h^{(j)}|^2 X_q^{(j)}[k] + W_q^{(j)}[k]$  is a Gaussian random variable with mean  $|h^{(j)}|^2 X_q^{(j)}[k]$ , variance  $\sigma_n^2$  and we have:

$$\begin{aligned} \hat{\mathbf{m}}_q &= \operatorname{argmax}_{\mathbf{m}_q \in \mathcal{Q}} \sum_{k=0}^{2^{SF}-1} \log \left( \frac{1}{\sqrt{\pi |h^{(j)}|^2 \sigma_n^2}} e^{-\frac{\left( Z_q^{(j)}[k] - |h^{(j)}|^2 X_q^{(j)}[k] \right)^2}{|h^{(j)}|^2 \sigma_n^2}} \right) \\ &= \operatorname{argmin}_{\mathbf{m}_q \in \mathcal{Q}} \|\mathbf{Z}_q^{(j)} - |h^{(j)}|^2 \mathbf{X}_q^{(j)}\|^2, \end{aligned} \quad (2.12)$$

where  $\mathcal{Q} := [0, \dots, 2^{SF} - 1]^N$  is the set of all possible symbols. As expected in the Gaussian independent noise case, maximizing the likelihood function  $\Lambda$  is equivalent to minimizing the Euclidean distance between the transmitted signal  $\mathbf{X}_q^{(j)}$ , and the received one  $\mathbf{Z}_q^{(j)}$ . However, this problem does not give an analytical expression for the solution. The difficulty is that  $m_q^{(i)}$  can take any integer value between 0 and  $2^{SF} - 1$ , meaning that with  $N$  users, the MLD is required to evaluate  $2^{N \cdot SF}$  possible source combinations, which is impractical.

One common approach to overcoming the combinatorial complexity is relaxing the problem by assuming that  $m$  has real-valued support. However, in our model, this relaxation would not simplify the solution due to the non-linear structure of the likelihood function, neither in time nor in frequency. We, therefore, develop an alternative solution that is based on a Monte Carlo sampling technique, known as the CEM [72].

### 2.3.2.1 Cross-Entropy Multiuser Detector

The CEM is a flexible Monte Carlo technique, which was originally developed for rare-event probability estimation, solving combinatorial, continuous, constrained, and noisy optimization problems [73].

The basic idea is to generate a set of candidate solutions ( $\mathbf{m}_q$  in our case consisting of  $N$  integers in  $\{0, \dots, 2^{SF} - 1\}$ ), select the best possible candidates, update the generating rule and iterate until convergence is obtained. One important step is the possible solution generation: what distribution for  $\mathbf{m}_q$  should be chosen? Let  $f_{\mathbf{m}}(\cdot)$  be the PMF of  $\mathbf{m}_q$ . The proposed cross-entropy algorithm is presented in algorithm 2.1.

Steps 1 to 3 define some parameters: the number of sequences we generate at each iteration, the number of sequences we keep to update the distribution, and a parameter that controls the convergence speed. Along with two parameters chosen for the initialization of the PMF of  $\mathbf{m}_q$ , these parameters are important and could be optimized because they represent a compromise between the complexity burden and the algorithm's accuracy. We chose parameters that ensure a good convergence rather than a reduced complexity to perform close to the true ML.

Steps 4 to 9 initialize the PMF of  $\mathbf{m}_q$ . All values are possible, but we give a slightly higher probability to the dominant peaks. This reduces the necessary number of iterations. An example is seen in Fig. 2.1, where the initial  $f_{\mathbf{m}}$  is represented. The same PMF is used for each user.

Step 10 starts the main loop. We set the end of iterations when for each user, the probability of a given value is at least 0.85. This probability is set empirically. From steps 11 to 17, we generate  $N_{seq}$  random sequences  $\tilde{\mathbf{m}}_q$  according to  $f_{\mathbf{m}}$  and the corresponding decoded vector  $\tilde{\mathbf{Z}}_q^{(j)}[k]$ . This requires the channel estimate  $\hat{h}^{(j)}$ . The distance with the true received sequence is also calculated. We chose  $N_{seq} = 2000$  to ensure enough variety in the generated sequences and a good convergence of the algorithm.

Steps 18 and 19 select the  $N_{keep}$  sequences leading to the closest received vectors from the truly received one. We chose  $N_{keep} = 100$ , also ensuring a good convergence of the algorithm. These sequences will be used in step 20 to update  $f_{\mathbf{m}}$  by reinforcing the weights on symbols that have been generated in the set of selected sequences. A parameter  $\delta P$  is needed for this purpose and is empirically set to 0.003, which has been shown to be a good compromise. A larger value increases the convergence speed but also the number of wrong decisions. The process is illustrated in Fig. 2.2 and Fig. 2.3, where we show the CEM values of  $f_{\mathbf{m}}$  per user after 15 and 30 iterations.

In practice, the CEM-MUD still incurs too high a computational complexity because it needs to generate many samples and keep generating for several rounds to converge

---

**Algorithm 2.1** CEM-MUD for downlink LoRa.

---

**Input:** Received vector  $\mathbf{Z}_q^{(j)}$ ,  $\hat{h}^{(j)}$ ,  $N$

**Output:** Decoded vector  $\mathbf{m}_q$

- 1:  $N_{seq} \leftarrow 2000$  (Number of generated sequences)
  - 2:  $N_{keep} \leftarrow 100$  (Number of selected sequences)
  - 3:  $\delta P \leftarrow 0.003$  (Update parameter)
  - 4:  $[p, l] \leftarrow$  find peak values and indices of  $\mathbf{Z}_q^{(j)}$
  - 5:  $u \leftarrow$  sort  $p$  in descending order
  - 6:  $pos \leftarrow l(u(1 : N))$  % Select the  $N$  strongest peaks
  - 7:  $f_{\mathbf{m}} \leftarrow N \times 2^{SF}$  matrix with all elements equal to 0.01
  - 8:  $f_{\mathbf{m}}(:, pos) \leftarrow 0.05$
  - 9:  $f_{\mathbf{m}} \leftarrow f_{\mathbf{m}} / \sum f_{\mathbf{m}}$  ( $\sum f_{\mathbf{m}}$  is the sum of all elements of  $f_{\mathbf{m}}$  to normalize and have a probability mass function.)
  - 10: **while** min of max of each line of  $f_{\mathbf{m}}$  less than 0.85 **do**
  - 11:   **for**  $idx = 1$  to  $N_{seq}$  **do**
  - 12:     Generate a vector  $\tilde{\mathbf{m}}_q$  according to  $f_{\mathbf{m}}$
  - 13:     Generate the source vector  $\tilde{\mathbf{X}}_q$  from  $\tilde{\mathbf{m}}_q$  and (2.2)
  - 14:      $\tilde{\mathbf{R}}_q^{(j)}[n] \leftarrow \hat{h}^{(j)} \tilde{\mathbf{X}}_q[n]$
  - 15:      $\tilde{\mathbf{Z}}_q^{(j)}[k] \leftarrow \text{Re}\{FFT(\hat{h}^{(l)*} \tilde{\mathbf{R}}_q^{(j)}[n])\}$
  - 16:      $d(idx) \leftarrow \|\mathbf{Z}_q^{(j)} - \tilde{\mathbf{Z}}_q^{(j)}[k]\|^2$
  - 17:   **end for**
  - 18:    $d \leftarrow$  sort  $d$  in ascending order
  - 19:   Keep  $N_{keep}$  sequences with the smallest  $d$
  - 20:   Update  $f_{\mathbf{m}}$  by adding  $\delta P$  at each position given by the selected sequences and normalizing.
  - 21: **end while**
  - 22: **return**  $\tilde{\mathbf{m}}_q$  corresponding to the smallest  $d$ .
-

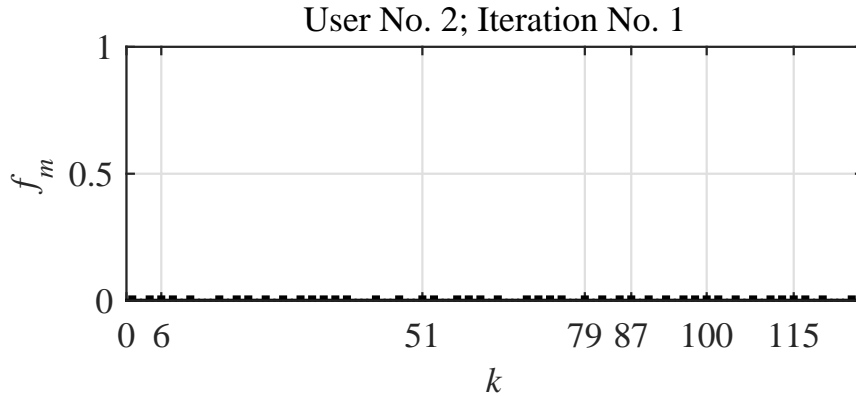


Figure 2.1: CEM-MUD as per Algorithm 2.1, with  $N = 8$  users and  $SF = 7$ . This figure represent  $f_{\mathbf{m}} = \mathbb{P}(m = k)$  at the beginning of the first iteration. Only one user is represented because the PMF  $f_{\mathbf{m}}$  is the same for all users.

into the true values. Therefore, we propose a new multiuser approach based on peak detection and collision studies.

*Remark: We implemented in Algorithm 2.1 the full MUD. In fact, when implemented at a specific receiver, the algorithm can simply focus on the selected user. The stopping rule can then be adapted (only the probability concerning the selected user has to exceed the threshold).*

### 2.3.2.2 Proposed Low-Complexity Detector

To reduce the complexity, we propose a simpler and more direct strategy. In fact, when a good number of peaks is found and because the power allocation scheme is known, it is straightforward to find the one corresponding to the selected user. The CSS in fact allows an interferer avoidance scheme in the Fourier domain at the receiver. In such a case, it is not necessary to cancel interference from stronger users. However, collisions, when two users transmit the same information at the same time, make things more difficult, and if not handled properly, may significantly limit the capabilities of the approach. Our proposed algorithm has the following two steps:

1. *Peak detection using a threshold:* The goal is to find the peaks, including the one from the selected user and the higher peaks. For instance, if the selected user is user  $j$  (the order of the users is from the strongest to the weakest allocated power), we define a low enough threshold that will allow us to detect the  $j$  strongest peaks but high enough such that the weaker peaks will not be

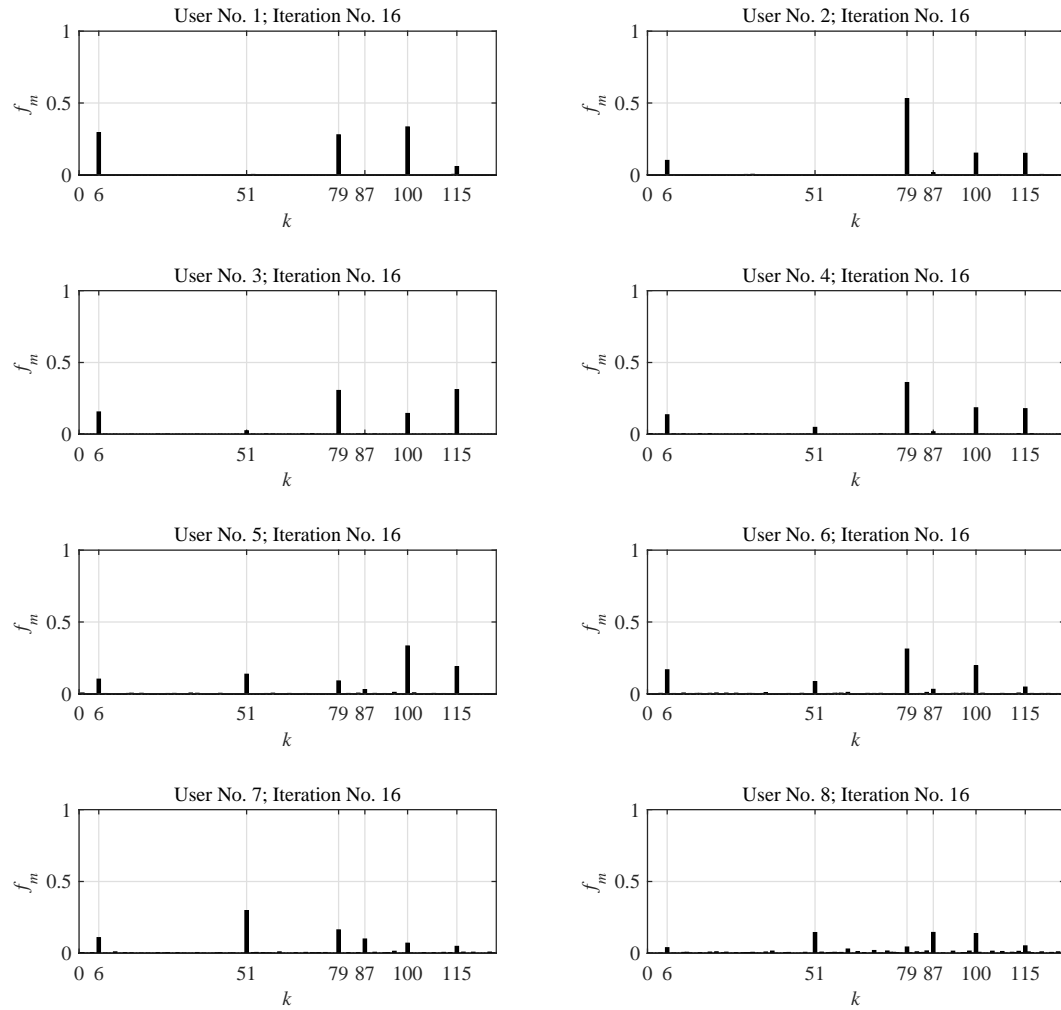


Figure 2.2: CEM-MUD as per Algorithm 2.1, with  $N = 8$  users and  $SF = 7$ . In this example two collisions occur ( $\mathbf{m}_q = \{6, 79, 115, 79, 100, 100, 51, 87\}$ ). The figures represent  $f_m$  at the beginning of the 16th iteration. We can see that if values tend to gain in probability, the decision cannot be made yet.

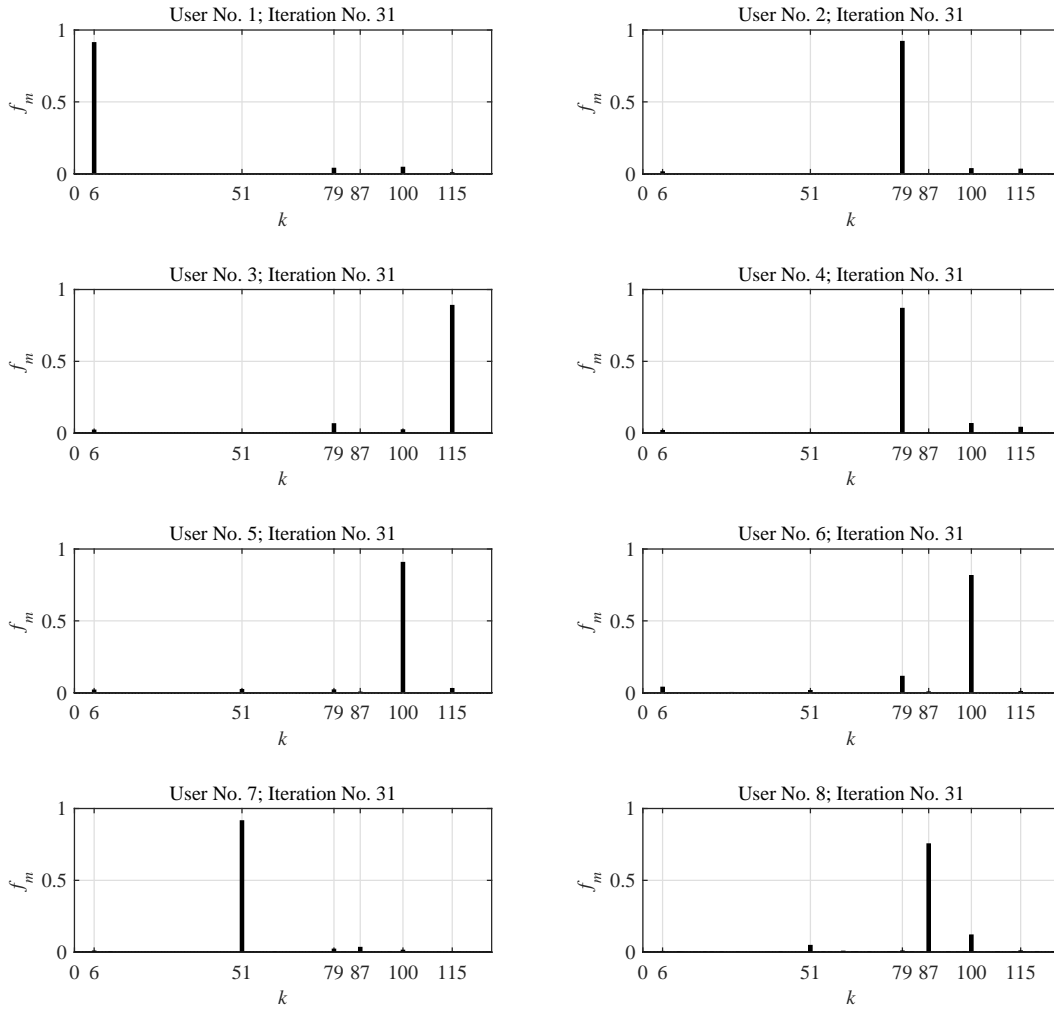


Figure 2.3: CEM-MUD as per Algorithm 2.1, with  $N = 8$  users and  $SF = 7$ . In this example two collisions occur ( $\mathbf{m}_q = \{6, 79, 115, 79, 100, 100, 51, 87\}$ ). The figures represent  $f_m$  at the beginning of the 31st iteration. We can see that the probability is clearly converging towards a single value equal to one for each user, all the others being zero. We also see that the decision is good despite the two collisions between users 2 and 4 and users 5 and 6.

detected.

2. *Peak selection using a search method:* If exactly  $j$  peaks are detected, we choose the closest one from the expected received amplitude, and its position gives the information of the selected user. Similarly, if more than  $j$  peaks are detected, weaker peaks have probably collided, and we choose the closest one from the expected received amplitude. Finally, if we detect less than  $j$  peaks, it means that collisions occurred between the  $j$  strongest users. In that case, we analyze all the possible collision cases to choose the most likely and decide.

Both steps (choosing the threshold and deciding when less than  $j$  peaks are detected) will be described in the following.

*Remark:* In the second step, when we detect exactly  $j$  peaks, there is a case where we can miss the information of the selected user, that is, when two or more weaker users collided and result in a peak larger than or equal to the selected user's peak but this selected peak is below the threshold or also collided with another peak. This case is infrequent and can be generally avoided by the power allocation scheme described in 2.3.3.1.

**A) Threshold definition:** Recall that we have  $N$  users ordered from the strongest allocated power to the weakest one. We consider user  $j$  that we want to decode. We fix a threshold to detect the  $j$  strongest peaks but not the  $N - j$  weakest ones. The expected amplitude for user  $i$  at receiver  $j$  is  $|h^{(j)}|\sqrt{p^{(i)}}$ . The objective for choosing the optimal threshold is by maximizing:

$$p_1 = \mathbb{P} \left( |h^{(j)}|\sqrt{p^{(j)}} + W_p^j[k] > \gamma \right),$$

and, at the same time, to minimize:

$$p_0 = \mathbb{P} \left( |h^{(j)}|\sqrt{p^{(j+1)}} + W_p^j[k'] > \gamma \right).$$

where  $W_p^j[k]$  is the Gaussian noise and  $k$  and  $k'$  denote the frequencies where the peaks fall. If user  $j$  is the weakest one ( $j = N$ ), we set  $p^{(N+1)} = 0$ :

$$\gamma_* = \underset{\gamma \in \gamma}{\operatorname{argmax}} \left[ \mathbb{P} \left( |h^{(j)}|\sqrt{p^{(j)}} + W_p^j[k] > \gamma \right), \right. \\ \left. 1 - \mathbb{P} \left( |h^{(j)}|\sqrt{p^{(j+1)}} + W_p^j[k'] > \gamma \right) \right]. \quad (2.13)$$

then, we have:

$$p_1 = Q\left(\frac{\gamma - h^{(j)}\sqrt{p^{(j)}}}{\sigma_n}\right), \quad (2.14)$$

$$p_0 = Q\left(\frac{\gamma - h^{(j)}\sqrt{p^{(j+1)}}}{\sigma_n}\right), \quad (2.15)$$

where  $Q(\cdot)$  is the Q-function [74]. Consequently, we have a multi-objective optimization problem, and the Pareto front is easy to obtain. As a starting point, we choose:

$$\gamma = h^{(j)}\frac{\sqrt{p^{(j+1)}} + \sqrt{p^{(j)}}}{2}, \quad (2.16)$$

but this parameter could be optimized to give more weight to  $p_1$ .

**B) Making a decision:** Let  $N_{pk}$  be the number of peaks above the threshold  $\gamma$ . The number of expected peaks is  $N_{exp} = j$ . The decision rule is the following:

- If  $N_{pk} \geq N_{exp}$ , we assume no collision between strong peaks and select the peak that has the closest value to the expected one.
- If  $N_{pk} < N_{exp}$ , we assume a collision occurred. We scan for all possible combinations between the users 1 to  $j$ . Let  $\check{m}$  be such a combination. We create a vector adding the amplitudes of the peaks that collide. We ordered the resulting values (including those that did not collide) and calculate the Euclidean distance with the ordered detected peaks. Scanning all possible combinations, we minimize the Euclidean distance in (2.12) to select the most probable one and deduce the estimated information of the selected user.

**C) Algorithm:** The resulting proposed solution is given in Algorithm 2.2.

Step 1 determines the threshold, and step 2 finds the peaks above the threshold. Steps 3 and 4 initialize the value of the decoded symbol ( $m_0$ ) and the minimum distance ( $M_0$ ).

Steps 5 to 16 are for the case when the number of peaks is less than the threshold: collision occurred. In that case, we scan all possible combinations giving the calculated number of collisions. If the vector received for a generated sequence is closer to the truly received vector (distance less than  $M_0$ ), we update the values of  $m_0$  and  $M_0$ . The number of combinations to scan can become important when the number of users and the number of collisions get large (see table 2.1), and alternative strategies should be found for these rare events.

When no collision is detected (the number of detected peaks is at least the one we expected), we choose the peak with the closest amplitude to the one we expect (step 18).

---

**Algorithm 2.2** Proposed Multiuser Detection Algorithm (single symbol)
 

---

**Input:** Received vector  $\mathbf{Z}_q^{(j)}$ ,  $\hat{h}^{(j)}$ ,  $N$ ,  $p^{(j)}$ ,  $p^{(j+1)}$

**Output:** Decoded symbol  $m_q^{(j)}$

- 1: Calculate  $\gamma$  according to (2.16)
  - 2:  $u \leftarrow \mathbf{Z}_q^{(j)} > \gamma$  % Get the position of peaks larger than  $\gamma$ .
  - 3:  $m_0 \leftarrow 0$  % Value of the selected combination
  - 4:  $M_0 \leftarrow \|\mathbf{Z}[u]\|^2$  % Initialize the distance
  - 5: **if**  $\text{length}(u) < j$  **then**
  - 6:   **while** another combination of  $j - \text{length}(u)$  collisions exist **do**
  - 7:     Choose a combination  $\tilde{\mathbf{m}}_q$  with  $m$  the symbol of user  $j$
  - 8:     Generate the source vector  $\tilde{\mathbf{X}}_q$  from  $\tilde{\mathbf{m}}_q$  and (2.2)
  - 9:      $\tilde{\mathbf{R}}_q^{(j)}[n] \leftarrow \hat{h}^{(j)} \tilde{\mathbf{X}}_q[n]$
  - 10:      $\tilde{\mathbf{Z}}_q^{(j)}[k] \leftarrow \text{Re}\{FFT(\hat{h}^{(j)} * \tilde{\mathbf{R}}_q^{(j)}[n])\}$
  - 11:     **if**  $\|\mathbf{Z}_q^{(j)}[u] - \tilde{\mathbf{Z}}_q^{(j)}[u]\|^2 < M_0$  **then**
  - 12:        $m_0 \leftarrow m$
  - 13:        $M_0 \leftarrow \|\mathbf{Z}_q^{(j)}[u] - \tilde{\mathbf{Z}}_q^{(j)}[u]\|^2$
  - 14:     **end if**
  - 15:   **end while**
  - 16:    $m_q^{(j)} \leftarrow m_0$
  - 17: **else**
  - 18:    $m_q^{(j)} \leftarrow \underset{u}{\text{argmin}} \left( \|\mathbf{Z}_q^{(j)}[u] - |\hat{h}^{(j)}|^2 \sqrt{p^{(j)}}\|^2 \right)$
  - 19: **end if**
  - 20: **return**  $m_q^{(j)}$
- 

### 2.3.2.3 Direct Peak Detection

As a reference, we also implement a detection based on finding the peak with the closest amplitude to the expected one. This receiver is the simplest one but does not provide the means to resolve collisions. The decoding process with  $N$  users is described as follows: search for the  $N$  strongest peaks; select the peak that minimizes the distance between its amplitude and the expected value  $|\hat{h}^{(j)}| \sqrt{p^{(j)}}$ .

### 2.3.3 Power allocation scheme

The power allocation allows us to differentiate the different users at the receiver. In order to optimize the NOMA scheme, we attribute the largest transmit power to the user with the worst channel [75, 76]. We can then allocate power based on two different objectives: (a) to suppress ambiguities when collisions occur and (b) to increase fairness between different users.

#### 2.3.3.1 Power Allocation 1: Suppressing ambiguities

The goal is to avoid colliding users giving rise to a peak with an amplitude equal to another user or a combination of other colliding users. We first order the users from the strongest to the weakest based on an estimate of the channels from a previous uplink ( $|\hat{h}^{(1)}| > |\hat{h}^{(2)}| > \dots > |\hat{h}^{(N)}|$ ). For user  $j$ , we allocate the power:

$$p^{(j)} = \frac{2^{j-1}}{\sum_{i=1}^N 2^{i-1}} p_t, \quad (2.17)$$

where  $p_t$  is the total power transmitted by the access point. This guarantees that whatever collision occurs, two peaks can not have the same amplitude at the receiver side. However, this results in a significant proportion of the available power to be allocated to further users, and the amplitude difference gets small for the closest ones.

#### 2.3.3.2 Power Allocation 2: Fair Spacing

We order the users based on an estimate of the channels from a previous uplink from the weakest to the strongest ( $|\hat{h}^{(1)}| < |\hat{h}^{(2)}| < \dots < |\hat{h}^{(N)}|$ ). We note  $h^{(0)} = 0$ . We want that whatever the receiver  $j$ , the gap between the peak amplitudes of user  $j$  and the weaker user  $j - 1$  always has the same value  $c$ ,

$$|\hat{h}^{(j)}| \sqrt{p^{(j)}} - |\hat{h}^{(j-1)}| \sqrt{p^{(j-1)}} = c. \quad (2.18)$$

We show in appendix **A** that the power allocated to user  $j$  in that case is:

$$p^{(j)} = p_t \frac{A_j^2}{\sum_{i=1}^N A_i^2}, \quad (2.19)$$

where,

$$A_i = \sum_{l=1}^i \frac{1}{|\hat{h}^{(l)}|^2}. \quad (2.20)$$

The drawback of this algorithm is that it depends on the channel coefficients. The access point can estimate them on previous uplinks, but the quality of the scheme will depend on the time coherence of the channels. We assume the time coherence of the channels is long in many static IoT cases, but the impact of time evolution needs to be further investigated. Theoretical performance analysis as the one in [77] for the uplink would have been a significant added value. However, contrary to other works on NOMA, performance is conditioned on collisions and gaps between allocated powers rather than on SIR, where interference is the sum of all interfering signals. It introduces combinatorial problems (probability of collisions, who collides, and so on), but we have not yet solved the problem.

## 2.4 Results

This section has four main objectives: first, we show that the MUD allows us to increase the LoRa network's capacity significantly. Second, we confirm that the proposed algorithm delivers performance close to the CEM-MUD. Third, we check the proposed PA schemes, including the users' performance according to their position (in terms of channel gain) in the group of users, simultaneously addressed. Fourth, we provide an analysis of the computational complexity.

### 2.4.1 Simulation setup

We define a circular region inside which users are uniformly distributed. The radius of the circle is  $R = 4, 5, 10$  km for SF = 7, 8, 10 respectively, and we choose the channel attenuation coefficient  $\eta = 3.5$ . A complex Gaussian random variable with mean 0 and variance 1 is drawn for each user to model the Rayleigh fading and obtain the channel coefficient as described in section 2.3.1.2:  $h^{(i)} = d^{(i)-\eta/2} \cdot \chi^{(i)}$ .

However, to be connected to the network with a given SF, the received power in the uplink has to be greater than the receiver sensitivity  $R_s$  (we assume a transmit power of 14 dBm). For instance,  $R_s = -121.5, -124, -129$  dBm for SF = 7, 8, 10 respectively, and  $B = 250$  kHz. Users that do not respect this condition are discarded and drawn again until  $N$  devices are connected. We consider that the access point has a sufficient number of users to address, but no selection scheme is implemented (users are independent and identically distributed). We fix this number, and the transmitted packet is the superposition of all corresponding signals.

The noise level of the receiver, as discussed in Section 2.3.1.1, is  $-114$  dBm. The

complete chirp spreading is simulated in the baseband, and the information is coded for all users. We use a total transmit power of 27 dBm.

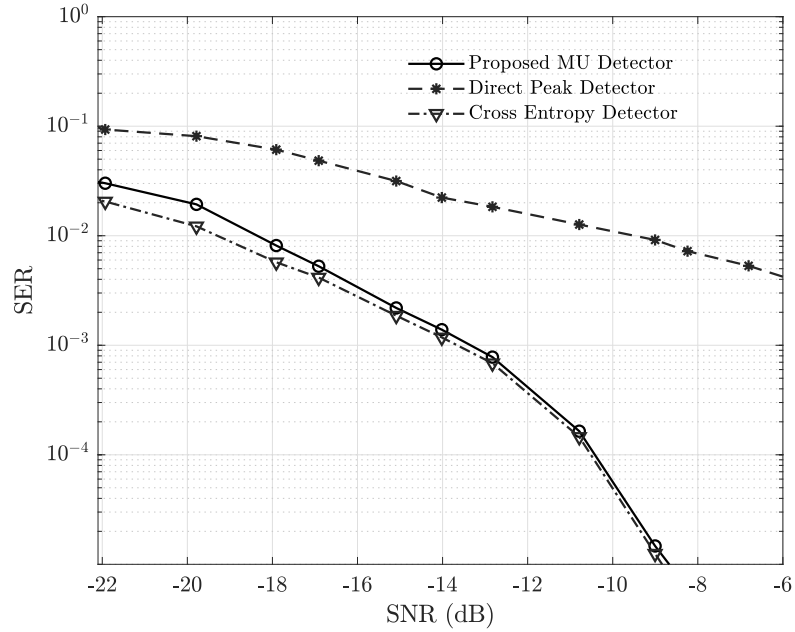
Monte Carlo simulations are used to evaluate the performance of the proposed scheme. The parameter settings for the cross-entropy decoder are as follows: we generate  $N_{seq} = 2000$  sequences and keep  $N_{keep} = 100$  sequences for the probability mass function update.

Packet detection and channel estimation are performed using correlation with the known preamble. Common to all users and transmitted with the full transmit power, it does not generate errors, and the channel estimation is accurate. We present the performance evaluation in terms of the average symbol error rate (SER). Error-correcting codes and a user selection scheme should be included to derive a higher layer Key Performance Indicator. This remains out of the scope of this paper because we are only interested in the Physical (PHY) layer.

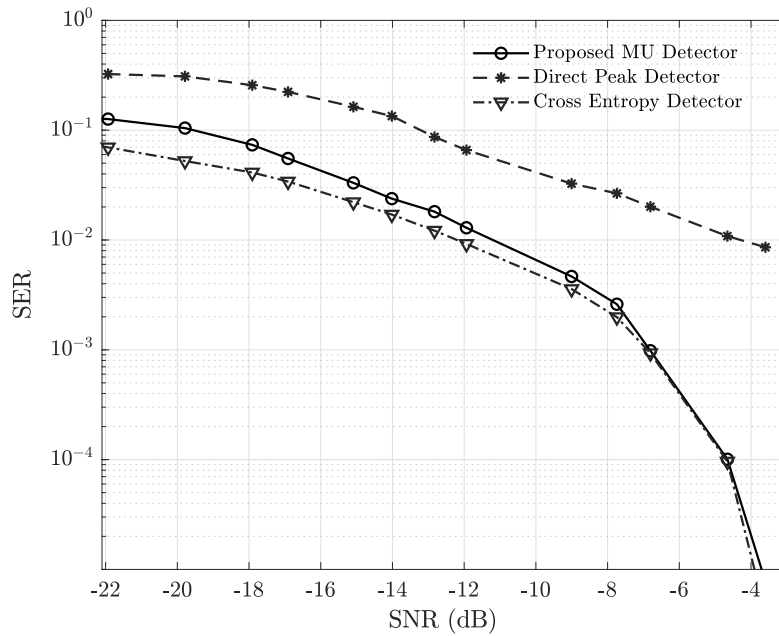
#### 2.4.2 Performance of the three receivers

Figs. 2.4a and 2.4b illustrate the SER of a single user with additive Gaussian noise (different SNR, which corresponds to different radio link quality) in the presence of, respectively, 4 and 9 interfering users. The spreading factor is  $SF = 7$ ,  $B = 250$  kHz, and  $R_s = -121.5$  dBm. Power allocation scheme 2 was used in these simulations. Slightly different results are obtained with scheme 1 but without changing the trends and conclusions. The impact of the other users and erroneous decisions due to peak ambiguities or collisions is shown. The MUD performance is outstanding compared to the direct peak receiver. At equivalent SNR, we see a significant gain in SER (one order of magnitude at -15 dB in the case of 5 simultaneous users).

The CEM-MUD has the best performance. It shows that the multiuser scheme can be implemented and significantly increases the number of users in the networks: 10 simultaneous users can be supported. These brute results are very encouraging, especially because we did not consider any user clustering scheme. If the network is highly populated, we should search for the best way to group users and ensure optimal performance. The CEM-MUD significantly outperforms the simplest receiver that only searches for the close peak amplitude. This shows that it is important to have a multiuser approach and implement a solution to account for collisions. Finally, our proposed receiver and the cross-entropy method have almost similar performance, especially at high SNR. This allows a solution for a low complexity implementation



(a) Performance of a single user in the presence of 4 interfering users.



(b) Performance of a single user in the presence of 9 interfering users.

Figure 2.4: SER for different SNR values of a single user, when  $SF = 7$ , and  $B = 250$  kHz.

of a multiuser detector.

### 2.4.3 Power allocation performance

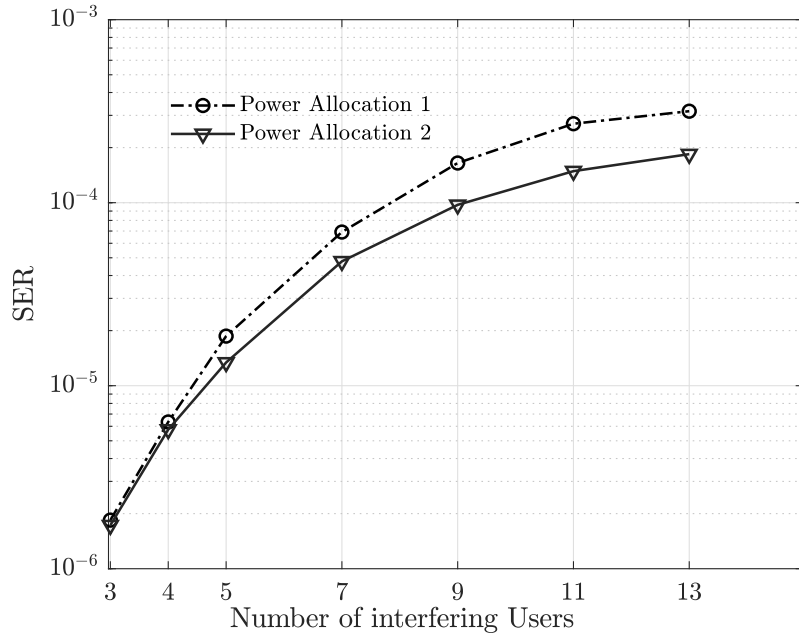
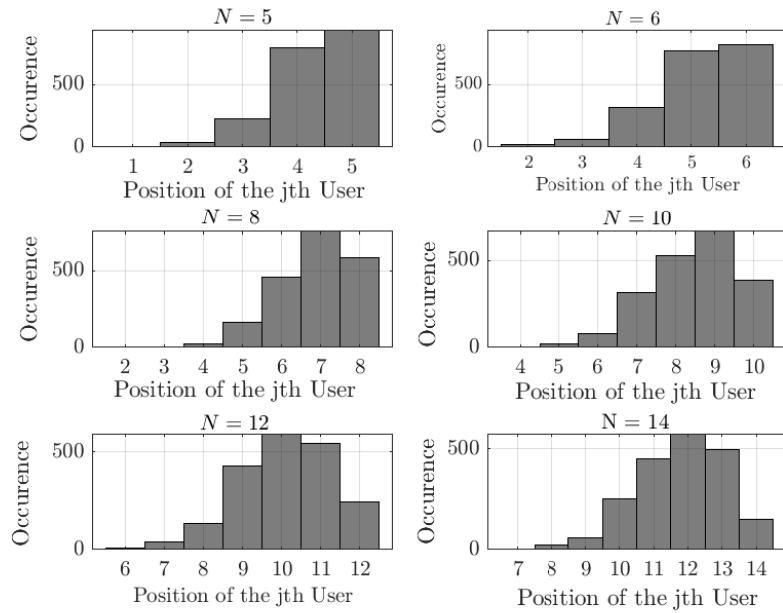
Figs. 2.5a and 2.6a show the symbol error rate of a single user with an additive Gaussian noise, SNR=  $-10$  and  $-12$  dB respectively, and an increasing number ( $N - 1$ ) of interfering users with  $N = 3, \dots, 13$ . In both cases, the power allocation scheme 2 (fair allocation) exhibits better performance. This is more significant in Fig. 2.6a when the SNR is smaller so that the user is in the weak users. This can be observed from Figs. 2.5b and 2.6b, where the histogram of the position of the selected user when users are ordered from the weakest channel (strongest allocated power) to the best channel. For instance, in the case with  $N = 12$ , it is seen that the mean position is between 3 and 4 in Fig. 2.6b (SNR=  $-12$  dB) when it is between 10 and 11 in Fig. 2.5b (SNR=  $-10$  dB). This latter case sees a larger benefit with the second power allocation scheme, which comes from the fairness approach and the fact that for the first allocation scheme, the gap between amplitudes is small for the users with the good channels.

This analysis is confirmed in Figs. 2.7 and 2.8 where the average symbol error rate is plotted for different SF (SF = 7, 8, 9, and 10) and the two power allocation schemes.

These two plots also show that the proposed MUD exhibits good performance whatever the SF. As a comparison, the actual implementation of LoRa allows us to address only one user at a time. This means that we can increase by one order of magnitude the number of users that can be addressed in a single time slot.

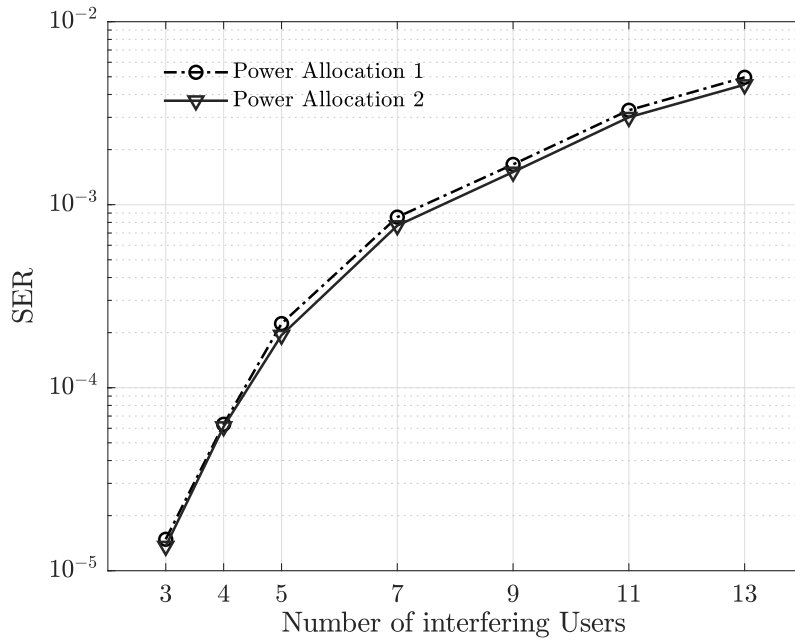
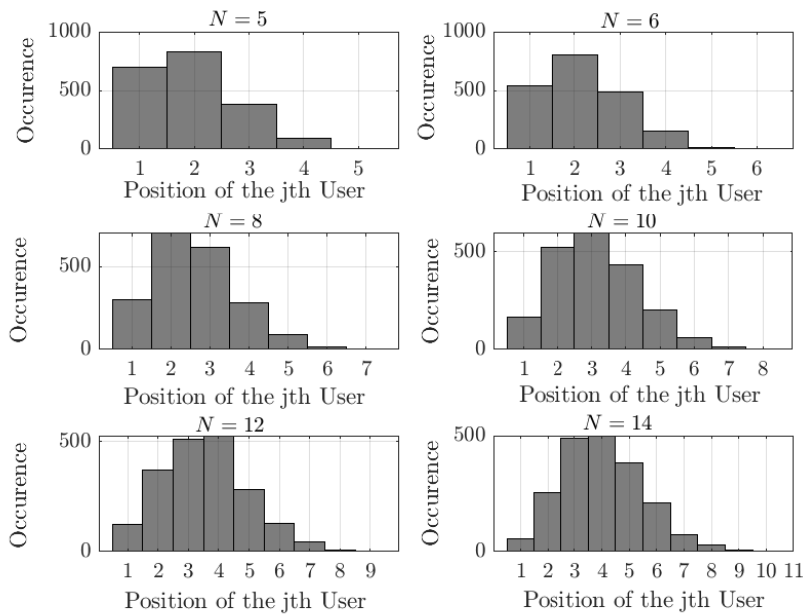
### 2.4.4 Fairness

The previous section analyzed the mean error (among all users) but did not consider the SER difference between users with a good or a bad channel. The SER difference between individual users is shown in Fig. 2.9. Users are randomly chosen at each round, but errors are added depending on their order (from the worst to the best channel). User one, for instance, is the one with the worst channel, so the one with the highest allocated power. Both power allocation schemes are considered, and we use  $N = 7$  and 13. In the first power allocation scheme, ambiguities are avoided, but the gap between allocated powers is rapidly decreasing and does not take the channel into account. For the last users (in fact, users with the best channel), the gap between allocated powers is insufficient, resulting in an increased SER. On the contrary, the second scheme offers a fairer allocation, slightly increasing the SER

(a) SER of a single user in the presence  $N - 1$  interfering users.

(b) Position of the selected user (jth) compared to the interfering users.

Figure 2.5: Performance of the proposed MUD when  $\text{SNR} = -10$  dB,  $\text{SF} = 8$ , and  $B = 250$  kHz.

(a) SER of a single user in the presence  $N - 1$  interfering users.

(b) Position of the selected user (jth) compared to the interfering users.

Figure 2.6: Performance of the proposed MUD when  $\text{SNR} = -12$  dB,  $\text{SF} = 8$ , and  $B = 250$  kHz.

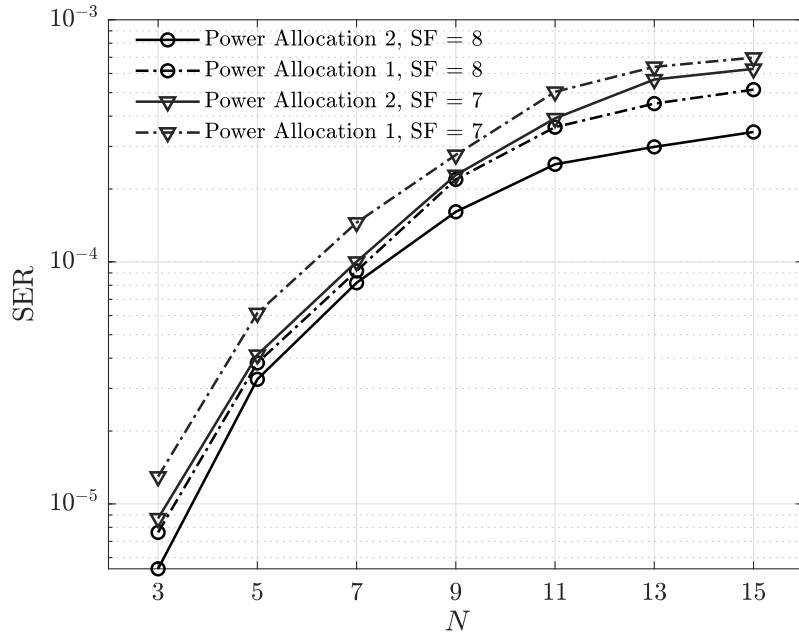


Figure 2.7: SER of the proposed MUD for different  $N$ , Noise level of  $-114$  dBm, SF=7, 8, and  $B = 250$  kHz.

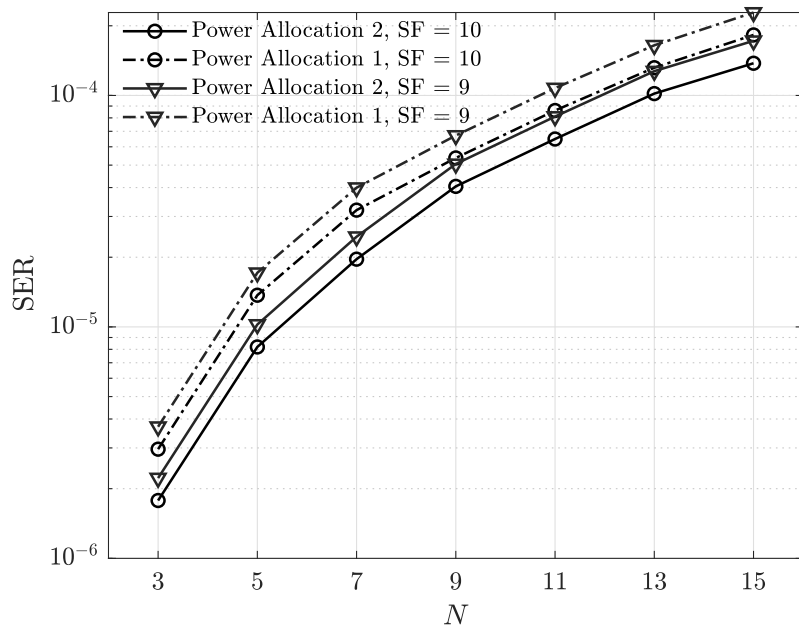


Figure 2.8: SER of the proposed MUD for different  $N$ , Noise level of  $-114$  dBm, SF=9, 10, and  $B = 250$  kHz.

for the far users (the first ones) but keeping a more constant value and significantly improving performance compared to the other allocation scheme for the last users.

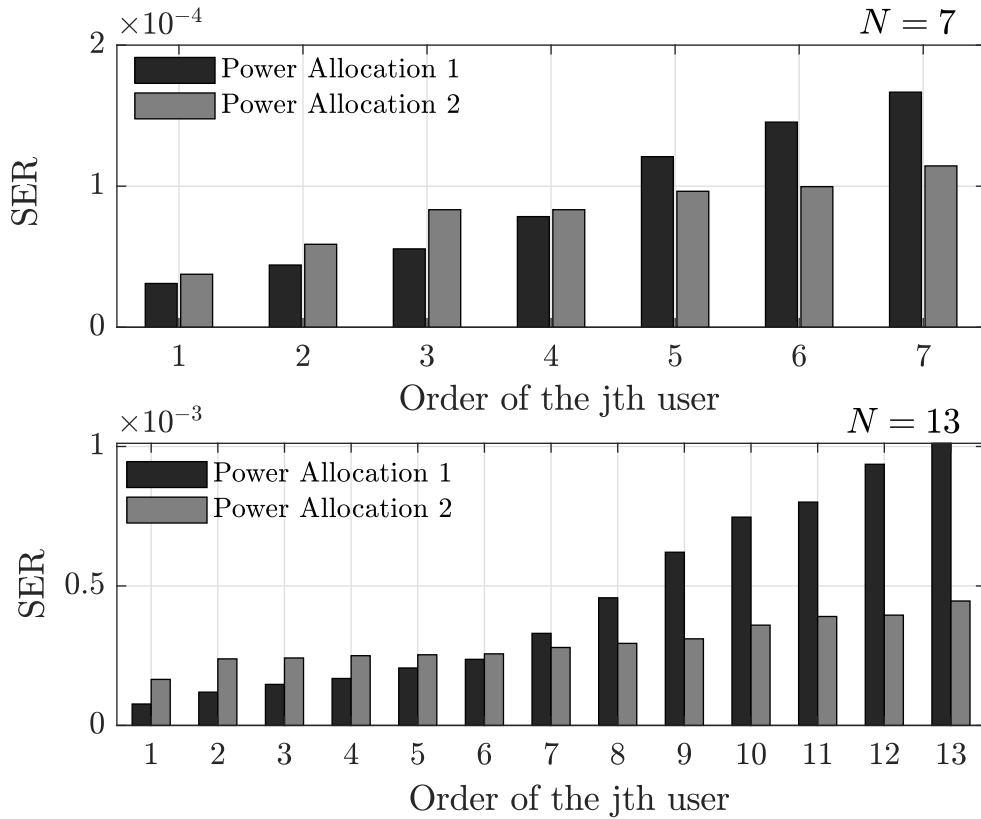


Figure 2.9: SER of individual users when  $N = 7$  and 13,  $SF = 8$ , Noise level of  $-114$  dBm, and  $B = 250$  kHz.

## 2.4.5 Computational Complexity Analysis

We compare the computational complexity of the three decoding algorithms, namely Direct peak detection, Cross-Entropy, and proposed receivers. Our evaluation is considering the decoding of a single symbol. This study gives a broad idea of the complexity, but we did not try to optimize the algorithm implementation.

### 2.4.5.1 Direct peak detection

For each symbol, we repeat the following operations:

1. Multiply by the down-chirp ( $2^{SF}$  multiplications),

2. FFT (complexity  $\mathcal{O}(2^{SF} \cdot \log(2^{SF}))$ ).

The final complexity for this simple receiver is  $\mathcal{O}(2^{SF} \cdot \log(2^{SF}))$ .

### 2.4.5.2 Cross Entropy Method

If we assume that generating a sample from a given PMF and updating a PMF are both  $\mathcal{O}(1)$ , the complexity of the CEM algorithm depends on the number of operations that are iterated. These operations, as depicted in algorithm 2.1 and their associated complexity for a single symbol are:

1. Line 12 (Generate  $\tilde{\mathbf{m}}_q$ ) is  $\mathcal{O}(N)$
2. Line 13 (Generate the source vector  $\tilde{\mathbf{X}}_q$ ) is  $\mathcal{O}(N \cdot 2^{SF})$
3. Line 14 ( $\tilde{\mathbf{R}}_q^{(j)}[n] \leftarrow \hat{h}^{(j)} \tilde{\mathbf{X}}_q[n]$ ) is  $\mathcal{O}(2^{SF})$
4. Line 15 (FFT) is  $\mathcal{O}(2^{SF} \log(2^{SF}))$
5. Line 16 (distance) is  $\mathcal{O}(2^{SF})$

The listed operations are repeated  $N_{seq} \cdot N_{ite}$  times, where  $N_{ite}$  is the number of iteration before convergence which was observed to be around 30. The PMF updating involves only additions and one normalization and will be  $\mathcal{O}(N_{keep})$ .

Therefore, the overall complexity is dominated by the  $2^{SF}$  repeated  $N$  times in line 13 and  $\log(2^{SF})$  in the FFT calculation done for each tested sequence. These figures are of similar order and fixed. In the end we can state that the complexity of the CEM is  $\mathcal{O}(N_{seq} \cdot N_{ite} \cdot N \cdot 2^{SF})$ .

### 2.4.5.3 Proposed Method

In our proposal, after peak detection, the complexity is equal to the first approach as long as the number of the detected peaks is equal to or larger than the number of expected peaks.

In the case where fewer peaks are detected, the complexity will be given by the FFT operation that we will need to repeat  $M_c$  times,  $M_c$  being the number of possible collision combinations we have to scan (steps 6-15 in algorithm 2.2). For a reasonable number of users and collisions, this number remains low (see table 2.1). So, finally, the overall complexity is  $\mathcal{O}(\mathbb{E}[M_c] \cdot 2^{SF} \log(2^{SF}))$ .

The time needed to decode a symbol is random and depends on  $M_c$ , which is directly

linked with the number of users  $N$  and collisions  $N_c$  occurring. It is easily seen that the probability of having no collision with  $N$  users independently and uniformly selecting a number in  $\{1, \dots, 2^{SF}\}$  is:

$$\mathbb{P}\{\text{No Collision}\} = \frac{\prod_{i=0}^{N-1} (2^{SF} - i)}{2^{N \cdot SF}} \quad (2.21)$$

It is, for instance, 0.697 when  $SF = 7$  and  $N = 10$  and goes up to 0.961 when  $SF = 8$  and  $N = 5$ . In the case when a collision occurs, the number of combinations to be scanned is presented in table 2.1 and can become very large in the rare cases when  $N$  is larger than 10 and  $N_c$  larger than 4, for instance.

#### 2.4.5.4 Comparison

It is clearly seen from the previous analysis that the CEM is much more complex than the two others. Our proposed approach is only complex in rare cases when the number of considered users is large and several collisions occur. Probably it will not be possible to implement these cases in low-cost devices, and alternative strategies to address them will be necessary.

To complement our study, table 2.2 compares the mean computational time  $R_t$  (in seconds) of the three receivers, which is required to decode a single user's packet when the length of the packet is  $Q = 100$  symbols, and  $B = 250$  kHz, and  $\text{SNR} = -12.5$  dB. To evaluate the differences, we used a MATLAB-based software implementation of the digital part of the receiver on a standard computer, but it gives us a general idea about the computational complexity.

As expected, the ordered peak receiver is much faster at the price of significantly degraded performance. On the other hand, the CEM-MUD has much better performance but with high computational complexity. The computation time is multiplied by 1200 for 5 users, and the coefficient increases with the number of users.

Our proposed receiver has performance close to the CEM-MUD with a significantly reduced computation time. Indeed, this time is more than 900 times less than the CEM-MUD except when the number of simultaneous packets becomes large (20 in table 2.2).

#### 2.4.6 SF Orthogonality

Fig. 2.10 and 2.11 study the impact of interfering users transmitting simultaneously but with another spreading factor. Fig. 2.10, five users are considered simultaneously

Table 2.1: Number of different combinations  $M_c$  when  $N_c$  collisions occur leading to  $N_{pk}$  observed peaks when  $N_{exp}$  were expected.

$N \backslash N_c$	1	2	3	4	5
1	0	0	0	0	0
2	1	0	0	0	0
3	3	1	0	0	0
4	6	7	1	0	0
5	10	25	15	1	0
6	15	65	90	31	1
7	21	140	350	301	63
8	28	266	1050	1701	966
9	36	462	2646	6951	7700
10	45	750	5880	22827	42525
11	55	1155	11880	63987	179487
12	66	1705	22275	159027	627396
13	78	2431	39325	359502	1899612
14	91	3367	66066	752752	5135130
15	105	4550	106470	1479478	12662650

with an SF 8. On the same frequency and at the same time, other users transmit using a different SF. Even if a slight degradation can be observed, it is seen that the performance is kept at a reasonable level.

The same conclusion can be drawn from Fig. 2.11, where 10 users are using an SF 8. Again with up to 10 interfering users transmitting with another SF, the loss in performance is limited.

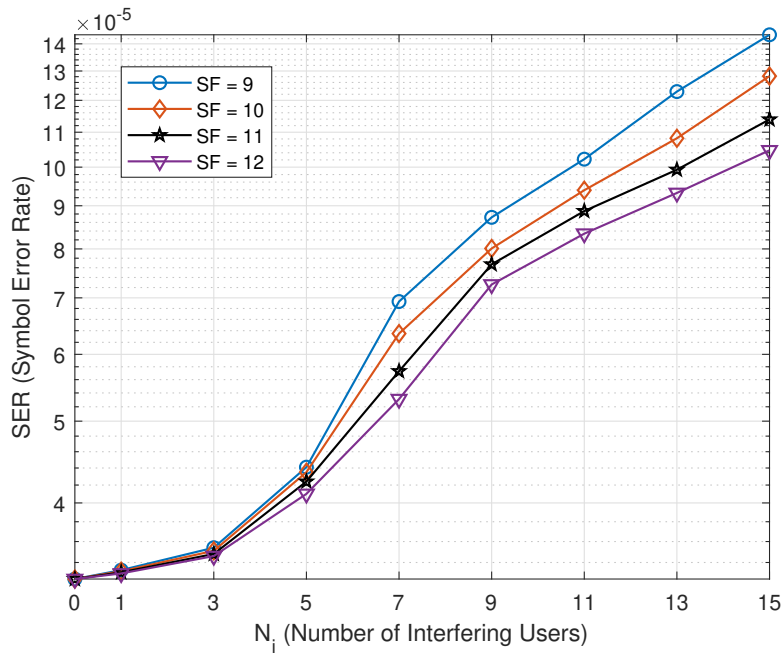


Figure 2.10: SER for fixed 5 users using SF = 8, for different SF and interfering users, when  $B = 250kHz$ .

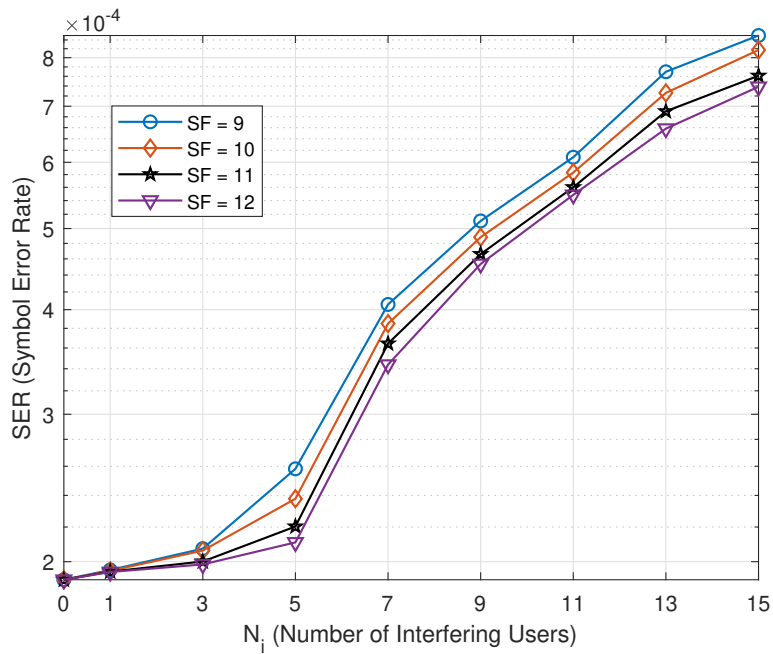


Figure 2.11: SER for fixed 10 users using SF = 8, for different SF and interfering users, when  $B = 250kHz$ .

Table 2.2: Average computational time  $R_t$  (in second) to decode a single user (jth) when SF = 7, and  $N$  users.

$N$	jth user position	Direct Peak	Proposed	CEM-MUD
5	5	0.0046	0.0059	5.5179
10	8	0.0062	0.0114	17.3731
15	13	0.0077	0.0233	32.6277
20	16	0.0093	0.4254	52.3609

## Conclusion

This chapter proposed a new joint multiuser receiver for downlink LoRa networks to face the scalability issue in the downlink. Our proposal is inspired by power domain NOMA but does not require the use of a SIC receiver. Doing so, we avoid the limitation of NOMA resulting from the residues remaining after each cancellation. A second concern for using NOMA in IoT is the low-cost end devices that cannot support computational complexity. The ML does not give an analytical solution and cannot be used. We proposed a suboptimal approach based on the CEM, which is efficient but remains too complex. Consequently, we derived a simplified method that allows resolving collision but keeps complexity low. We have shown that instead of one single packet per time slot, we could transmit more than 10 packets per time slot and even more, keeping the symbol error rate (without error-correcting codes) below  $10^{-3}$ .

The next chapter will discuss the uplink communications in LoRa-like networks and presents a new multi-user receiver to decode multiple signals from different users using the same spreading factor. Additionally, new single-user detectors based on a deep learning approach are also presented.



# Chapter 3

## Uplink Communication in LoRa-like Networks

### Contents

---

<b>3.1 Multi-user Detection: Serial Interference Cancellation . . . . .</b>	<b>52</b>
3.1.1 System Model . . . . .	53
3.1.2 Proposed SIC Receiver . . . . .	57
3.1.3 Results . . . . .	58
3.1.3.1 Performance for a given selected link . . . . .	59
3.1.3.2 Mean Performance . . . . .	59
3.1.3.3 SF Orthogonality . . . . .	60
<b>3.2 Single User Detection: Deep learning-based . . . . .</b>	<b>65</b>
3.2.1 System Model . . . . .	66
3.2.2 Deep Learning-based Receiver . . . . .	67
3.2.2.1 Deep Feedforward Neural Network-based receiver . . . . .	68
3.2.2.2 Convolutional Neural Networks-based receiver . . . . .	68
3.2.3 Results . . . . .	69
3.2.3.1 Results for $N_i \sim \mathcal{P}(\lambda)$ . . . . .	70
3.2.3.2 Capture Effect – $N_i = 1$ . . . . .	71
3.2.3.3 Computational complexity . . . . .	71
<b>Conclusion . . . . .</b>	<b>75</b>

---

*In Chapter 2, we presented a solution for the scalability issues in the downlink communications of LoRa-like networks. This chapter introduces other solutions for uplink communication in LoRa-like networks, which can cope with co-spreading factor interference coming from other LoRa users. First, a multi-user detector based on a Serial Interference Cancellation (SIC) technique is discussed. Then two deep learning-based receivers are modeled for single-user detection based on deep feedforward neural network and a convolutional neural network.*

### 3.1 Multi-user Detection: Serial Interference Cancellation

As mentioned earlier, in LoRa, when two or more devices use the same transmission settings (B and SF) for simultaneous transmission, destructive collision will occur. Therefore, the main objective of this section is to introduce a solution that enables two or more users to transmit their signals using the same SF and frequency band at the same time. In the rest of this section, we reviewed related works.

The authors in [38] examines the interfering signal and analytically derives the performance of LoRa under the same SF interference. Unfortunately, information about interferers is lost in the process. Recent work [45] proposes an algorithm to decode the correct symbols of synchronized or slightly desynchronized signals using their timing information. However, ensuring synchronization is complex in the uplink of long-range networks.

Recently, the authors in [78] proposed a receiver that can decode two signals received at the same time, with the same spreading factor using SIC. Asynchronicity is processed by estimating the time shift between the two received signals. However, the authors presumed that the signal with the highest power was received first, which is not necessarily the case. The extension of this work, which can process multiple simultaneously received signals with the same SF is presented in [46]. However, the power ratio between two successive received signals is assumed to be constant.

The work in [42], closely related to ours, proposes SIC to decode information from all users. A synchronized reception is considered, which is not realistic in the uplink.

We proposed a SIC technique to enable a receiver to decode multiple signals simultaneously. We extend the work in [42] to a more general case where transmitters are asynchronous. Our main contributions are to develop a complete receiver structure,

including the detection of packets, channel estimation, detection of symbols, and interference cancellation. We analyze the performance in the presence of multiple interfering nodes and show that this approach can significantly improve the scalability of the network.

This section is divided into three subsections. In 3.1.1, we introduce the system model. In 3.1.2, we present the SIC algorithm while in 3.1.3 we discuss the simulation results.

### 3.1.1 System Model

Recall that the transmitted modulating symbol of the  $i$ th user at time  $qT_s$ ,  $q = 0, \dots, Q - 1$ , with  $Q$  the number of symbols transmitted in a packet is described in section 1.3, see eq. 1.3. Then, the complex envelope of the transmitted signal of user  $i$ ,  $x^{(i)}(t)$ , is given by:

$$x^{(i)}(t) = \sum_{q=0}^{Q-1} s_q^{(i)}(t - qT_s) \quad (3.1)$$

The transmitted LoRa packet is finally obtained by adding the preamble consisting of consecutive raw chirps as explained in section 1.2.

The rest of this section deals with the reception of a LoRa frame in the presence of interfering users. Indeed, when two users simultaneously transmit their data using the same spreading factor and frequency band, a collision can occur at the reception. Without loss of generality, only one interfering user is considered, and the complete expressions with  $N_u$  interferers are directly obtained by adding all interfering terms, all of which have a similar expression. Therefore, in this analysis, we consider a collision between a symbol of a selected user of interest and two consecutive symbols of an interfering user. The derivation of the expressions of the two consecutive symbols of an interfering user is shown in appendix B.1 in details and can be written as:

$$x_{q,1}^{(j,i)}(t) = \begin{cases} \exp\left(2j\pi\left(\frac{B}{2T_s}t^2 + \left(\frac{m_{q,1}^{(i)} - B\Delta^{(j,i)}}{T_s}\right)t + \phi_{q,1}^{(j,i)}\right)\right), \\ \quad t \in A_{q,1} = \left[-\frac{T_s}{2} + \Delta^{(j,i)}, \frac{T_s}{2} + \Delta^{(j,i)} - \tau_{q,1}^{(i)}\right], \\ \exp\left(2j\pi\left(\frac{B}{2T_s}t^2 + \left(\frac{m_{q,1}^{(i)} - B\Delta^{(j,i)}}{T_s}\right)t + \phi_{q,1}^{(j,i)} - B(t - \Delta^{(j,i)})\right)\right), \\ \quad t \in B_{q,1} = \left[\frac{T_s}{2} + \Delta^{(j,i)} - \tau_{q,1}^{(i)}, \frac{T_s}{2}\right]. \end{cases} \quad (3.2)$$

$$x_{q,2}^{(j,i)}(t) = \begin{cases} \exp\left(2j\pi\left(\frac{B}{2T_s}t^2 + \left(\frac{m_{q,2}^{(i)} + B(T_s - \Delta^{(j,i)})}{T_s}\right)t + \phi_{q,2}^{(j,i)}\right)\right), \\ \quad t \in B_{q,2} = \left[-\frac{T_s}{2}, -\frac{T_s}{2} + \Delta^{(j,i)} - \tau_{q,2}^{(i)}\right], \\ \exp\left(2j\pi\left(\frac{B}{2T_s}t^2 + \left(\frac{m_{q,2}^{(i)} + B(T_s - \Delta^{(j,i)})}{T_s}\right)t + \phi_{q,2}^{(j,i)} - B(t + T_s - \Delta^{(j,i)})\right)\right), \\ \quad t \in A_{q,2} = \left[-\frac{T_s}{2} + \Delta^{(j,i)} - \tau_{q,2}^{(i)}, -\frac{T_s}{2} + \Delta^{(j,i)}\right]. \end{cases} \quad (3.3)$$

$$\text{where } \phi_{q,1}^{(j,i)} = \frac{B(\Delta^{(j,i)})^2 - 2m_{q,1}^{(j,i)}\Delta^{(j,i)}}{2T_s}, \text{ and}$$

$$\phi_{q,2}^{(j,i)} = \frac{B(T_s - \Delta^{(j,i)})^2 + 2m_{q,2}^{(j,i)}(T_s - \Delta^{(j,i)})}{2T_s}.$$

Now we describe the collision between a  $q$ th symbol of the selected user of interest  $j$  and two consecutive symbols of an interfering user  $i$  as shown in Fig. 3.1. Recall that  $x_q^{(j)}(t)$  denotes the modulated symbol (or chirp) at time  $qT_s$  of user  $j$  (see eq. (1.3)). The two consecutive interfering symbols of user  $i$  are denoted by  $x_{q,1}^{(j,i)}(t)$  and  $x_{q,2}^{(j,i)}(t)$ , the index  $j$  indicating that the synchronization is carried out on user  $j$ . The shifts carrying the corresponding modulating symbols are given by  $\tau_{q,1}^{(i)} = m_{q,1}^{(i)}T$  and  $\tau_{q,2}^{(i)} = m_{q,2}^{(i)}T$ . The delay between user  $j$  and user  $i$  (accounting for asynchronous transmissions) is denoted by  $\Delta^{(j,i)}$ .

To formulate the mathematical expression for the interfering signals in Fig. 3.1, we consider two conditions that define the positions of the shifts of the interfering symbols:

$$C_1: \tau_{q,1}^{(i)} > \Delta^{(j,i)}, \quad C_2: \tau_{q,2}^{(i)} < \Delta^{(j,i)}. \quad (3.4)$$

Depending on these conditions, there could be two to four contributions to the interference. The expression for the interfering signal is given in (3.2) and (3.3). The second case in (3.2) (respectively the first in (3.3)) contributes only if  $C_1$  (respectively  $C_2$ ) in (3.4) is satisfied, see appendix **B.1**.

To synchronize, we perform a correlation between the received signal and the preamble. The highest peak indicates the strongest user, indexed by  $j$ , that we will try to decode first, so we synchronize on it. The received signal associated with symbol  $q$  of user  $j$  sampled at  $t = nT$ ,  $n = 0, \dots, M - 1$  is:

$$y_q^{(j)}[n] = h^{(j)}\sqrt{P_t}x_q^{(j)}[n] + h^{(i)}\sqrt{P_t}\left(x_{q,1}^{(j,i)}[n] + x_{q,2}^{(j,i)}[n]\right) + w_q[n]. \quad (3.5)$$

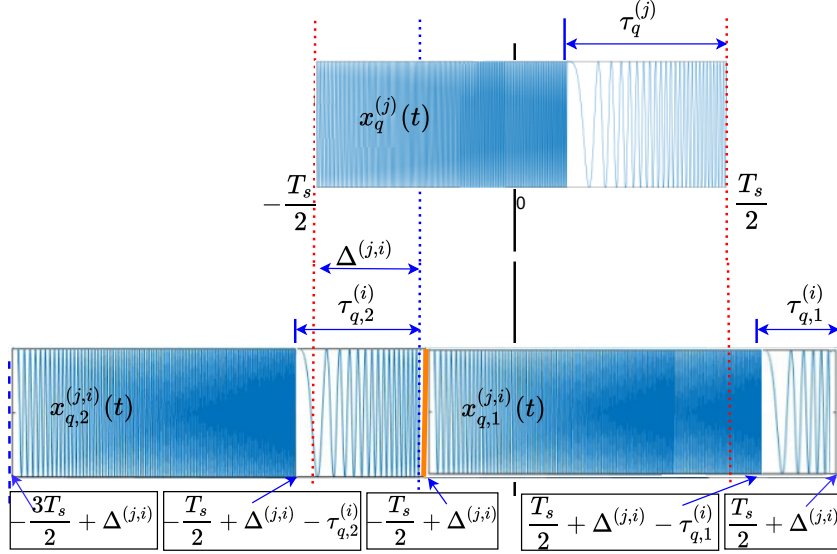


Figure 3.1: LoRa-like Interfering symbols.

where we have used the notation  $x[n] = x(nT_s)$  for any modulated signal  $x(t)$ .  $w_q[n] \sim \mathcal{CN}(0, \sigma_n^2)$  is a complex Gaussian noise,  $h^{(j)}$  and  $h^{(i)}$  are the channel attenuations for users  $j$  and  $i$ ,  $P_t$  is the transmitted power (we consider the same transmit power for each user). Details are shown in appendix **B.2**.

$$\begin{aligned}
r_q[n] &= h^{(j)} \sqrt{P_t} e^{2j\pi \frac{m_q^{(j)}}{M} n} + h^{(i)} \sqrt{P_t} \left( \sum_{l=1}^2 e^{2j\pi \phi_{q,l}^{(j,i)}} e^{2j\pi \left( \frac{\varphi_{q,l}^{(j,i)}}{M} \right) n} \mathbb{1}_{A_{q,l}}[n] \right. \\
&\quad \left. + e^{2j\pi (\phi_{q,l}^{(j,i)} + B\Delta^{(j,i)})} e^{2j\pi \left( \frac{\varphi_{q,l}^{(j,i)}}{M} - (-1)^{l+1} \right) n} \mathbb{1}_{B_{q,l}}[n] \right) + w_q[n], \tag{3.6}
\end{aligned}$$

$$\begin{aligned}
R'_q[k] &= P^{(j)} \delta[k - m_q^{(j)}] + P^{(i)} \left( \sum_{l=1}^2 e^{j\beta_{q,l}^{(j,i)}} \frac{\sin \left( \pi \left( \frac{k - \varphi_{q,l}^{(j,i)}}{M} \right) \Delta A_{q,l} \right)}{\sin \left( \pi \left( \frac{k - \varphi_{q,l}^{(j,i)}}{M} \right) \right)} \right. \\
&\quad \left. + e^{j\gamma_{q,l}^{(j,i)}} \frac{\sin \left( \pi \left( \frac{k - \varphi_{q,l}^{(j,i)}}{M} - (-1)^l \right) \Delta B_{q,l} \right)}{\sin \left( \pi \left( \frac{k - \varphi_{q,l}^{(j,i)}}{M} - (-1)^l \right) \right)} \right) + W'_q[k]. \tag{3.7}
\end{aligned}$$

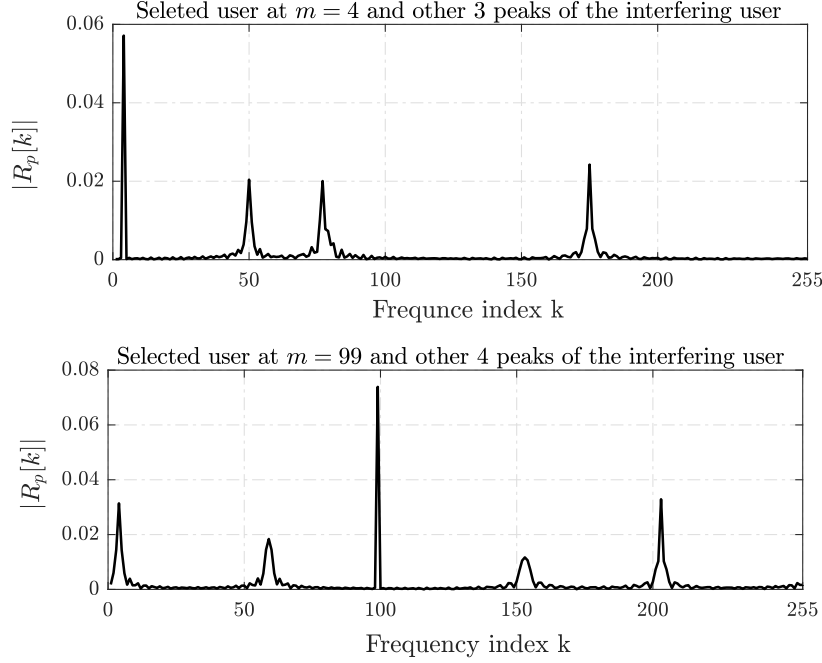


Figure 3.2: FFT of coded chirp of the user of interest at the values of 4 and 99 in the presence of one interfering user using SF = 8,  $B = 250$  KHz.

where  $\beta_{q,l}^{(j,i)} = 2\pi\phi_{q,l}^{(j,i)} - \pi\left(\frac{k - \varphi_{q,l}^{(j,i)}}{M}\right)(\Delta A_{q,l} - 1)$ ,

$$\gamma_{q,l}^{(j,i)} = 2\pi(\phi_{q,l}^{(j,i)} + B\Delta^{(j,i)}) - \pi\left(\frac{k - \varphi_{q,l}^{(j,i)}}{M} - (-1)^l\right)(\Delta B_{q,l} - 1),$$

$$\varphi_{q,l}^{(j,i)} = m_{q,l}^{(i)} - B\Delta^{(j,i)},$$

$\Delta A_{q,l}$ ,  $\Delta B_{q,l}$  are the length of the intervals  $A_{q,l}$  and  $B_{q,l}$  for  $l \in \{1, 2\}$ .

To demodulate, the samples of the received signal are multiplied by the conjugate of the raw chirp: i.e.,  $r_q[n] = y_q^{(j)}[n]c^*[n]$ , where  $c^*[n] = c^*(nT)$ . The resulting signal is given in (3.6), with  $A_{q,l}$  and  $B_{q,l}$ ,  $l \in \{1, 2\}$ , from (3.2) and (3.3). Taking the absolute value of the FFT of (3.6), the useful information creates a peak whose amplitude depends on the channel attenuation. Eq. (3.6) also shows that user  $i$  can create up to four peaks in the Fourier domain (and this is the same for any interfering user). The height of these peaks is determined not only by the channel attenuation but also by the length of the overlaps, and this is good news for our SIC scheme. Fig. 3.2 illustrates this phenomenon by showing the results of the FFT processing for two coded chirps with  $m = 4$  and  $m = 99$  for the user of interest. The parameters are as

follows: Noise level of  $-114$  dBm, SF = 8,  $B = 250$  kHz and one interfering user.

### 3.1.2 Proposed SIC Receiver

We consider SIC as a pure receiver technique, without any power control or any types of adjustment at the transmitter side. First, the strongest signal is decoded. Its contribution can then be reconstructed using an estimate of the channel and subtracted from the received signal. From the resulting residue, the second strongest signal can then be extracted [79]. The performance of the decoding will be degraded by two facts: if the difference in received powers from two different users is too close (which means that their channel is similar because we do not perform any power control); and if other peaks collide, making the peak of interest, not the strongest one or significantly deviating from its expected amplitude. It is important to notice in this case that the signal to interference plus noise power ratio, with an interference power evaluated through the sum of all interfering signal powers, is not a reliable metric. We can also note that the wide range of the communications should allow a large dispersion in the received powers, allowing our approach to performing well.

The decoding of a user can be described as follows. First, the strongest preamble is detected by calculating the correlation between the received signal and the preamble and taking the maximal value, denoted by  $C_{\max}$ . This allows us to detect the beginning of the packet of the strongest user and to estimate its channel  $\hat{h}^{(j)}$ . Multiplication by the down-chirp is then performed; see (3.6). We apply an FFT to  $r_q[n]$  and divide it by the estimated channel, which is shown in (3.7), where  $R'_q[k] = R_q[k]/\hat{h}^{(j)}$ ,  $P^{(j)} = \sqrt{P_t} h^{(j)}/\hat{h}^{(j)}$ ,  $P^{(i)} = \sqrt{P_t} h^{(i)}/\hat{h}^{(j)}$ ,  $W'_q[k] = W_q[k]/\hat{h}^{(j)}$ , and  $W_q[k]$  is the FFT of the Gaussian noise. In (3.7), it is shown that the received power varies according to the standard deviation  $\sigma_n$  of the noise term  $W'_q[k]$ . (Expressions are still given for two users and are simply extended to  $N_u$  users.)

The next step is to search for the peaks of the selected user. Instead of the usual maximum search, we propose to search for the peak having the closest value to  $P^{(j)}$  by minimizing the difference between the detected peaks in  $R'_q[k]$  and  $P^{(j)}$ . This avoids mistakes when interferers collide and create peaks with a larger amplitude than the desired one. We also check that  $|R'_q[k] - P^{(j)}| < \varepsilon$  to detect collisions on the desired peak, where  $\varepsilon$  is tuned by grid-search, yielding an optimal value of  $3\sigma_n$ . If the above condition is not verified, we choose the maximum peak. Once the symbol of the selected user is decoded, its contribution is re-constructed and subtracted from the composite received discrete signal  $y_q[n]$ . The process then starts again to detect

the next strongest user. This detection and suppression process is repeated until no more preamble can be found or a packet is not correctly decoded. Algorithm 3.1 illustrates the proposed receiver. The input is only the combined received signal.

---

**Algorithm 3.1** SIC Receiver for LoRa-like Networks
 

---

**Input:** Received samples  $y_q[n]$ , number of transmitted symbols  $Q$ , detection threshold  $\varepsilon$

**Output:** Decoded symbols  $m_q^{(j)}$

```

1: Detected  $\leftarrow 1$ 
2: while Detected == 1 do
3:   if  $|C_{\max}| < \varepsilon$  then
4:     Detected  $\leftarrow 0$ 
5:   else
6:     Estimate  $\hat{h}^{(j)}$ 
7:      $r_q[n] \leftarrow y_q^{(j)}[n]c^*[n]$ 
8:      $R'_q[k] \leftarrow |FFT(r_q[n])|$ 
9:     for  $q = 1$  to  $Q$  do
10:       $u \leftarrow \underset{k}{\operatorname{argmin}} |R'_q[k] - P^{(j)}|$ 
11:      if  $|R'_q[u] - P^{(j)}|^2 < \varepsilon$  then
12:         $m_q^{(j)} \leftarrow u$ 
13:      else
14:         $m_q^{(j)} \leftarrow \underset{k}{\operatorname{argmax}} (|R'_q[k]^2|)$ 
15:      end if
16:    end for
17:     $\hat{x}_q^{(j)}[n] \leftarrow$  CSS Modulation of  $m_q^{(j)}$ 
18:     $y_q[n] \leftarrow y_q[n] - \hat{h}^{(j)} \hat{x}_q^{(j)}[n]$ 
19:  end if
20: return  $m_q^{(j)}$ 
21: end while

```

---

### 3.1.3 Results

To evaluate the performance of our proposed scheme, we rely on Monte Carlo simulations. We consider a circle of radius  $R$  with one gateway at the center. Multiple users are uniformly distributed within the circle. The distance from user  $i$  to the gateway is denoted by  $d^{(i)}$ . We consider a set of users transmitting their data through block

fading channels during the time interval of interest. All users employ CSS modulation with a symbol duration  $T_s$  (same SF). They transmit their signals with the same power  $P_t$ , i.e., there is no power control. We consider asynchronous transmission among the nodes, different devices operating autonomously. We consider path loss and Rayleigh multi-path fading  $\chi_i$ . For path loss, the signal amplitude decays with distance according to  $d^{(i)-\eta/2}$ , where  $\eta$  is the path loss exponent. The channel attenuation (in amplitude) is then  $h^{(i)} = d^{(i)-\eta/2}\chi_i$ . In the following, we take a maximum range  $R = 5$  km, and we choose  $\eta = 3.5$ . However, the channel attenuation has to be such that the user can be connected to the network with the chosen SF, in other words, if their received power is greater than the receiver sensitivity  $S$ , for instance,  $S = -124$  dBm for SF = 8 and  $B = 250$  kHz. Users that do not respect this condition are discarded and drawn again. The noise level of a receiver at room temperature is  $-174 + 10 \log_{10}(B) + \text{NF} = -114$  dBm, where NF is the receiver noise figure and a classic 6 dB is considered [21].

We consider a window of size  $W = 3T_f$ , where  $T_f$  is the frame length.  $N$  devices are transmitting in this window and asynchronicity is ensured through a random variable  $\Delta^{(i)}$ , uniformly distributed over  $[0, 2T_f]$ . Indeed,  $2T_f$  is the vulnerability period of an ALOHA protocol, and to be sure we receive all full packets, we need to end our study frame at  $3T_f$ . A perfect time-division would allow 3 users (3 packets) in this frame if collisions are not allowed. No channel coding is performed, and we are interested in the symbol error rate (SER).

### 3.1.3.1 Performance for a given selected link

For a given selected link characterized by its SNR  $\frac{|h|^2 P}{\sigma_n^2}$ , Fig. 3.3 shows the performance of this specific receiver when there is no other interfering user ( $N_u = 1$ ) as well as when  $N_u = 4, 7$ , and 10 interfering users are present. The positions and channels of these interfering users are randomly chosen at each round. For an SNR of  $-10$  dB, a typical value for SF = 8 and  $B = 250$  kHz, the performance is good even for 10 interfering users; we reach a SER of  $10^{-3}$  at SNR of  $-10$  dB which is a target SER for LoRa under same SF interference [38].

### 3.1.3.2 Mean Performance

We now evaluate the performance for any user, whatever their channel (so their SNR) is. Fig. 3.4 shows the average symbol error rate of the proposed receiver with SF = 8 when the position of all users is randomly drawn at each round and

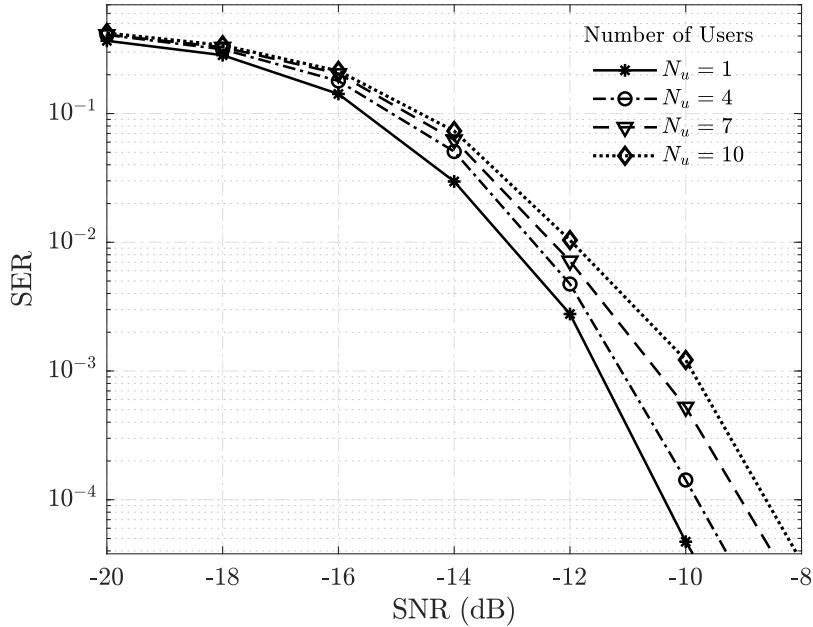


Figure 3.3: SER for  $N_u = 1, 4, 7,$  and  $10$ , with  $SF = 8, B = 250$  kHz.

when different noise levels are considered. It can be seen that instead of the three users that could be handled with a perfect TDMA, which is even more than what an ALOHA protocol as the one used in LoRa can handle, a SIC approach allows having about 20 users with a SER under  $10^{-2}$ .

SIC receiver can be affected by error propagation, which is the consequence of the serial decoding, reconstruction, and suppression process. The result is a higher SER for users with lower power. Fig. 3.5 illustrates the SER of each users when  $N_u = 7, 10, 13,$  and  $16$ . According to their received power, the users are ordered from the highest (1) to the lowest (7, 10, 13, and 16) (cf. Figs. 3.5a, 3.5b, 3.5c, and 3.5d), confirming the error propagation.

### 3.1.3.3 SF Orthogonality

It was shown in [80] that SFs have imperfect orthogonality. Fig. 3.6 presents the average SER for 10 users, which transmit their signal using  $SF = 8$ . We consider an additional  $N_u$  of interfering users transmitting their signal using a different SF (9, 10 or 12). As long as these added interferers are less than four, their impact is negligible. However, the spreading factors are not perfectly orthogonal so that the

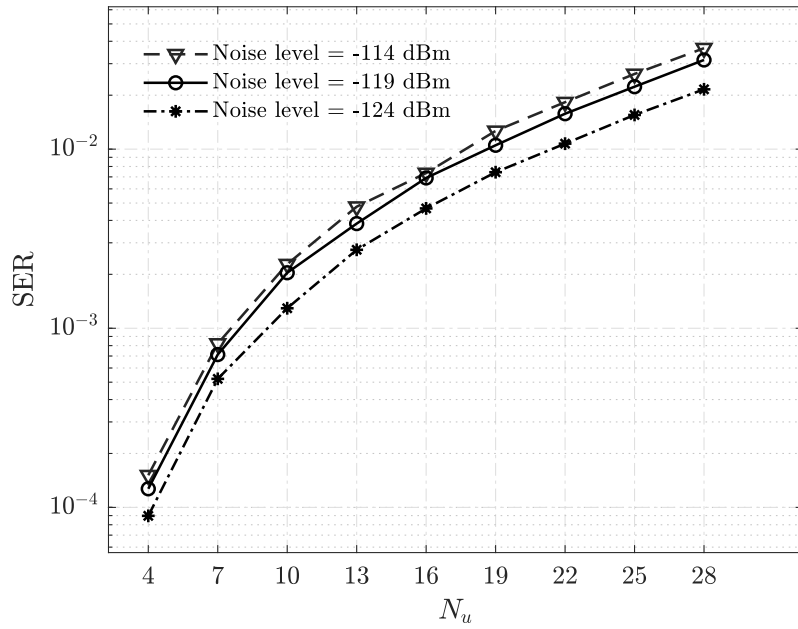
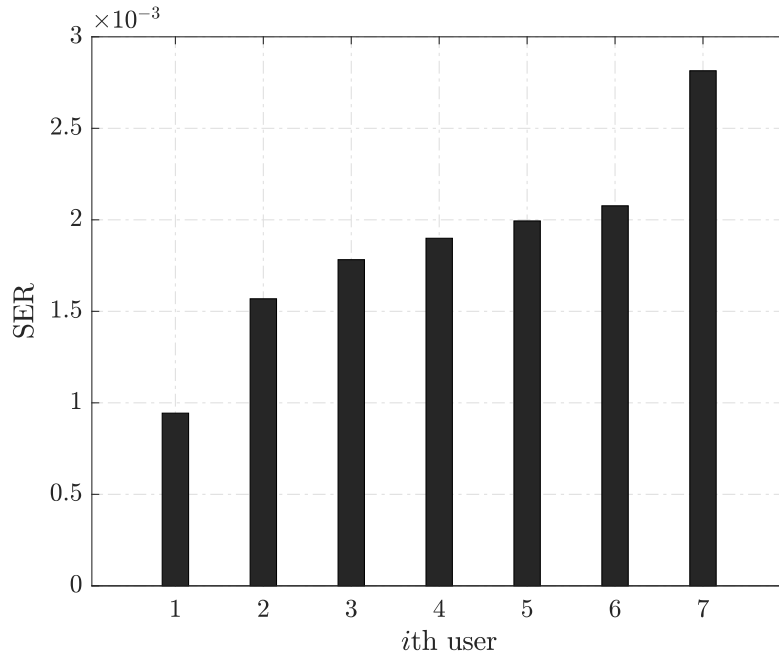
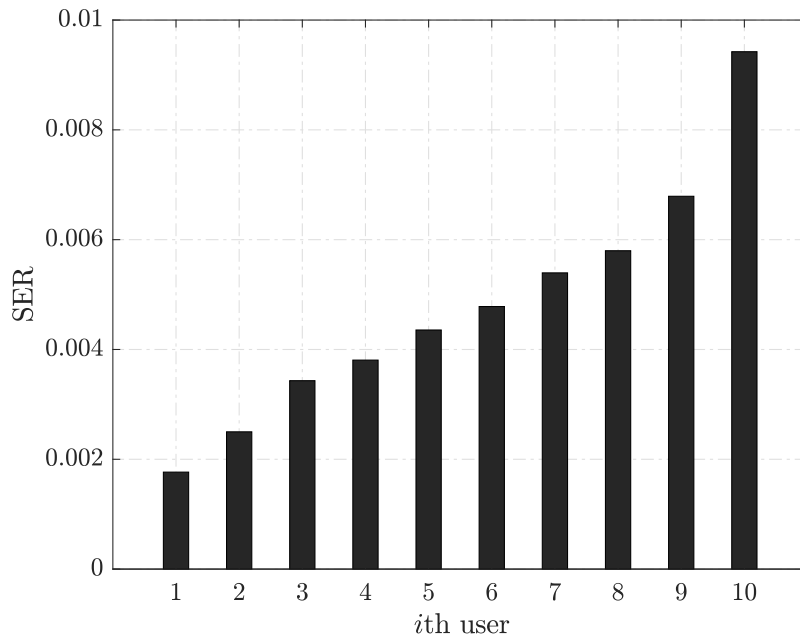
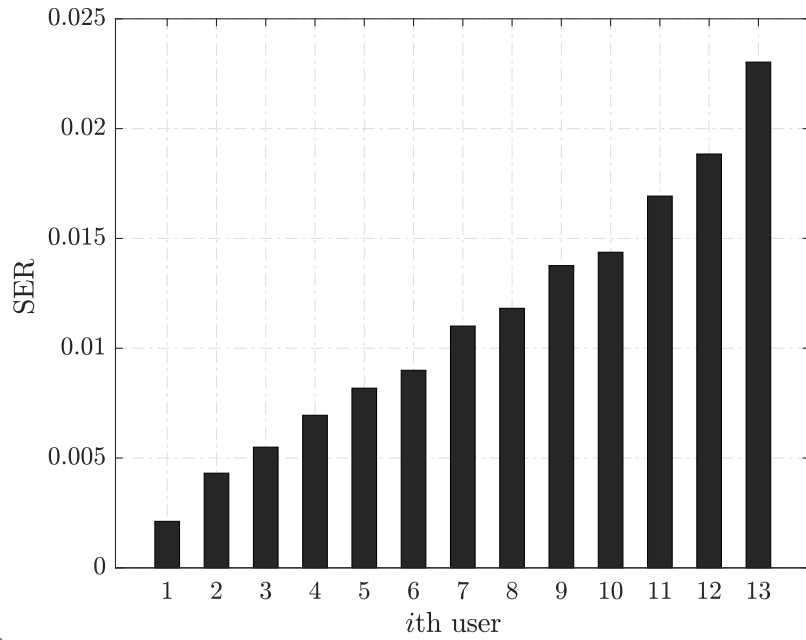
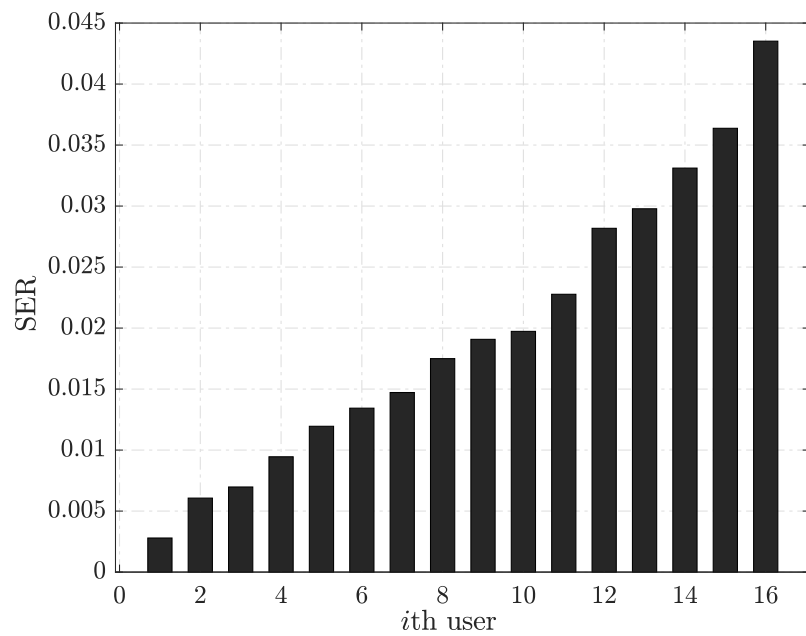


Figure 3.4: SER for different values of  $N_u$ , SF = 8,  $B = 250$  kHz.

performance of the 10 users using SF = 8 degrades when the number of interfering users with a different SF gets larger. We also notice that the shorter SF (9) impacts more than, the longer ones.

(a)  $N_u = 7$ (b)  $N_u = 10$ Figure 3.5: SER of each users for SF = 8,  $B = 250$  kHz, Noise level of  $-114$  dBm.

(c)  $N_u = 13$ (d)  $N_u = 16$ Figure 3.5: SER of each users for SF = 8,  $B = 250$  kHz, Noise level of  $-114$  dBm.

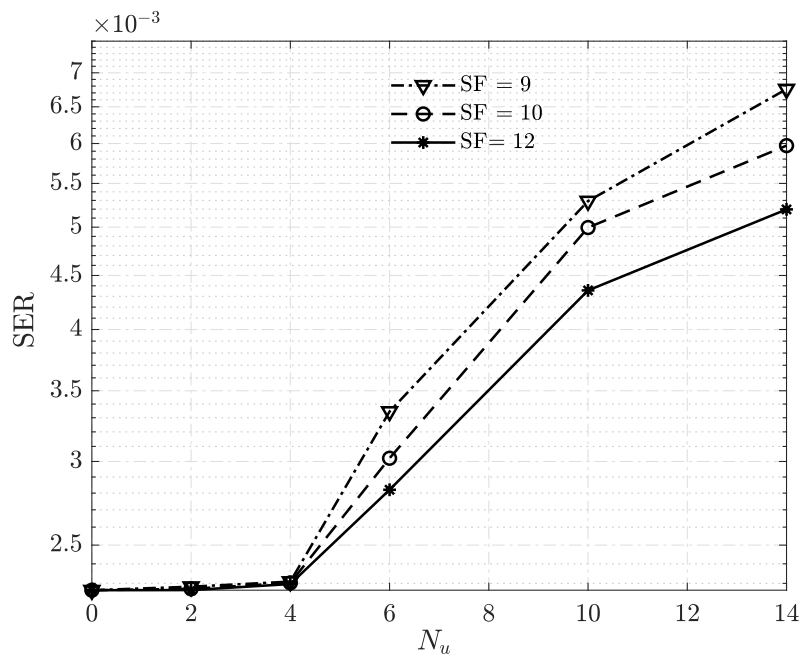


Figure 3.6: SER of Fixed 10 users using SF = 8 and additional interfering users using different SF (9, 10, 12),  $B = 250$  kHz, Noise level of  $-114$  dBm.

## 3.2 Single User Detection: Deep learning-based

In this section, the main focus is to design a single user detector for LoRa-like networks. Generally, in LoRa, when a collision occurred at the receiver, it results in packet loss [81]. Sometimes, one packet can be correctly decoded despite the collision due to a capture effect. It can be achieved when the desired signal is sufficiently stronger than the interfering one. Such results have been presented in LoRa communications in [82]. However, an interleaved chirp spreading (ICS) modulation scheme is used, which is not directly backward compatible with the standard LoRa. This principle is also used in serial interference cancellation schemes. In [47], the strongest user can be decoded, then suppressed, and the second strongest can, in turn, be decoded. The capture effect is also used in [45], where two superposed signals, synchronized or slightly desynchronized, can be decoded using timing information. However, ensuring synchronization is not realistic in the uplink of wide-area networks.

Nevertheless, the capture effect requires a sufficient power gap between the desired and the interfering signal. This section proposes two schemes based on deep learning that significantly improve the receiver's ability to correctly retrieve a signal, even when an interfering user is present. In the literature, some works employ the deep learning approach for IoT networks [83, 84], but not for signal detection. To our knowledge, there are no works yet that investigate detection in that context using deep learning.

The contributions are three-fold:

1. Designing two new receivers based on deep learning for detection in LoRa networks. The first one deals with *bit* detection with a regression approach, as in [85] for the OFDM context, and the second one deals with *symbol* detection with a classification approach. These receivers can cope with interference coming from other LoRa users, and both strongly improve the capture effect compared to the classical LoRa receiver;
2. It is shown that, once they have information on the power levels, the designed receivers are further efficient, mainly if the interfering users are stronger than the user to be decoded; and
3. The outstanding performance of the new receivers is achieved while maintaining an efficient complexity order.

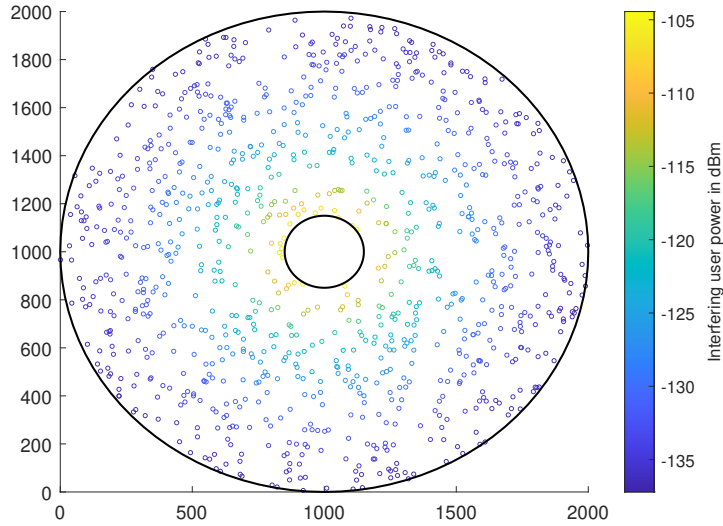


Figure 3.7: Uniform distribution of interfering user around the gateway. There exist no interfering devices within the radius of the guard-zone.

The rest of this section is organized as follows. Subsection 3.2.1 describes the system model, 3.2.2 presents the proposed deep learning-based receivers, and 3.2.3 shows simulation results and discussions.

### 3.2.1 System Model

A circle of radius  $r_{max}$  with one gateway located at the center is considered, including a user-free guard-zone around the gateway with radius  $r_{min}$ , see Fig. 3.7. We assume  $N_i$  interfering users are using the same SF.  $N_i$  is randomly drawn from a Poisson distribution with parameter  $\lambda$ . The 2D coordinates of the  $N_i$  interfering users are uniformly distributed while considering only positions within the disc defined by  $r_{max}$  and  $r_{min}$ . Since different devices operate autonomously, the transmission between nodes is asynchronous.

The collision between the  $p$ th symbol of the selected user  $j$  and two consecutive symbols of an interfering user  $i$  is illustrated in Fig. 3.8. The interfering part of user  $i$  is denoted by  $x_{q,interf}^{(j,i)}$ . The delay between user  $j$  and user  $i$  (accounting for asynchronous transmissions between the nodes) is  $\Delta^{(j,i)}$ .

The synchronization is carried out as follows: a correlation is first performed between the received signal and preamble. Then the highest peak of the correlation is selected,

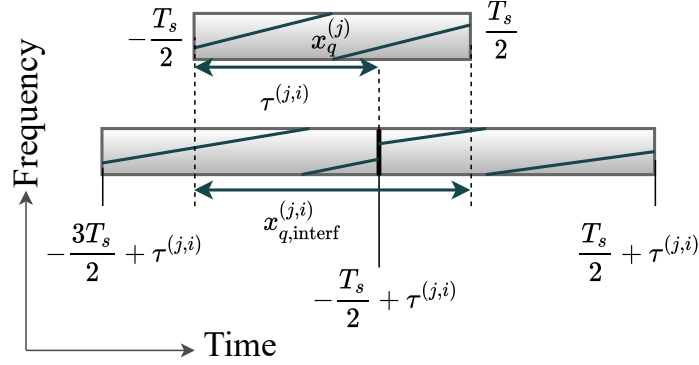


Figure 3.8: Collision between a symbol of selected user and two consecutive symbols of the interfering user.

and the received signal is synchronized on it. The user corresponding to this peak is the selected user to be decoded, indexed by  $j$ . The received signal associated with symbol  $q$  of user  $j$  sampled at  $t = nT$ ,  $n = 0, \dots, M - 1$  is:

$$r_q[n] = h^{(j)} x_q^{(j)}[n] + \sum_{i \in \mathcal{I}} h^{(i)} x_{q,interf}^{(j,i)}[n] + w_q[n], \quad (3.8)$$

where  $x_q^{(j)}[n] = x_q^{(j)}(nT)$ ,  $\mathcal{I}$  is the set of interfering users ( $|\mathcal{I}| = N_i$ ) and  $w_q[n] \sim \mathcal{CN}(0, \sigma^2)$  is a circularly symmetrical complex Gaussian noise.  $h^{(j)}$  and  $h^{(i)}$  are the channel coefficients for users  $j$  and  $i$ , respectively.

To demodulate, the classical LoRa receiver first multiplies the samples of the received signal by the conjugate of the raw chirp, yielding  $y_q[n] = r_q[n]c^*[n]$ , where  $c^*[n] = c^*(nT)$ . Then, a FFT is applied:

$$Y_q[k] = \sum_{n=0}^{M-1} y_q[n] e^{-2i\pi \frac{nk}{M}}, \quad k = 0, \dots, M - 1. \quad (3.9)$$

The symbol  $m_q^{(j)}$  is estimated by searching for the frequency index where the modulus of (3.9) is maximum. However, collisions occur when multiple users transmit simultaneously using the same SF, yielding possible detection errors.

### 3.2.2 Deep Learning-based Receiver

This section presents two receivers based on Deep Feedforward Neural Network (DFNN) and a convolutional neural network (CNN).

### 3.2.2.1 Deep Feedforward Neural Network-based receiver

As indicated in Fig. 3.9, the detector relies on a DFNN architecture with four hidden layers. The number of nodes in each hidden layer is  $8M$ ,  $4M$ ,  $2M$ , and  $M$ . The input is the modulus of the de-chirped received samples after the FFT (3.9), yielding  $M$  input nodes. The output is the bits of the transmitted symbol, yielding SF output nodes. The ReLU function is used as the activation function in the hidden layers. The sigmoid function is applied to map the outputs to the interval  $[0, 1]$  in the output layer. Batch normalization (BN) is embedded in the hidden layers to prevent overfitting. The DFNN is trained so that the error between the outputs and the transmitted bits is minimized. The error is evaluated through the  $L_2$  mean squared error function. Then, the detected bits are obtained by thresholding the outputs. For the sigmoid function, the corresponding threshold is 0.5.

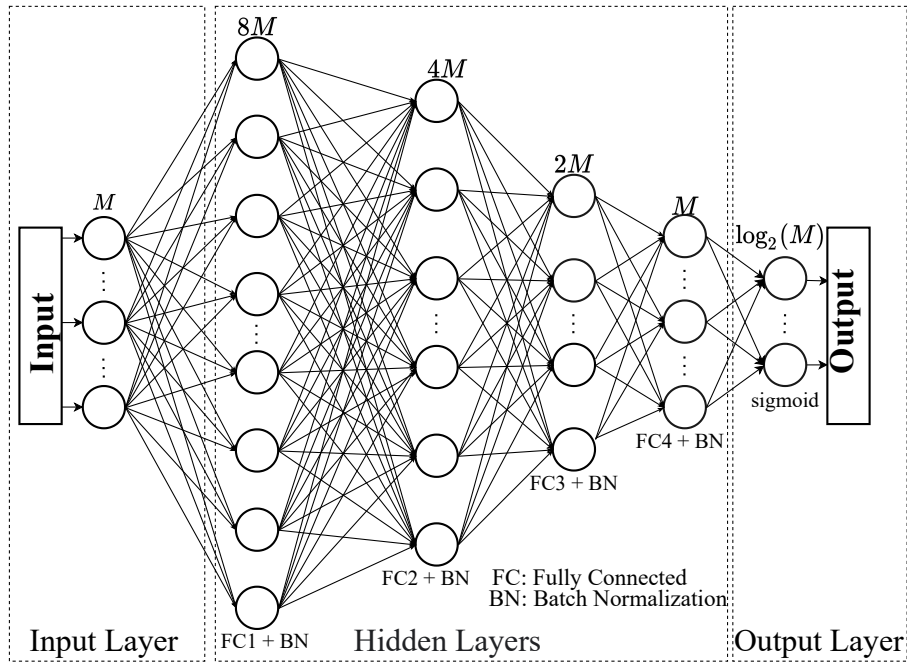


Figure 3.9: Deep Feedforward Neural Network architecture.

### 3.2.2.2 Convolutional Neural Networks-based receiver

Differently from the common feedforward architecture, CNN relies mainly on convolution operations within the so-called convolutional layers. For this architecture, the input is an  $M \times M$  image containing the modulus plots of (3.9), as illustrated in Fig. 3.10. The  $M$  nodes at the output layer correspond to the  $M$  symbols to be

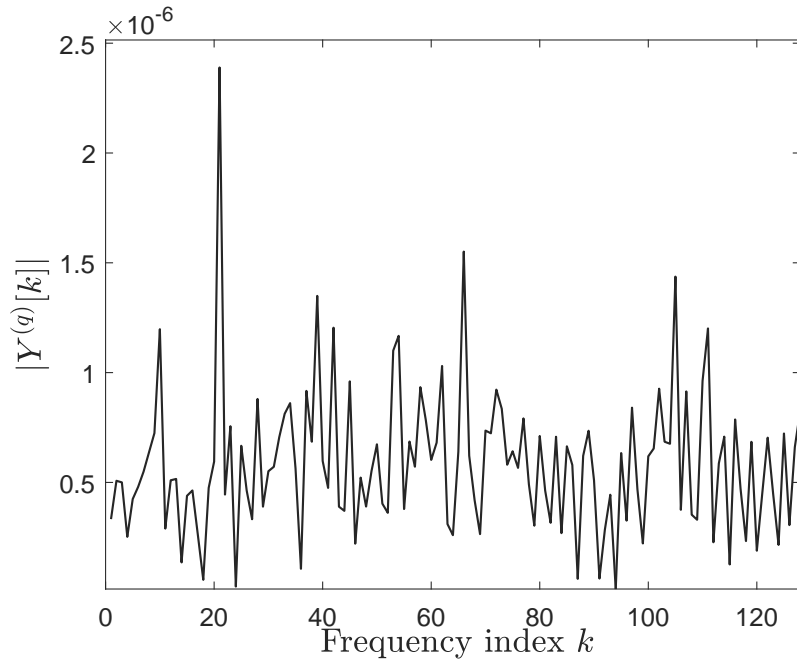


Figure 3.10: Plot of  $|Y_q[k]|$  ( $k = 0, \dots, M - 1$ ) for a symbol of  $m_q = 20$  with  $\text{SNR} = -10$  dB and  $\text{SF} = 7$ .

detected. Here, we use a structure that includes two convolutional layers and two fully connected layers (cf. Fig. 3.11).

We set  $M/4$  and  $M/2$  kernels for the first and second convolutional layers, respectively. The kernel size is set to  $4 \times 4$  for both layers. A pooling layer follows convolution steps to reduce the feature map's dimension while keeping the most relevant information. The filter used for the average pooling layer is of size  $2 \times 2$ , and the stride is 2. The output of the second pooling layer is flattened to be the input of the fully connected layer. The first fully connected layer has  $4M$  nodes and the second one has  $2M$  nodes. Similarly to the DFNN, the ReLU function is used as the activation function, and batch normalization is performed. For the output classification layer, we employ the softmax function. The CNN is trained to minimize the cross-entropy loss between the output and the transmitted symbols.

### 3.2.3 Results

In this section, we provide simulation results to evaluate the proposed DFNN and CNN-based receivers' performance. For the LoRa modulation, the bandwidth  $B =$

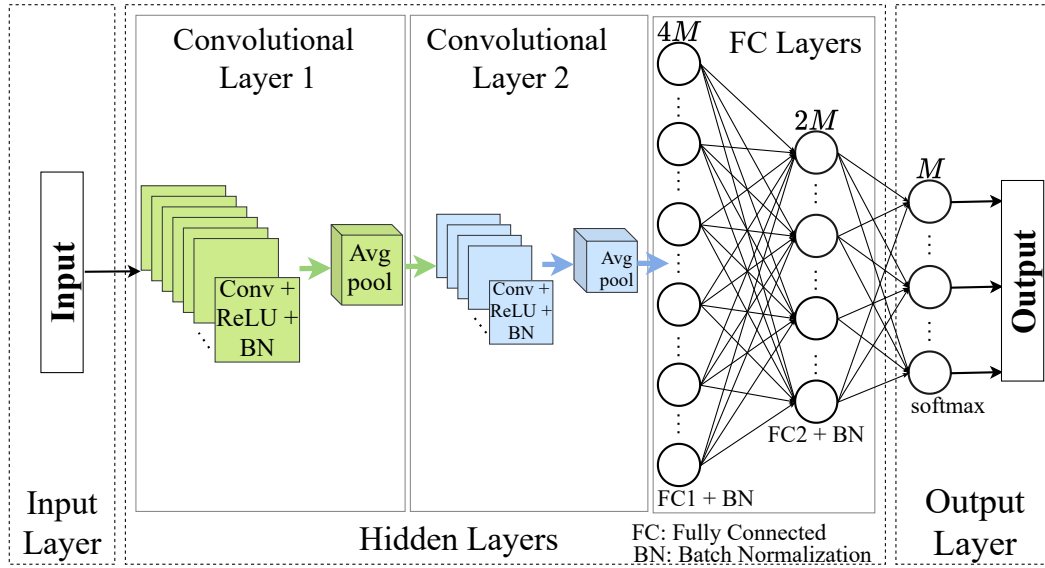


Figure 3.11: Convolutional Neural Network architecture.

250 kHz is considered, with  $SF = 7$ , yielding  $M = 128$ .  $r_{max}$  and  $r_{min}$  are set to 1 km and 200 m, respectively. The proposed detectors are compared with the classical LoRa detector in terms of symbol error rate (SER).

In the following, first, we present results where  $N_i$  is a random variable. Then, in order to investigate the capture effect, the number of interfering users is forced to one ( $N_i = 1$ ). Capture effect is the receiver's ability to decode one out of two (or more) colliding users correctly, usually the strongest one but not necessarily with the proposed receiver.

### 3.2.3.1 Results for $N_i \sim \mathcal{P}(\lambda)$

As described in section 3.2.1, the total number of interfering users  $N_i$ , in the time interval of interest, is drawn from a Poisson distribution, i.e.,  $N_i \sim \mathcal{P}(\lambda)$ , with the following values for  $\lambda$ : 0.25, 0.5, and 0.7. Training and test are done for each (SNR,  $\lambda$ ) couple. Note that LoRa receivers can estimate the SNR. Results are presented in Fig. 3.12. As a lower bound, the case when there is no interfering user, i.e.,  $\lambda = 0$ , is considered (gray curves). It is shown that the proposed receivers have better performance compared to the classical LoRa one for  $\lambda \neq 0$ . For  $\lambda = 0$ , the SER of the CNN is close to that of the classical LoRa receiver, whereas the DFNN is not as efficient with a 2 dB penalty for a target SER of  $10^{-4}$ .

For the lowest number of interfering users ( $\lambda = 0.25$  and  $0.5$ ), the SER of the two proposed receivers is in the order of  $10^{-3}$  for  $\text{SNR} = -7.5$  dB (cf. Figs. 3.12a and 3.12b). For the same SNR value, in the case of the higher number of interfering users ( $\lambda = 0.7$ ), the SER of the CNN-based receiver remains in the order of  $10^{-3}$  whereas the SER of the other receivers degrades (cf. Fig. 3.12c and 3.12d). Besides, as the number of interfering users increases, the classic LoRa receiver endures higher performance loss than the CNN-based receiver.

### 3.2.3.2 Capture Effect – $N_i = 1$

The goal is now to analyze the impact of one interfering user with different levels of signal-to-interference ratio (SIR). This is done by generating a new test set for which  $N_i$  is forced to one and testing the previously trained networks with this specific test set. The one that was trained for the ( $\lambda = 0.25$ ,  $\text{SNR} = -6$  dB) couple is considered. Fig. 3.13 plots the obtained SER as a function of the SIR (solid line). Additionally, as a perspective, we also investigate what would happen if the SIR could be estimated at the receiver. To do so, we do a new training of the networks for the different (SIR,  $\text{SNR} = -6$  dB) couples with  $N_i = 1$ , and we use the appropriate network for the test. Clearly, in this context, the deep learning-based approaches outperform the classical receiver for  $\text{SIR} \leq 4$  dB.

When  $\text{SIR} > 0$  dB, that is, the selected user's signal is the strongest, the capture effect happens for all receivers while being improved for the CNN-based receiver when the SIR is under 6 dB. However, when  $\text{SIR} < 0$  dB, i.e., the interfering user is the strongest, performance can be further improved if we have information on the SIR, i.e., learning is performed given the SIR value. In fact, when the SIR is known, the deep learning-based approach makes it possible to distinguish between the two users based on their power level, unless there is ambiguity, i.e.,  $\text{SIR} = 0$  dB.

### 3.2.3.3 Computational complexity

The computational complexity of the classical LoRa receiver is of  $\mathcal{O}(M \log(M))$  [67]. For the DFNN-based receiver, the complexity results in  $\mathcal{O}(M^2)$ . Based on [86], where the complexity order for the convolutional layers is derived, the overall complexity of the CNN-based receiver is also of  $\mathcal{O}(M^2)$ . Even though the proposed receivers and the classical LoRa receiver have different complexity orders, the proposed schemes' running time remains polynomial. According to [87], one of the definitions for computational efficiency is the following: “an algorithm is efficient if it has a polynomial

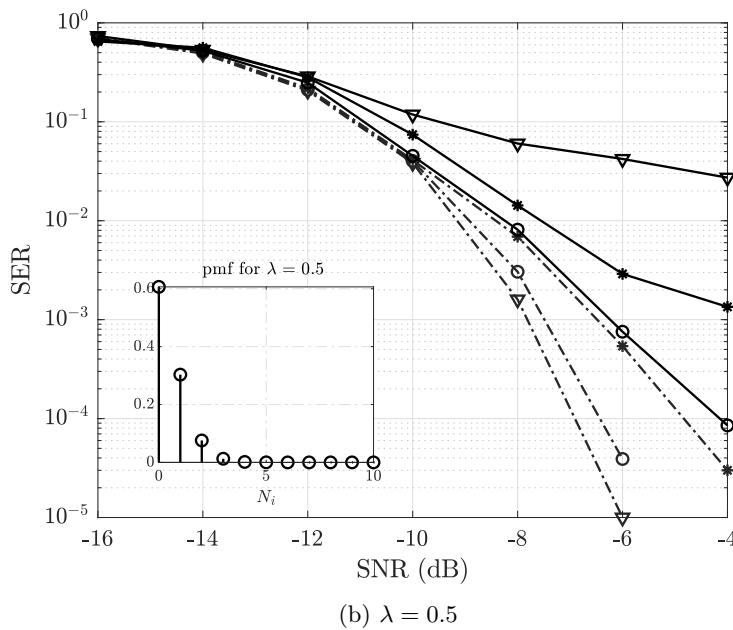
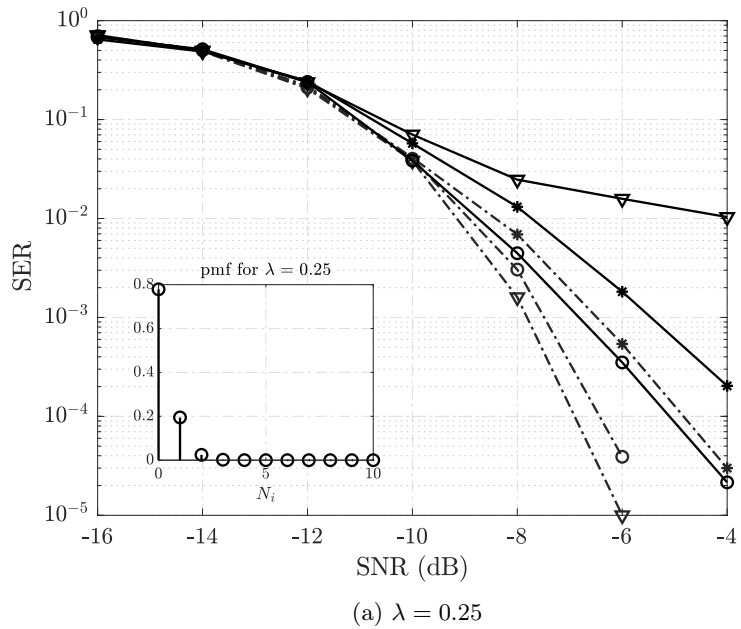


Figure 3.12: Symbol error rate as a function of the SNR for different detection approaches: classical decoder [ $\nabla$ ], DFNN-based [ $*$ ], and CNN-based [ $\circ$ ]. For all figures, two scenarios are considered: no possible interference (plots in dash-dot line [---]) and when interference can happen (plots in solid line [—]). The plot inside show the probability mass function (pmf) related to the number of interfering users.

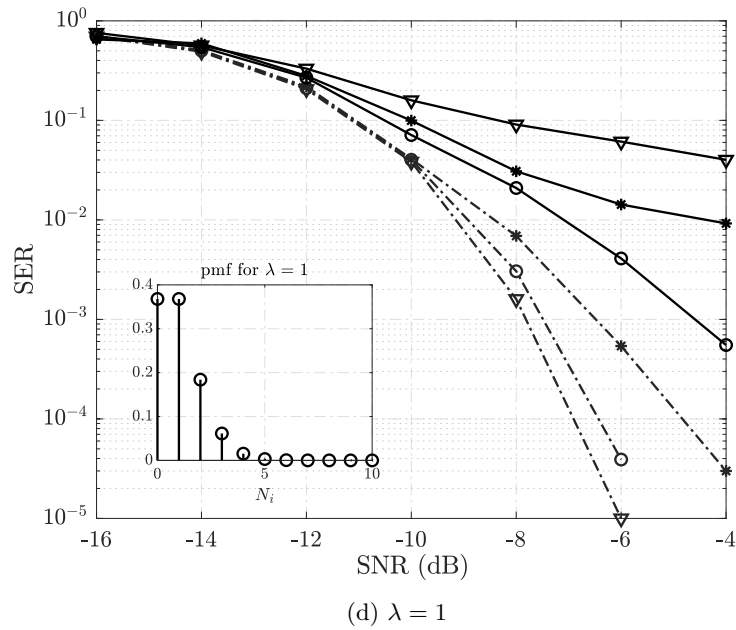
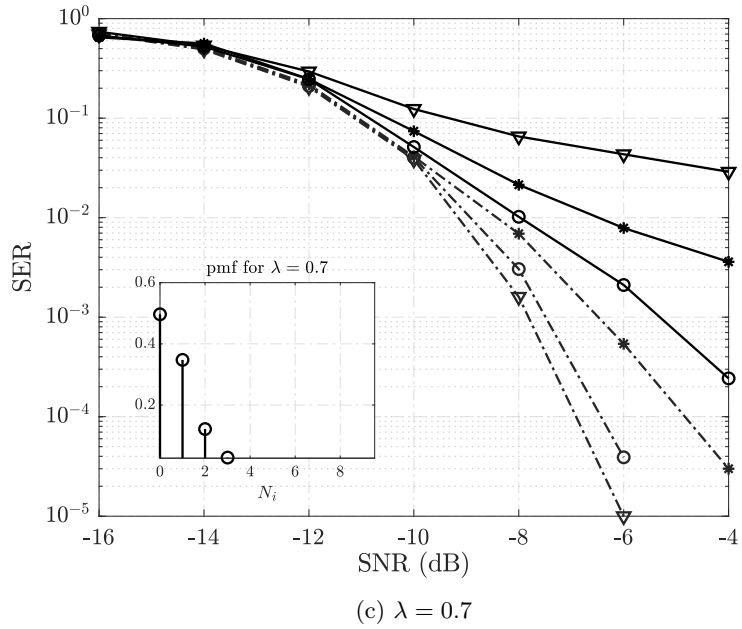


Figure 3.12: Symbol error rate as a function of the SNR for different detection approaches: classical decoder [ $\nabla$ ], DFNN-based [ $*$ ], and CNN-based [ $\circ$ ]. For all figures, two scenarios are considered: no possible interference (plots in dash-dot line [-.-]) and when interference can happens (plots in solid line [—]). The plot inside show the probability mass function (pmf) related to the number of interfering users.

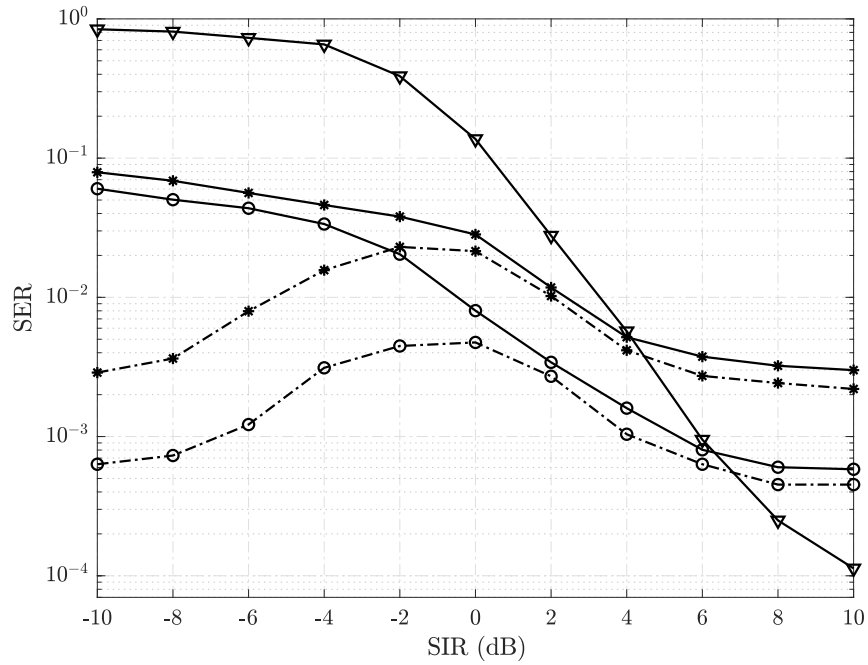


Figure 3.13: SER as a function of the SIR for the classical detector [▽], the DFNN-based [\*], and the CNN-based [○]. The SNR for the selected user is set to  $-6$  dB. Two different cases are considered: networks trained for  $\lambda = 0.25$  [—], networks trained for each SIR value [---].

running time”.

## Conclusion

Scalability is a major concern in IoT networks and actual deployed solutions cannot face it. However, due to the star topology of LP-WANs, complexity can be added at the receiver to improve the system performance, without modifying the low consumption transmission scheme. It allows us to propose a serial interference cancellation scheme for chirp spread spectrum based physical layer. Assuming uncoordinated transmitting devices, we use the power-domain NOMA idea to recover multiple signals arriving simultaneously, on the same bandwidth and with the same SF. The diversity in received powers is ensured by the random radio channels faced by the devices. A SIC receiver allows then to recover the multiple signals. The proposed solution allows to support 20 times more devices without any modification of the transmission scheme. This is attained with a first simple implementation of the SIC and further improvement can certainly be obtained with a judicious choice of the PHY layer parameters.

This chapter also investigated a deep learning-based approach for LoRa-like networks to decode a selected user's signals while considering interfering users that transmit simultaneously over the same frequency channel with the same SF. From the simulation results, we observed that in terms of SER, the two proposed receivers, the DFNN-based and the CNN-based, outperform the classical LoRa decoder in the presence of interference. In the absence of interference, the CNN-based receiver performs closely to the classical LoRa receiver, which is the optimal receiver for the interference-free case. However, the DFNN-based receiver has endured a slight loss in performance, e.g., a 2 dB penalty in SNR for a target SER of  $10^{-4}$ . The good performance shown by the proposed schemes is achieved while keeping an efficient complexity order, i.e., a polynomial running time of order two. For the future, the deep learning-based approach seems to be a promising candidate to tackle the issue of interference in LoRa networks due to the exponential growth of connected devices. In addition to improving the capture effect, i.e., decoding the selected user when its power is higher than that of the interference, we have shown that the deep-learning-based approach makes it possible to decode the selected user when it is weaker than the interference. This requires information on the SIR. As a perspective, an SIR estimation technique could be combined with the deep learning-based decoder to improve the receiver's performance further.



# Conclusion and Perspectives

In Internet of Things (IoT) networks, scalability is a significant issue, and current solutions cannot deal with it. In this thesis, different solutions are proposed to enhance the scalability of LoRa-like networks in both downlink and uplink communication.

To address the downlink's scalability limitations caused by the duty cycle, we introduce a new joint multiuser receiver for downlink LoRa-like networks. Although our approach is based on power-domain Non-Orthogonal Multiple Access (NOMA), it does not require a Serial Interference Cancellation (SIC) receiver. As a result, we avoid the NOMA constraint caused by the residue after each cancellation step. The low-cost end devices that cannot handle high computational complexity are other concerns for employing NOMA in IoT. The Maximum Likelihood (ML) cannot be applied since it does not provide an analytical solution. We presented a suboptimal Cross-Entropy Method (CEM) based method that is efficient but too complicated. As a result, we developed a simpler approach for resolving collisions while maintaining a low level of complexity. We showed that instead of transmitting a single packet each time slot, we could transmit more than ten packets, if not more, while keeping the symbol error rate below  $10^{-3}$ . This is achieved without using error-correcting codes.

In uplink communication, due to the LPWANs' star topology, the receiver can be complex to improve the system performance without modifying the low consumption transmission scheme. As a result, we propose a SIC technique for the physical layer based on the chirp spread spectrum. We apply the power-domain NOMA approach to recover numerous signals received simultaneously, over the same bandwidth, using the same SF, and assuming uncoordinated transmitting devices. The devices' received power varies according to the random radio channels they encounter. Multiple signals can be recovered using a SIC receiver. Without modifying the transmission system, the proposed method can handle 20 times more devices. This is obtained

with a simple SIC implementation, and additional improvement can be achieved with a proper choice of PHY layer settings.

Finally, we studied a deep learning-based technique for LoRa-like networks to decode a single user's signal while taking into account interfering users that transmit over the same frequency channel, with the same SF at the same time. In the presence of interference, the two proposed receivers, the DFNN-based and the CNN-based, outperform the classical LoRa decoder in terms of SER, according to the simulation findings. In the absence of interference, however, the CNN-based receiver performs similarly to the traditional LoRa receiver, which is the optimal decoder in the interference-free scenario. The DFNN-based receiver has sustained slight performance loss, such as a 2 dB SNR penalty for a target SER of  $10^{-4}$ . The proposed methods achieve good performance while maintaining an efficient complexity order, i.e., a polynomial running time of order two. As a result, the deep learning-based technique appears to be a potential choice for addressing interference issues in LoRa networks that have arisen due to the exponential increase of connected devices. We have demonstrated that, in addition to improving the capture effect, i.e., decoding the useful user when its power is higher than the interference, the deep-learning-based technique also allows us to decode the useful user when its power is less than the interference. This requires information on the signal-to-interference ratio (SIR).

## Perspectives

This thesis proposes different receivers which can increase LoRa-like networks' scalability and cope with co-spreading factor interference from other LoRa users. In the future, the extension of the work in this thesis can be from several perspectives and can be summarized as follows:

1. As demonstrated in Chapter 2, different power allocation strategies have distinct impacts on the overall system performance. Two power allocation schemes are proposed; the first one helps suppress ambiguities when collisions occur, and the other one increases fairness between users. As a result, to optimize signal detection performance even further, this work may be extended to identify a better trade-off between the two power allocation approaches that can minimize ambiguities when collisions occur while also increasing user fairness.
2. In this thesis, it is mentioned that the achieved performance is without the use of error-correcting codes. Therefore, another perspective to improve the

performance is to implement error-correcting codes. In LoRa, Forward error correction (FEC) techniques are used to further increase receiver sensitivity, and FEC schemes can add redundant bits to the valuable information using Hamming codes to correct the errors [42].

3. The findings in section 3.2.3.2 showed that the signal detection performance could be enhanced if the information about the SIR is provided. For LoRa-like networks where resources are shared dynamically among users, SIR estimation is critical. As a result, the SIR estimation technique in [88] could be combined with the proposed deep learning-based decoders to further improve the receiver's signal detection performance.
4. In LoRa, the signal is transmitted under the noise level, meaning with a low SNR value. The proposed receivers in section 3, specifically the convolutional neural network (CNN)-based receiver, can be more efficient if we can manage to reduce the received signal's noise level. Thus, a denoising auto-encoder can be combined with CNN to denoise the received signals before further processing, enabling CNN to extract better features for classification. Subsequently, the signal detection performance can be optimized.
5. In this study, we considered only interference only coming from other LoRa users. Finally, we can extend the analysis by considering interference from other IoT networks such as Sigfox, Zigbee.



## Appendix A

# Appendix related to Down-link Communication in LoRa

### A.1 Power allocation 2

Let us consider  $N$  users with estimated channels  $\hat{h}^{(i)}$ ,  $i = 1, \dots, N$  order from the weakest to the strongest channel:  $|\hat{h}^{(1)}| < |\hat{h}^{(2)}| < \dots < |\hat{h}^{(N)}|$ . We note  $\hat{h}^{(0)} = 0$ . We want that whatever the receiver  $j$ , the gap between the peak amplitudes of user  $j$  and  $j - 1$  is always the same,  $c$ . We denote  $p_t$  the total transmit power. We write  $h^{(i)} = |\hat{h}^{(i)}|$  for the rest of this annex for lighter expressions. We want:

$$\left\{ \begin{array}{l} h^{(1)}\sqrt{p^{(1)}} - 0 = c \\ h^{(2)}\sqrt{p^{(2)}} - h^{(2)}\sqrt{p^{(1)}} = c \\ \vdots \\ h^{(N)}\sqrt{p^{(N)}} - h^{(N)}\sqrt{p^{(N-1)}} = c \\ p^{(1)} + p^{(2)} + p^{(3)} + \dots + p^{(N)} = p_t \end{array} \right.$$

We note

$$A_i = \sum_{j=1}^i \frac{1}{(h^{(j)})^2}, \quad (\text{A.1})$$

Starting with the weakest user ( $i = 1$ ) we have

$$p^{(1)} = \left( \frac{c}{h^{(1)}} \right)^2 = c^2 A_1, \quad (\text{A.2})$$

If we assume

$$p^{(l)} = c^2 A_l, \quad (\text{A.3})$$

then from

$$h^{(l+1)}\sqrt{p^{(l+1)}} - h^{(l+1)}\sqrt{p^{(l)}} = c, \quad (\text{A.4})$$

and using (A.3), we have

$$\begin{aligned} \sqrt{p^{(l+1)}} &= \frac{c}{h^{(l+1)}} + \sqrt{p^{(l)}}, \\ &= c \left( \frac{1}{h^{(l+1)}} + \sum_{j=1}^l \frac{1}{h^{(j)}} \right), \\ &= c \left( \sum_{j=1}^{l+1} \frac{1}{h^{(j)}} \right), \\ &= c\sqrt{A_{l+1}}. \end{aligned} \quad (\text{A.5})$$

which proves that (A.3) is true for all  $i = 1, \dots, N$ .

We then use the final equation in (A.1)

$$P_t = \sum_{j=1}^N p^{(j)} = c^2 \sum_{j=1}^N A_j, \quad (\text{A.6})$$

which gives

$$c = \sqrt{\frac{p_t}{\sum_{j=1}^N A_j}}. \quad (\text{A.7})$$

We finally obtain  $p^{(l)} = p_t \frac{A_l^2}{\sum_{i=1}^N A_i^2}$  which is (2.19).

## Appendix B

# Appendix related to Up-link Communication in LoRa-like Networks

### B.1 Chirp Formulation

A chirp (up or down) over the entire  $T_s$  is regarded as a raw chirp and its instantaneous frequency is given by  $f(t) = \frac{B}{T_s}t$ . Its baseband expression is:  $c(t) = e^{j2\pi\frac{B}{2T_s}t^2}$  for  $t \in [-\frac{T_s}{2}, \frac{T_s}{2}]$ . Let's consider multiple users in the network. For the  $i$ th user the instantaneous frequency of the chirp transmitted at time  $qT_s$  is defined as the derivative of the phase  $\vartheta_q^{(i)}(t)$ :  $f_q^{(i)}(t) = \frac{1}{2\pi} \frac{d\vartheta_q^{(i)}(t)}{dt}$ . We denote the transmit symbol of the  $i$ th user at time  $qT_s$  as  $m_p^{(i)} \in \{0, \dots, M-1\}$ . Information is carried by performing a cyclic shift of the up-chirp and the position of the shift depends on the symbol value. Delaying the frequency ramp of the chirp by  $\tau_q^{(i)} = m_q^{(i)}/B$  will give us the coded chirp as it shown in Fig. 1.5, where  $\tau_q^{(i)}$  is the time shift that corresponds to the  $q$ th symbol. The coded chirp of the  $q$ th symbol of user  $i$  is:

$$\vartheta_q^{(i)}(t) = \begin{cases} 2\pi\left(\frac{B}{2T_s}t^2 + \frac{m_q^{(i)}}{T_s}t\right), & \text{for } t \in \left[-\frac{T_s}{2}, \frac{T_s}{2} - \tau_q^{(i)}\right), \\ 2\pi\left(\frac{B}{2T_s}t^2 + \left(\frac{m_q^{(i)}}{T_s} - B\right)t\right), & \text{for } t \in \left[\frac{T_s}{2} - \tau_q^{(i)}, \frac{T_s}{2}\right]. \end{cases} \quad (\text{B.1})$$

The complex envelope of the transmitted signal of the  $i$ th user,  $x^{(i)}(t)$ , can be written as:

$$x^{(i)}(t) = \sum_{p=0}^Q x_q^{(i)}(t - qT_s) = \sum_{q=0}^Q e^{j\vartheta_q^{(i)}(t - qT_s)}. \quad (\text{B.2})$$

where  $x_q^{(i)}(t) = e^{j\vartheta_q^{(i)}(t)}$ , and  $Q$  is the transmitted symbols of user  $i$  inside a packet.

Assume that the users transmit simultaneously their data using the same spreading factor. As a result a collision occurs between the  $q$ th symbol of the user of interest  $j$  and two consecutive symbols of other user  $i$  as shown in Fig. B.1.  $x_q^{(j)}$  is the symbol of the user  $j$  we try to decode.  $x_{q,1}^{(j,i)}$  and  $x_{q,2}^{(j,i)}$  are the two consecutive symbols from the  $i$ th user that are interfering with user of interest  $j$ . The delay between the user of interest  $j$  and  $x_{q,1}^{(j,i)}$  is denoted by  $\Delta^{(j,i)}$ . The interference from user  $i$  in  $x_q^{(j)}$  is the combination of the interference from two successive symbols,  $x_{q,1}^{(j,i)}$  and  $x_{q,2}^{(j,i)}$ , carrying their own information defined by the shifts  $\tau_{q,1}^{(j,i)} = m_{q,1}^{(j,i)}/B$  and  $\tau_{q,2}^{(j,i)} = m_{q,2}^{(j,i)}/B$ .

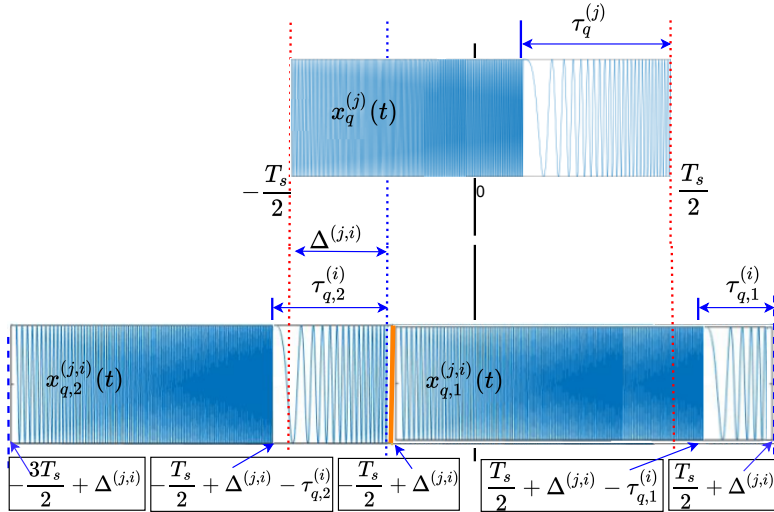


Figure B.1: Interfering symbols at the receiver.

$$x_{q,1}^{(j,i)}(t) = \begin{cases} \exp\left(2j\pi\left(\frac{B}{2T_s}t^2 + \left(\frac{m_{q,1}^{(i)} - B\Delta^{(j,i)}}{T_s}\right)t + \phi_{q,1}^{(j,i)}\right)\right), \\ \quad t \in A_{q,1} = \left[\frac{-T_s}{2} + \Delta^{(j,i)}, \frac{T_s}{2} + \Delta^{(j,i)} - \tau_{q,1}^{(i)}\right), \\ \exp\left(2j\pi\left(\frac{B}{2T_s}t^2 + \left(\frac{m_{q,1}^{(i)} - B\Delta^{(j,i)}}{T_s}\right)t + \phi_{q,1}^{(j,i)} - B(t - \Delta^{(j,i)})\right)\right), \\ \quad t \in B_{q,1} = \left[\frac{T_s}{2} + \Delta^{(j,i)} - \tau_{q,1}^{(i)}, \frac{T_s}{2}\right). \end{cases} \quad (\text{B.3})$$

$$x_{q,2}^{(j,i)}(t) = \begin{cases} \exp\left(2j\pi\left(\frac{B}{2T_s}t^2 + \left(\frac{m_{q,2}^{(i)} + B(T_s - \Delta^{(j,i)})}{T_s}\right)t + \phi_{q,2}^{(j,i)}\right)\right), \\ \quad t \in B_{q,2} = \left[\frac{-T_s}{2}, \frac{-T_s}{2} + \Delta^{(j,i)} - \tau_{q,2}^{(i)}\right), \\ \exp\left(2j\pi\left(\frac{B}{2T_s}t^2 + \left(\frac{m_{q,2}^{(i)} + B(T_s - \Delta^{(j,i)})}{T_s}\right)t + \phi_{q,2}^{(j,i)} - B(t + T_s - \Delta^{(j,i)})\right)\right), \\ \quad t \in A_{q,2} = \left[\frac{-T_s}{2} + \Delta^{(j,i)} - \tau_{q,2}^{(i)}, \frac{-T_s}{2} + \Delta^{(j,i)}\right). \end{cases} \quad (\text{B.4})$$

$$\text{where } \phi_{q,1}^{(j,i)} = \frac{B(\Delta^{(j,i)})^2 - 2m_{q,1}^{(j,i)}\Delta^{(j,i)}}{2T_s}, \text{ and}$$

$$\phi_{q,2}^{(j,i)} = \frac{B(T_s - \Delta^{(j,i)})^2 + 2m_{q,2}^{(j,i)}(T_s - \Delta^{(j,i)})}{2T_s}.$$

To formulate the mathematical expression for the interfering signals in Fig. B.1, we consider two conditions that define the positions of the shifts of the interfering symbols:

$$\begin{aligned} C_1: \frac{T_s}{2} + \Delta^{(j,i)} - \tau_{q,1}^{(j,i)} < \frac{T_s}{2}, \quad \text{and} \quad C_2: -\frac{T_s}{2} + \Delta^{(j,i)} - \tau_{q,1}^{(j,i)} > -\frac{T_s}{2} \\ C_1: \tau_{q,1}^{(j,i)} > \Delta^{(j,i)}, \quad \text{and} \quad C_2: \tau_{q,2}^{(j,i)} < \Delta^{(j,i)}. \end{aligned} \quad (\text{B.5})$$

The expression for the **first interfering symbol** of the  $i$ th user,  $x_{q,1}^{(j,i)}(t)$  is derived as:

$$x_{q,1}^{(j,i)}(t) = e^{j\vartheta_{p,1}^{(j,i)}(t)}, \quad \text{and} \quad \vartheta_{q,1}^{(j,i)}(t) = \vartheta_q^{(j)}(t - \Delta^{(j,i)}).$$

1) For  $t \in A_{q,1} = \left[ \frac{-T_s}{2} + \Delta^{(j,i)}, \frac{T_s}{2} + \Delta^{(j,i)} - \tau_{q,1}^{(j,i)} \right)$ , we have:

$$\begin{aligned}
 \vartheta_{q,1}^{(j,i)}(t) &= 2\pi \left[ \frac{B}{2T_s} (t - \Delta^{(j,i)})^2 + \frac{m_{q,1}^{(j,i)}}{T_s} (t - \Delta^{(j,i)}) \right] \\
 &= 2\pi \left[ \frac{B}{2T_s} (t^2 + (\Delta^{(j,i)})^2 - 2t\Delta^{(j,i)}) + \frac{m_{q,1}^{(j,i)}}{T_s} t - \frac{m_{q,1}^{(j,i)}}{T_s} \Delta^{(j,i)} \right] \quad (\text{B.6}) \\
 &= 2\pi \left[ \frac{B}{2T_s} t^2 + \left( \frac{m_{q,1}^{(j,i)}}{T_s} - B\Delta^{(j,i)} \right) t + \phi_{q,1}^{(j,i)} \right]
 \end{aligned}$$

2) For  $t \in B_{q,1} = \left[ \frac{T_s}{2} + \Delta^{(j,i)} - \tau_{q,1}^{(j,i)}, \frac{T_s}{2} \right]$ , we have:

$$\begin{aligned}
 \vartheta_{q,1}^{(j,i)}(t) &= 2\pi \left[ \frac{B}{2T_s} (t - \Delta^{(j,i)})^2 + \frac{m_{q,1}^{(j,i)}}{T_s} (t - \Delta^{(j,i)}) - B(t - \Delta^{(j,i)}) \right] \\
 &= 2\pi \left[ \frac{B}{2T_s} (t^2 + (\Delta^{(j,i)})^2 - 2t\Delta^{(j,i)}) + \frac{m_{q,1}^{(j,i)}}{T_s} t - \frac{m_{q,1}^{(j,i)}}{T_s} \Delta^{(j,i)} - B(t - \Delta^{(j,i)}) \right] \quad (\text{B.7}) \\
 &= 2\pi \left[ \frac{B}{2T_s} t^2 + \left( \frac{m_{q,1}^{(j,i)}}{T_s} - B\Delta^{(j,i)} \right) t + \phi_{q,1}^{(j,i)} - B(t - \Delta^{(j,i)}) \right]
 \end{aligned}$$

The expression for the **second interfering symbol** of the  $i$ th user,  $x_{q,2}^{(j,i)}(t)$  is derived as:

$$x_{q,2}^{(j,i)}(t) = e^{j\vartheta_{q,2}^{(j,i)}(t)}, \quad \text{and} \quad \vartheta_{q,2}^{(j,i)}(t) = \vartheta_q^{(j)}(t + T_s - \Delta^{(j,i)}).$$

1) For  $t \in B_{q,2} = \left[ \frac{-T_s}{2}, -\frac{T_s}{2} + \Delta^{(j,i)} - \tau_{q,2}^{(j,i)} \right)$ , we have:

$$\begin{aligned}
 \vartheta_{q,2}^{(j,i)}(t) &= 2\pi \left[ \frac{B}{2T_s} (t + T_s - \Delta^{(j,i)})^2 + \frac{m_{q,2}^{(j,i)}}{T_s} (t + T_s - \Delta^{(j,i)}) \right] \\
 &= 2\pi \left[ \frac{B}{2T_s} (t^2 + T_s^2 + (\Delta^{(j,i)})^2 + 2tT_s - 2T_s\Delta^{(j,i)} - 2t\Delta^{(j,i)}) \right. \\
 &\quad \left. + \frac{m_{q,2}^{(j,i)}}{T_s} (t + T_s - \Delta^{(j,i)}) \right] \\
 &= 2\pi \left[ \frac{B}{2T_s} t^2 + \left( \frac{m_{q,2}^{(j,i)}}{T_s} - B(T_s - \Delta^{(j,i)}) \right) t + \phi_{q,2}^{(j,i)} \right] \quad (\text{B.8})
 \end{aligned}$$

2) For  $t \in A_{q,2} = [-\frac{T_s}{2} + \Delta^{(j,i)} - \tau_{q,2}^{(j,i)}, -\frac{T_s}{2} + \Delta^{(j,i)}]$ , we have:

$$\begin{aligned}
\vartheta_{q,2}^{(j,i)}(t) &= 2\pi \left[ \frac{B}{2T_s} (t + T_s - \Delta^{(j,i)})^2 + \frac{m_{q,2}^{(j,i)}}{T_s} (t + T_s - \Delta^{(j,i)}) - B(t + T_s - \Delta^{(j,i)}) \right] \\
&= 2\pi \left[ \frac{B}{2T_s} (t^2 + T_s^2 + (\Delta^{(j,i)})^2 + 2tT_s - 2T_s\Delta^{(j,i)} - 2t\Delta^{(j,i)}) \right. \\
&\quad \left. + \frac{m_{q,2}^{(j,i)}}{T_s} (t + T_s - \Delta^{(j,i)}) - B(t + T_s - \Delta^{(j,i)}) \right] \\
&= 2\pi \left[ \frac{B}{2T_s} t^2 + \left( \frac{m_{q,2}^{(j,i)}}{T_s} - B(T_s - \Delta^{(j,i)}) \right) t + \phi_{q,2}^{(j,i)} - B(t + T_s - \Delta^{(j,i)}) \right]
\end{aligned} \tag{B.9}$$

## B.2 Received Signal and De-chirping

The received signal associated with the  $p$ th user symbol of the strongest user sampled at  $t = nT$ , where  $T = \frac{1}{B}$ , is:

$$y^{(j)}[n] = h^{(j)} \sqrt{p_e} x_q^{(j)}[n] + h^{(i)} \sqrt{p_e} (x_{q,1}^{(j,i)}[n] + x_{q,2}^{(j,i)}[n]) + w[n] \tag{B.10}$$

where  $y^{(j)}[n] \forall n \in [0, \dots, M-1]$ ,  $h^{(j)}$  and  $h^{(i)}$  are the channel coefficients of the user of interest and the interfering users respectively,  $w[n] \sim \mathcal{N}(0, \sigma_N^2)$  is a complex Gaussian noise, and  $p_e$  is the transmit power which is equal to all users.

To demodulate the samples of the received signal  $y^{(j)}[n]$  is multiplied by the conjugate of the raw chirp,  $c^*[n]$ , i.e.,  $r[n] = y^{(j)}[n]c^*[n]$  for all  $t = nT$ :

$$\begin{aligned}
r[n] &= y^{(j)}[n]c^*[n] \\
r[n] &= \underbrace{h^{(j)} \sqrt{p_e} x_q^{(j)}[n] e^{-j2\pi \frac{1}{2M} n^2}}_{\text{User of interest}} + h^{(i)} \sqrt{p_e} \left( \underbrace{x_{q,1}^{(j,i)}[n] e^{-j2\pi \frac{1}{2M} n^2}}_{\text{1st interfering symbol}} + \underbrace{x_{q,2}^{(j,i)}[n] e^{-j2\pi \frac{1}{2M} n^2}}_{\text{2nd interfering symbol}} \right) \\
&\quad + w[n] e^{-j2\pi \frac{1}{2M} n^2}
\end{aligned} \tag{B.11}$$

It should be noted that the intervals  $A_{q,l}$ ,  $B_{q,l}$  for  $l \in \{1, 2\}$  are given in (B.3) and (B.4), for  $t = nT$ ,  $T = \frac{1}{B}$ .

1. Selected user of interest,  $t = nT$ :

$$\begin{aligned}
x_q^{(j)}[n] \times c^*[n] &= e^{j2\pi \left( \frac{1}{2M} n^2 + \frac{m_q^{(j)}}{M} n \right)} e^{-j2\pi \frac{1}{2M} n^2} \\
&= e^{j2\pi \frac{m_q^{(j)}}{M} n} \mathbb{1}_{[-\frac{M}{2}, \frac{M}{2}-1]}[n].
\end{aligned} \tag{B.12}$$

2. 1st interfering symbol of user  $i$ :

$$\begin{aligned}
 \text{1st Part: } x_{q,1}^{(j,i)}[n] \times c^*[n] &= e^{j2\pi\left(\frac{1}{2M}n^2 + \left(\frac{m_{q,1}^{(j,i)} - B\Delta^{(j,i)}}{M}\right)n + \phi_{q,1}^{(j,i)}\right)} e^{-j2\pi\frac{1}{2M}n^2} \mathbb{1}_{[A_{q,1}]}[n] \\
 &= e^{j2\pi\phi_{q,1}^{(j,i)}} e^{j2\pi\left(\frac{m_{q,1}^{(j,i)} - B\Delta^{(j,i)}}{M}\right)n} \mathbb{1}_{[A_{q,1}]}[n]. \quad (\text{B.13})
 \end{aligned}$$

$$\begin{aligned}
 \text{2nd Part: } x_{q,1}^{(j,i)}[n] \times c^*[n] &= e^{j2\pi\left(\frac{1}{2M}n^2 + \left(\frac{m_{q,1}^{(j,i)} - B\Delta^{(j,i)}}{M}\right)n + \phi_{q,1}^{(j,i)} - B\left(\frac{n}{B} - \Delta^{(j,i)}\right)\right)} \\
 &\quad \times e^{-j2\pi\frac{1}{2M}n^2} \mathbb{1}_{[B_{q,1}]}[n] \\
 &= e^{j2\pi(\phi_{q,1}^{(j,i)} + B\Delta^{(j,i)})} e^{j2\pi\left(\frac{m_{q,1}^{(j,i)} - M - B\Delta^{(j,i)}}{M}\right)n} \mathbb{1}_{[B_{q,1}]}[n]. \quad (\text{B.14})
 \end{aligned}$$

3. 2nd interfering symbol of user  $i$ :

$$\begin{aligned}
 \text{1st Part: } x_{q,2}^{(j,i)}[n] \times c^*[n] &= e^{j2\pi\left(\frac{1}{2M}n^2 + \left(\frac{m_{q,2}^{(j,i)} - B(T_s - \Delta^{(j,i)})}{M}\right)n + \phi_{q,2}^{(j,i)}\right)} \\
 &\quad \times e^{-j2\pi\frac{1}{2M}n^2} \mathbb{1}_{[B_{q,2}]}[n] \\
 &= e^{j2\pi\phi_{q,2}^{(j,i)}} e^{j2\pi\left(\frac{m_{q,2}^{(j,i)} + M - B\Delta^{(j,i)}}{M}\right)n} \mathbb{1}_{[B_{q,2}]}[n]. \quad (\text{B.15})
 \end{aligned}$$

$$\begin{aligned}
 \text{2nd Part: } x_{q,2}^{(j,i)}[n] \times c^*[n] &= e^{j2\pi\left(\frac{1}{2M}n^2 + \left(\frac{m_{q,2}^{(j,i)} - B\left(\frac{M}{B} - \Delta^{(j,i)}\right)}{M}\right)n + \phi_{q,2}^{(j,i)} - B\left(\frac{n}{B} + \frac{M}{B} - \Delta^{(j,i)}\right)\right)} \\
 &\quad \times e^{-j2\pi\frac{1}{2M}n^2} \mathbb{1}_{[A_{q,2}]}[n] \\
 &= e^{j2\pi(\phi_{q,2}^{(j,i)} - M + B\Delta^{(j,i)})} e^{j2\pi\left(\frac{m_{q,2}^{(j,i)} - B\Delta^{(j,i)}}{M}\right)n} \mathbb{1}_{[A_{q,2}]}[n] \\
 &\quad (\text{B.16}) \\
 &= e^{j2\pi(\phi_{q,2}^{(j,i)} + B\Delta^{(j,i)})} e^{j2\pi\left(\frac{m_{q,2}^{(j,i)} - B\Delta^{(j,i)}}{M}\right)n} \mathbb{1}_{[A_{q,2}]}[n].
 \end{aligned}$$

Therefore, the final term can be written as:

$$\begin{aligned}
 r[n] &= h^{(j)} \sqrt{p_e} e^{j2\pi\frac{m_q^{(j)}}{M}n} + h^{(i)} \sqrt{p_e} \left( \sum_{l=1}^2 e^{j2\pi\phi_{q,l}^{(j,i)}} e^{j2\pi\left(\frac{\varphi_{q,l}^{(j,i)}}{M}\right)n} \mathbb{1}_{[A_{q,l}]}[n] \right. \\
 &\quad \left. + e^{j2\pi(\phi_{q,l}^{(j,i)} + B\Delta^{(j,i)})} e^{j2\pi\left(\frac{\varphi_{q,l}^{(j,i)}}{M} - (-1)^{l+1}\right)n} \mathbb{1}_{[B_{q,l}]}[n] \right) + w[n]. \quad (\text{B.17})
 \end{aligned}$$

where  $\varphi_{q,l}^{(j,i)} = m_{q,l}^{(j,i)} - B\Delta^{(j,i)}$  for  $l \in \{1, 2\}$ .

Applying FFT to  $r[n]$  in (B.17), we have:

$$\begin{aligned}
R[k] &= \sum_{n=-\frac{M}{2}}^{\frac{M}{2}-1} r[n] e^{-j2\pi \frac{n}{M} k} \\
R[k] &= \underbrace{h^{(j)} \sqrt{p_e} \sum_{n=-\frac{M}{2}}^{\frac{M}{2}-1} e^{j2\pi \frac{m_q^{(j)}}{M} n} e^{-j2\pi \frac{n}{M} k}}_{R_0[k]} + \underbrace{h^{(i)} \sqrt{p_e} \left( e^{j2\pi \phi_{q,1}^{(j,i)}} \sum_{n \in A_{q,1}} e^{j2\pi \left( \frac{\varphi_{q,1}^{(j,i)}}{M} \right) n} e^{-j2\pi \frac{n}{M} k} \right)}_{R_1[k]} \\
&\quad + \underbrace{e^{j2\pi (\phi_{q,1}^{(j,i)} + B\Delta^{(j,i)})} \sum_{n \in B_{q,1}} e^{j2\pi \left( \frac{\varphi_{q,1}^{(j,i)} - M}{M} \right) n} e^{-j2\pi \frac{n}{M} k}}_{R_2[k]} + \underbrace{e^{j2\pi \phi_{q,2}^{(j,i)}} \sum_{n \in B_{q,2}} e^{j2\pi \left( \frac{\varphi_{q,2}^{(j,i)} + M}{M} \right) n} e^{-j2\pi \frac{n}{M} k}}_{R_3[k]} \\
&\quad + \underbrace{e^{j2\pi (\phi_{q,2}^{(j,i)} + B\Delta^{(j,i)})} \sum_{n \in A_{q,2}} e^{j2\pi \left( \frac{\varphi_{q,2}^{(j,i)}}{M} \right) n} e^{-j2\pi \frac{n}{M} k}}_{R_4[k]}
\end{aligned} \tag{B.18}$$

1.  $R_0[k]$

$$\begin{aligned}
R_0[k] &= h^{(j)} \sqrt{p_e} \sum_{n=-\frac{M}{2}}^{\frac{M}{2}-1} e^{j2\pi \frac{m_q^{(j)}}{M} n} e^{-j2\pi \frac{n}{M} k} \\
R_0[k] &= h^{(j)} \sqrt{p_e} \sum_{n=-\frac{M}{2}}^{\frac{M}{2}-1} e^{-j2\pi \left( \frac{k - m_q^{(j)}}{M} \right) n} = h^{(j)} \sqrt{p_e} \delta[k - m_q^{(j)}]
\end{aligned} \tag{B.19}$$

2.  $R_1[k]$

$$\begin{aligned}
 R_1[k] &= h^{(i)} \sqrt{p_e} e^{j2\pi\phi_{q,1}^{(j,i)}} \sum_{n \in A_{q,1}} e^{j2\pi\left(\frac{\varphi_{q,1}^{(j,i)}}{M}\right)n} e^{-j2\pi\frac{n}{M}k} \\
 R_1[k] &= h^{(i)} \sqrt{p_e} e^{j2\pi\phi_{q,1}^{(j,i)}} \sum_{n \in A_{q,1}} e^{-j2\pi\left(\frac{k-\varphi_{q,1}^{(j,i)}}{M}\right)n} \\
 R_1[k] &= h^{(i)} \sqrt{p_e} e^{j2\pi\phi_{q,1}^{(j,i)}} \left( \frac{1 - e^{-j2\pi\left(\frac{k-\varphi_{q,1}^{(j,i)}}{M}\right)\Delta A_{q,1}}}{1 - e^{-j2\pi\left(\frac{k-\varphi_{q,1}^{(j,i)}}{M}\right)}} \right) \\
 R_1[k] &= h^{(i)} \sqrt{p_e} \underbrace{e^{j2\pi\phi_{q,1}^{(j,i)}} e^{-j\pi\left(\frac{k-\varphi_{q,1}^{(j,i)}}{M}\right)(\Delta A_{q,1}-1)}}_{e^{j\beta_1^{(j,i)}}} \\
 &\quad \times \left( \frac{e^{j\pi\left(\frac{k-\varphi_{q,1}^{(j,i)}}{M}\right)\Delta A_{q,1}} - e^{-j\pi\left(\frac{k-\varphi_{q,1}^{(j,i)}}{M}\right)\Delta A_{q,1}}}{e^{j\pi\left(\frac{k-\varphi_{q,1}^{(j,i)}}{M}\right)} - e^{-j\pi\left(\frac{k-\varphi_{q,1}^{(j,i)}}{M}\right)}} \right) \\
 R_1[k] &= h^{(i)} \sqrt{p_e} e^{j\beta_1^{(j,i)}} \frac{\sin\left(\pi\left(\frac{k-\varphi_{q,1}^{(j,i)}}{M}\right)\Delta A_{q,1}\right)}{\sin\left(\pi\left(\frac{k-\varphi_{q,1}^{(j,i)}}{M}\right)\right)} \tag{B.20}
 \end{aligned}$$

$$\begin{aligned}
 3. \quad R_2[k] \quad R_2[k] &= h^{(i)} \sqrt{p_e} e^{j2\pi(\phi_{q,1}^{(j,i)} + B\Delta^{(j,i)})} \sum_{n \in B_{q,1}} e^{j2\pi\left(\frac{\varphi_{q,1}^{(j,i)} - M}{M}\right)n} e^{-j2\pi\frac{n}{M}k} \\
 R_2[k] &= h^{(i)} \sqrt{p_e} e^{j2\pi(\phi_{q,1}^{(j,i)} + B\Delta^{(j,i)})} \sum_{n \in B_{q,1}} e^{-j2\pi\left(\frac{k+M-\varphi_{q,1}^{(j,i)}}{M}\right)n} \\
 R_2[k] &= h^{(i)} \sqrt{p_e} e^{j2\pi(\phi_{q,1}^{(j,i)} + B\Delta^{(j,i)})} \left( \frac{1 - e^{-j2\pi\left(\frac{k+M-\varphi_{q,1}^{(j,i)}}{M}\right)\Delta B_{q,1}}}{1 - e^{-j2\pi\left(\frac{k+M-\varphi_{q,1}^{(j,i)}}{M}\right)}} \right) \\
 R_2[k] &= h^{(i)} \sqrt{p_e} \underbrace{e^{j2\pi(\phi_{q,1}^{(j,i)} + B\Delta^{(j,i)})} e^{-j\pi\left(\frac{k+M-\varphi_{q,1}^{(j,i)}}{M}\right)\Delta(B_{q,1}-1)}}_{e^{j\beta_2^{(j,i)}}} \\
 &\quad \times \left( \frac{e^{j\pi\left(\frac{k+M-\varphi_{q,1}^{(j,i)}}{M}\right)\Delta B_{q,1}} - e^{-j\pi\left(\frac{k+M-\varphi_{q,1}^{(j,i)}}{M}\right)\Delta B_{q,1}}}{e^{j\pi\left(\frac{k+M-\varphi_{q,1}^{(j,i)}}{M}\right)} - e^{-j\pi\left(\frac{k+M-\varphi_{q,1}^{(j,i)}}{M}\right)}} \right) \\
 R_2[k] &= h^{(i)} \sqrt{p_e} e^{j\beta_2^{(j,i)}} \frac{\sin\left(\pi\left(\frac{k+M-\varphi_{q,1}^{(j,i)}}{M}\right)\Delta B_{q,1}\right)}{\sin\left(\pi\left(\frac{k+M-\varphi_{q,1}^{(j,i)}}{M}\right)\right)} \tag{B.21}
 \end{aligned}$$

4.  $R_3[k]$ 

$$\begin{aligned}
R_3[k] &= h^{(i)} \sqrt{p_e} e^{j2\pi\phi_{q,2}^{(j,i)}} \sum_{n \in B_{q,2}} e^{j2\pi\left(\frac{\varphi_{q,2}^{(j,i)} + M}{M}\right)n} e^{-j2\pi\frac{n}{M}k} \\
R_3[k] &= h^{(i)} \sqrt{p_e} e^{j2\pi\phi_{q,2}^{(j,i)}} \sum_{n \in B_{q,2}} e^{-j2\pi\left(\frac{k-M-\varphi_{q,2}^{(j,i)}}{M}\right)n} \\
R_3[k] &= h^{(i)} \sqrt{p_e} e^{j2\pi\phi_{q,2}^{(j,i)}} \left( \frac{1 - e^{-j2\pi\left(\frac{k-M-\varphi_{q,2}^{(j,i)}}{M}\right)\Delta B_{q,2}}}{1 - e^{-j2\pi\left(\frac{k-M-\varphi_{q,2}^{(j,i)}}{M}\right)}} \right) \\
R_3[k] &= h^{(i)} \sqrt{p_e} \underbrace{e^{j2\pi\phi_{q,2}^{(j,i)}} e^{-j\pi\left(\frac{k-M-\varphi_{q,1}^{(j,i)}}{M}\right)\Delta(B_{q,2}-1)}}_{e^{j\beta_3^{(j,i)}}} \\
&\quad \times \left( \frac{e^{j\pi\left(\frac{k-M-\varphi_{q,2}^{(j,i)}}{M}\right)\Delta B_{q,2}} - e^{-j\pi\left(\frac{k-M-\varphi_{q,2}^{(j,i)}}{M}\right)\Delta B_{q,2}}}{e^{j\pi\left(\frac{k-M-\varphi_{q,2}^{(j,i)}}{M}\right)} - e^{-j\pi\left(\frac{k-M-\varphi_{q,2}^{(j,i)}}{M}\right)}} \right) \\
R_3[k] &= h^{(i)} \sqrt{p_e} e^{j\beta_3^{(j,i)}} \frac{\sin\left(\pi\left(\frac{k-M-\varphi_{q,1}^{(j,i)}}{M}\right)\Delta B_{q,2}\right)}{\sin\left(\pi\left(\frac{k-M-\varphi_{q,2}^{(j,i)}}{M}\right)\right)} \tag{B.22}
\end{aligned}$$

5.  $R_4[k]$

$$\begin{aligned}
 R_4[k] &= h^{(i)} \sqrt{p_e} e^{j2\pi(\phi_{q,2}^{(j,i)} + B\Delta^{(j,i)})} \sum_{n \in A_{q,2}} e^{j2\pi\left(\frac{\varphi_{q,2}^{(j,i)}}{M}\right)n} e^{-j2\pi\frac{n}{M}k} \\
 R_4[k] &= h^{(i)} \sqrt{p_e} e^{j2\pi(\phi_{q,2}^{(j,i)} + B\Delta^{(j,i)})} \sum_{n \in A_{q,2}} e^{-j2\pi\left(\frac{k-\varphi_{q,2}^{(j,i)}}{M}\right)n} \\
 R_4[k] &= h^{(i)} \sqrt{p_e} e^{j2\pi(\phi_{q,2}^{(j,i)} + B\Delta^{(j,i)})} \left( \frac{1 - e^{-j2\pi\left(\frac{k-\varphi_{q,2}^{(j,i)}}{M}\right)\Delta A_{q,2}}}{1 - e^{-j2\pi\left(\frac{k-\varphi_{q,2}^{(j,i)}}{M}\right)}} \right) \\
 R_4[k] &= h^{(i)} \sqrt{p_e} \underbrace{e^{j2\pi(\phi_{q,2}^{(j,i)} + B\Delta^{(j,i)})} e^{-j\pi\left(\frac{k-\varphi_{q,2}^{(j,i)}}{M}\right)\Delta(A_{q,2}-1)}}_{e^{j\beta_4^{(j,i)}}} \\
 &\quad \times \left( \frac{e^{j\pi\left(\frac{k-\varphi_{q,2}^{(j,i)}}{M}\right)\Delta A_{q,2}} - e^{-j\pi\left(\frac{k-\varphi_{q,2}^{(j,i)}}{M}\right)\Delta A_{q,2}}}{e^{j\pi\left(\frac{k-\varphi_{q,2}^{(j,i)}}{M}\right)} - e^{-j\pi\left(\frac{k-\varphi_{q,2}^{(j,i)}}{M}\right)}} \right) \\
 R_4[k] &= h^{(i)} \sqrt{p_e} e^{j\beta_4^{(j,i)}} \frac{\sin\left(\pi\left(\frac{k-\varphi_{q,2}^{(j,i)}}{M}\right)\Delta A_{q,2}\right)}{\sin\left(\pi\left(\frac{k-\varphi_{q,2}^{(j,i)}}{M}\right)\right)} \\
 &\quad \approx h^{(i)} \sqrt{p_e} e^{j\beta_4^{(j,i)}} \frac{\pi\left(\frac{k-\varphi_{q,2}^{(j,i)}}{M}\right)\Delta A_{q,2}}{\pi\left(\frac{k-\varphi_{q,2}^{(j,i)}}{M}\right)} \\
 &\quad \approx h^{(i)} \sqrt{p_e} e^{j\beta_4^{(j,i)}} \Delta A_{q,2} \tag{B.23}
 \end{aligned}$$

$$R[k] = R_0[k] + R_1[k] + R_2[k] + R_3[k] + R_4[k] \tag{B.24}$$

### B.3 Amplitudes of the Peaks

- The amplitude of the 1st peak is written as:

$$= h^{(i)} \sqrt{p_e} e^{j2\pi\phi_{q,1}^{(j,i)}} e^{j\pi\left(\frac{k-m_{q,1}^{(i)}+B\Delta^{(j,i)}}{M}\right)(M-m_{q,1}^{(i)}-1)} \tag{B.25}$$

- The amplitude of the 2nd peak is written as:

$$= h^{(i)} \sqrt{p_e} e^{j2\pi(\phi_{q,1}^{(j,i)} + B\Delta^{(j,i)})} e^{j\pi\left(\frac{k-m_{q,1}^{(i)}+B\Delta^{(j,i)}+M}{M}\right)(B\Delta^{(j,i)}-m_{q,1}^{(i)}-1)} \tag{B.26}$$

- The amplitude of the 3rd peak is written as:

$$= h^{(i)} \sqrt{p_e} e^{j2\pi(\phi_{q,2}^{(j,i)} + B\Delta^{(j,i)})} e^{j\pi\left(\frac{k-m_{q,2}^{(i)} + B\Delta^{(j,i)} - M}{M}\right)(B\Delta^{(j,i)} - m_{q,2}^{(i)} - 1)} \quad (\text{B.27})$$

- The amplitude of the 4th peak is written as:

$$= h^{(i)} \sqrt{p_e} e^{j2\pi\phi_{q,2}^{(j,i)}} e^{j\pi\left(\frac{k-m_{q,2}^{(i)} + B\Delta^{(j,i)}}{M}\right)(m_{q,2}^{(i)} - 1)} \quad (\text{B.28})$$

where  $\phi_{q,1}^{(j,i)} = \frac{B(\Delta^{(j,i)})^2 - 2m_{q,1}^{(i)}\Delta^{(j,i)}}{2T_s}$ , and

$$\phi_{q,2}^{(j,i)} = \frac{B(T_s - \Delta^{(j,i)})^2 + 2m_{q,2}^{(i)}(T_s - \Delta^{(j,i)})}{2T_s}.$$



# Bibliography

- [1] Sandro Nižetić, Petar Šolić, Diego López-de-Ipiña González-de-Artaza, and Luigi Patrono. Internet of things (iot): Opportunities, issues and challenges towards a smart and sustainable future. *Journal of Cleaner Production*, 274:122877, 2020.
- [2] Luigi Patrono, Luigi Atzori, Petar Šolić, Marina Mongiello, and Aitor Almeida. Challenges to be addressed to realize internet of things solutions for smart environments. *Future Generation Computer Systems*, 111:873–878, 2020.
- [3] Arpan Pal and Balamuralidhar Purushothaman. *IoT technical challenges and solutions*. Artech House, 2016.
- [4] Lueth. Knud Lasse. State of the iot 2018: Number of iot devices, Aug 2018. (Accessed on 05/22/2020).
- [5] Jetmir Haxhibeqiri, Eli De Poorter, Ingrid Moerman, and Jeroen Hoebeke. A survey of lorawan for iot: From technology to application. *Sensors*, 18:3995, 11 2018.
- [6] N. Shahid and S. Aneja. Internet of things: Vision, application areas and research challenges. In *2017 International Conference on I-SMAC (IoT in Social, Mobile, Analytics and Cloud) (I-SMAC)*, pages 583–587, 2017.
- [7] Luigi Atzori, Antonio Iera, and Giacomo Morabito. Understanding the internet of things: definition, potentials, and societal role of a fast evolving paradigm. *Ad Hoc Networks*, 56:122–140, 2017.
- [8] N. Shah and S. Sundar. Smart electric meter using lora protocols and lot applications. In *2018 Second International Conference on Electronics, Communication and Aerospace Technology (ICECA)*, pages 1178–1180, 2018.

- [9] Y. Bagariang, M. I. Nashiruddin, and N. Mufti Adriansyah. Lora-based iot network planning for advanced metering infrastructure in urban, suburban and rural scenario. In *2019 International Seminar on Research of Information Technology and Intelligent Systems (ISRITI)*, pages 188–193, 2019.
- [10] R. Vishnubhotla, P. S. Rao, A. Ladha, S. Kadiyala, A. Narmada, B. Ronanki, and S. Illapakurthi. Zigbee based multi-level parking vacancy monitoring system. In *2010 IEEE International Conference on Electro/Information Technology*, pages 1–4, 2010.
- [11] Semtech. Iot-enabled smart parking management: Lora technology application brief. (Accessed on 05/23/2020).
- [12] J. Jose and T. Sasipraba. Indoor air quality monitors using iot sensors and lpwan. In *2019 3rd International Conference on Trends in Electronics and Informatics (ICOEI)*, pages 633–637, 2019.
- [13] R. K. Kodali, S. Yerroju, and S. Sahu. Smart farm monitoring using lora enabled iot. In *2018 Second International Conference on Green Computing and Internet of Things (ICGCIoT)*, pages 391–394, 2018.
- [14] K. I. Wang, S. Wu, A. Ivoghlian, Z. Salcic, A. Austin, and X. Zhou. Lws: A lorawan wireless underground sensor network simulator for agriculture applications. In *2019 IEEE SmartWorld, Ubiquitous Intelligence Computing, Advanced Trusted Computing, Scalable Computing Communications, Cloud Big Data Computing, Internet of People and Smart City Innovation (SmartWorld/SCALCOM/UIC/ATC/CBDCOM/IOP/SCI)*, pages 475–482, 2019.
- [15] N. Shahid and S. Aneja. Internet of things: Vision, application areas and research challenges. In *2017 International Conference on I-SMAC (IoT in Social, Mobile, Analytics and Cloud) (I-SMAC)*, pages 583–587, 2017.
- [16] Z. Sheng, S. Yang, Y. Yu, A. V. Vasilakos, J. A. Mccann, and K. K. Leung. A survey on the ietf protocol suite for the internet of things: standards, challenges, and opportunities. *IEEE Wireless Communications*, 20(6):91–98, 2013.
- [17] Antonio Cilfone, Luca Davoli, Laura Belli, and Gianluigi Ferrari. Wireless mesh networking: An iot-oriented perspective survey on relevant technologies. *Future Internet*, 11(4), 2019.

- [18] U. Raza, P. Kulkarni, and M. Sooriyabandara. Low power wide area networks: An overview. *IEEE Communications Surveys Tutorials*, 19(2):855–873, 2017.
- [19] U. Raza, P. Kulkarni, and M. Sooriyabandara. Low power wide area networks: An overview. *IEEE Communications Surveys Tutorials*, 19(2):855–873, 2017.
- [20] Patent. Low power long range transmitter, Jan 2014.
- [21] Semtech. AN1200.22: LoRa Modulation Basics. Technical report, Semtech Corporation, 2015.
- [22] Rashmi Sharan Sinha, Yiqiao Wei, and Seung-Hoon Hwang. A survey on lpwa technology: Lora and nb-iot. *ICT Express*, 3(1):14–21, 2017.
- [23] J. P. Shanmuga Sundaram, W. Du, and Z. Zhao. A survey on lora networking: Research problems, current solutions, and open issues. *IEEE Communications Surveys Tutorials*, 22(1):371–388, 2020.
- [24] Capture effect - wikipedia. [https://en.wikipedia.org/wiki/Capture\\_effect](https://en.wikipedia.org/wiki/Capture_effect). (Accessed on 06/20/2021).
- [25] LoRaAlliance. What is LoRaWAN. Technical report, LoRa Alliance, 2015.
- [26] LoRaAlliance. LoRaWAN 1.0 Specification. Technical report, LoRa Alliance, 2015.
- [27] LoRaAlliance. LoRaWAN 1.1 Specification. Technical report, LoRa Alliance, 2017.
- [28] LoRaAlliance. LoRaWAN 1.0.3 Specification. Technical report, LoRa Alliance, 2018.
- [29] Jeferson Rodrigues Cotrim and João Henrique Kleinschmidt. Lorawan mesh networks: A review and classification of multihop communication. *Sensors*, 20(15), 2020.
- [30] Jorge Ortín, Matteo Cesana, and Alessandro Redondi. How do aloha and listen before talk coexist in lorawan? In *2018 IEEE 29th Annual International Symposium on Personal, Indoor and Mobile Radio Communications (PIMRC)*, pages 1–7, 2018.
- [31] Luca Beltramelli, Aamir Mahmood, Patrik Österberg, and Mikael Gidlund. Lora beyond aloha: An investigation of alternative random access protocols. *IEEE Transactions on Industrial Informatics*, 17(5):3544–3554, 2021.

- [32] D. Croce, M. Gucciardo, S. Mangione, G. Santaromita, and I. Tinnirello. Impact of lora imperfect orthogonality: Analysis of link-level performance. *IEEE Communications Letters*, 22(4):796–799, 2018.
- [33] A. Waret, M. Kaneko, A. Guitton, and N. El Rachkidy. Lora throughput analysis with imperfect spreading factor orthogonality. *IEEE Wireless Communications Letters*, 8(2):408–411, 2019.
- [34] D. Bankov, E. Khorov, and A. Lyakhov. On the limits of lorawan channel access. In *2016 International Conference on Engineering and Telecommunication (EnT)*, pages 10–14, 2016.
- [35] A. Mahmood, E. Sisinni, L. Guntupalli, R. Rondón, S. A. Hassan, and M. Gidlund. Scalability analysis of a lora network under imperfect orthogonality. *IEEE Transactions on Industrial Informatics*, 15(3):1425–1436, 2019.
- [36] G. Zhu, C. Liao, M. Suzuki, Y. Narusue, and H. Morikawa. Evaluation of lora receiver performance under co-technology interference. In *2018 15th IEEE Annual Consumer Communications Networking Conference (CCNC)*, pages 1–7, 2018.
- [37] D. Magrin, M. Centenaro, and L. Vangelista. Performance evaluation of lora networks in a smart city scenario. In *2017 IEEE International Conference on Communications (ICC)*, pages 1–7, 2017.
- [38] T. Elshabrawy and J. Robert. Analysis of ber and coverage performance of lora modulation under same spreading factor interference. In *2018 IEEE 29th Annual International Symposium on Personal, Indoor and Mobile Radio Communications (PIMRC)*, pages 1–6, 2018.
- [39] O. Afisiadis, M. Cotting, A. Burg, and A. Balatsoukas-Stimming. Lora symbol error rate under non-aligned interference. In *2019 53rd Asilomar Conference on Signals, Systems, and Computers*, pages 1957–1961, 2019.
- [40] J. Markkula, K. Mikhaylov, and J. Haapola. Simulating lorawan: On importance of inter spreading factor interference and collision effect. In *ICC 2019 - 2019 IEEE International Conference on Communications (ICC)*, pages 1–7, 2019.

- [41] A. A. Kherani and K. M. P. Maurya. Improved packet detection in lora-like chirp spread spectrum systems. In *2019 IEEE International Conference on Advanced Networks and Telecommunications Systems (ANTS)*, pages 1–4, 2019.
- [42] U. Noreen, L. Clavier, and A. Bounceur. Lora-like css-based phy layer, capture effect and serial interference cancellation. In *European Wireless 2018; 24th European Wireless Conference*, pages 1–6, 2018.
- [43] Congduc Pham, Ahe e'ne Bounceur, Laurent Clavier, Umber Noreen, and Muhammad Ehsan. Radio channel access challenges in lora low-power wide-area networks. In Bharat S. Chaudhari and Marco Zennaro, editors, *LPWAN Technologies for IoT and M2M Applications*, pages 65–102. Academic Press, Jan 2020.
- [44] B. Laporte-Fauret, M. A. Ben Temim, G. Ferré, D. Dallet, B. Minger, and L. Fuché. An enhanced lora-like receiver for the simultaneous reception of two interfering signals. In *2019 IEEE 30th Annual International Symposium on Personal, Indoor and Mobile Radio Communications (PIMRC)*, pages 1–6, 2019.
- [45] N. E. Rachkidy, A. Guitton, and M. Kaneko. Decoding superposed lora signals. In *2018 IEEE 43rd Conference on Local Computer Networks (LCN)*, pages 184–190, 2018.
- [46] M. A. B. Temim, G. Ferré, B. Laporte-Fauret, D. Dallet, B. Minger, and L. Fuché. An enhanced receiver to decode superposed lora-like signals. *IEEE Internet of Things Journal*, pages 1–1, 2020.
- [47] A. A. TESFAY, E. P. SIMON, G. FERRÉ, and L. CLAVIER. Serial interference cancellation for improving uplink in lora-like networks. In *2020 IEEE 31st Annual International Symposium on Personal, Indoor and Mobile Radio Communications*, pages 1–6, 2020.
- [48] T. Voigt, M. Bor, U. Roedig, and J. Alonso. Mitigating inter-network interference in lora networks. In *Proceedings of the 2017 International Conference on Embedded Wireless Systems and Networks*, page 323–328, USA, 2017.
- [49] L. Beltramelli, A. Mahmood, M. Gidlund, P. Österberg, and U. Jennehag. Interference modelling in a multi-cell lora system. In *2018 14th International Conference on Wireless and Mobile Computing, Networking and Communications (WiMob)*, pages 1–8, 2018.

- [50] K. Mikhaylov, J. Petäjäljärvi, and J. Janhunen. On lorawan scalability: Empirical evaluation of susceptibility to inter-network interference. In *2017 European Conference on Networks and Communications (EuCNC)*, pages 1–6, 2017.
- [51] P. Edward, S. Elzeiny, M. Ashour, and T. Elshabrawy. On the coexistence of lora- and interleaved chirp spreading lora-based modulations. In *2019 International Conference on Wireless and Mobile Computing, Networking and Communications (WiMob)*, pages 1–6, 2019.
- [52] L. Vangelista, L. Dell’Anna, and I. Calabrese. On the coexistence of lorawan and legacy short range devices in unlicensed bands in europe. In *2019 International Conference on Software, Telecommunications and Computer Networks (SoftCOM)*, pages 1–5, 2019.
- [53] O. Georgiou and U. Raza. Low power wide area network analysis: Can lora scale? *IEEE Wireless Communications Letters*, 6(2):162–165, 2017.
- [54] K. Mikhaylov, J. Petäejäjaervi, and T. Haenninen. Analysis of capacity and scalability of the lora low power wide area network technology. In *22th European Wireless Conference*, pages 1–6, 2016.
- [55] Martin C. Bor, Utz Roedig, Thiemo Voigt, and Juan M. Alonso. Do lora low-power wide-area networks scale? In *Proceedings of the 19th ACM International Conference on Modeling, Analysis and Simulation of Wireless and Mobile Systems*, MSWiM ’16, pages 59–67, New York, NY, USA, 2016. Association for Computing Machinery.
- [56] F. Adelantado, X. Vilajosana, P. Tuset-Peiro, B. Martinez, J. Melia-Segui, and T. Watteyne. Understanding the limits of lorawan. *IEEE Communications Magazine*, 55(9):34–40, Sep. 2017.
- [57] S. Abboud, N. el Rachkidy, A. Guitton, and H. Safa. Gateway selection for downlink communication in lorawan. In *2019 IEEE Wireless Communications and Networking Conference (WCNC)*, pages 1–6, 2019.
- [58] M. Centenaro, L. Vangelista, and R. Kohno. On the impact of downlink feedback on lora performance. In *2017 IEEE 28th Annual International Symposium on Personal, Indoor, and Mobile Radio Communications (PIMRC)*, pages 1–6, Oct 2017.

- [59] A. Pop, U. Raza, P. Kulkarni, and M. Sooriyabandara. Does bidirectional traffic do more harm than good in lorawan based lpwa networks? In *GLOBECOM 2017 - 2017 IEEE Global Communications Conference*, pages 1–6, 2017.
- [60] K. Mikhaylov, J. Petaejaevaerv, and A. Pouttu. Effect of downlink traffic on performance of lorawan lpwa networks: Empirical study. In *2018 IEEE 29th Annual International Symposium on Personal, Indoor and Mobile Radio Communications (PIMRC)*, pages 1–6, Sep. 2018.
- [61] F. Van den Abeele, J. Haxhibeqiri, I. Moerman, and J. Hoebeke. Scalability analysis of large-scale lorawan networks in ns-3. *IEEE Internet of Things Journal*, 4(6):2186–2198, Dec 2017.
- [62] M. A. Ullah, J. Iqbal, A. Hoeller, R. Souza, and H. Alves. K-means spreading factor allocation for large-scale lora networks. *Sensors*, 19(21):4723, 2019.
- [63] A. Farhad, D. Kim, and J. Pyun. Scalability of lorawan in an urban environment: A simulation study. In *2019 Eleventh International Conference on Ubiquitous and Future Networks (ICUFN)*, pages 677–681, July 2019.
- [64] V. Di Vincenzo, M. Heusse, and B. Tourancheau. Improving downlink scalability in lorawan. In *ICC 2019 - 2019 IEEE International Conference on Communications (ICC)*, pages 1–7, May 2019.
- [65] B. Reynders, Q. Wang, P. Tuset-Peiro, X. Vilajosana, and S. Pollin. Improving reliability and scalability of lorawans through lightweight scheduling. *IEEE Internet of Things Journal*, 5(3):1830–1842, 2018.
- [66] J. Lim and Y. Han. Spreading factor allocation for massive connectivity in lora systems. *IEEE Communications Letters*, 22(4):800–803, 2018.
- [67] A. A. Tesfay, E. P. Simon, I. Nevat, and L. Clavier. Multiuser detection for downlink communication in LoRa- Like networks. *IEEE Access*, 8:199001–199015, 2020.
- [68] S. M. R. Islam, N. Avazov, O. A. Dobre, and K. Kwak. Power-domain non-orthogonal multiple access (noma) in 5g systems: Potentials and challenges. *IEEE Communications Surveys Tutorials*, 19(2):721–742, 2017.
- [69] S. Shieh, C. Lin, Y. Huang, and C. Wang. On gray labeling for downlink non-orthogonal multiple access without sic. *IEEE Communications Letters*, 20(9):1721–1724, 2016.

- [70] M. Qiu, Y. Huang, and J. Yuan. Downlink non-orthogonal multiple access without sic for block fading channels: An algebraic rotation approach. *IEEE Transactions on Wireless Communications*, 18(8):3903–3918, 2019.
- [71] ETSI. Etsi en 300 220-1 v2.4.1: Electromagnetic compatibility and radio spectrum matters (erm); short range devices (srd); radio equipment to be used in the 25 mhz to 1 000 mhz frequency range with power levels ranging up to 500 mw; part 1: Technical characteristics and test methods. Technical report, European Telecommunications Standards Institute (ETSI), 2012.
- [72] Reuven Y. Rubinstein. Optimization of computer simulation models with rare events, 1997.
- [73] D. Ernst, M. Glavic, G. Stan, S. Mannor, and L. Wehenkel. The cross-entropy method for power system combinatorial optimization problems. In *2007 IEEE Lausanne Power Tech*, pages 1290–1295, 2007.
- [74] J. G. Proakis and M. Saleh. *Digital Communications 5th Edition*. McGraw Hill, 2007.
- [75] L. Dai, B. Wang, Y. Yuan, S. Han, C. I, and Z. Wang. Non-orthogonal multiple access for 5g: solutions, challenges, opportunities, and future research trends. *IEEE Communications Magazine*, 53(9):74–81, 2015.
- [76] H. Tabassum, M. S. Ali, E. Hossain, M. J. Hossain, and D. I. Kim. Uplink vs. downlink noma in cellular networks: Challenges and research directions. In *2017 IEEE 85th Vehicular Technology Conference (VTC Spring)*, pages 1–7, 2017.
- [77] J. M. d. S. Sant’Ana, A. Hoeller, R. D. Souza, H. Alves, and S. Montejo-Sánchez. Lora performance analysis with superposed signal decoding. *IEEE Wireless Communications Letters*, pages 1–1, 2020.
- [78] B. Laporte-Fauret, M. A. Ben Temim, G. Ferre, D. Dallet, B. Minger, and L. Fuché. An enhanced lora-like receiver for the simultaneous reception of two interfering signals. In *2019 IEEE 30th Annual International Symposium on Personal, Indoor and Mobile Radio Communications (PIMRC)*, pages 1–6, 2019.
- [79] J. G. Andrews. Interference cancellation for cellular systems: a contemporary overview. *IEEE Wireless Communications*, 12(2):19–29, 2005.

- [80] D. Croce, M. Gucciardo, S. Mangione, G. Santaromita, and I. Tinnirello. Impact of lora imperfect orthogonality: Analysis of link-level performance. *IEEE Communications Letters*, 22(4):796–799, 2018.
- [81] Q. M. Qadir. Analysis of the reliability of LoRa. *IEEE Communications Letters*, pages 1–1, 2020.
- [82] P. Edward, S. Elzeiny, M. Ashour, and T. Elshabrawy. On the coexistence of LoRa- and Interleaved Chirp Spreading LoRa-Based modulations. In *2019 International Conference on WiMob*, 2019.
- [83] P. Zhang, X. Kang, D. Wu, and R. Wang. High-Accuracy Entity State Prediction Method Based on Deep Belief Network Toward IoT Search. *IEEE Wireless Communications Letters*, 8(2):492–495, 2019.
- [84] J. Zhou, Y. Wang, K. Ota, and M. Dong. AAIoT: Accelerating Artificial Intelligence in IoT Systems. *IEEE Wireless Communications Letters*, 8(3):825–828, 2019.
- [85] Hao Ye, Geoffrey Ye Li, and Biing-Hwang Juang. Power of deep learning for channel estimation and signal detection in ofdm systems. *IEEE Wireless Communications Letters*, 7(1):114–117, 2017.
- [86] K. He and J. Sun. Convolutional Neural Networks at constrained time cost. In *2015 IEEE Conference on Computer Vision and Pattern Recognition (CVPR)*, pages 5353–5360, 2015.
- [87] Jon Kleinberg and Éva Tardos. *Algorithm Design*, chapter Basics of Algorithm Analysis, pages 30–35. Pearson Education, 1st edition, 2005.
- [88] A. Sampath and D.R. Jeske. Analysis of signal-to-interference ratio estimation methods for wireless communication systems. In *ICC 2001. IEEE International Conference on Communications. Conference Record (Cat. No.01CH37240)*, volume 8, pages 2499–2503 vol.8, 2001.